Nuclear structure corrections in muonic atoms

Dissertation

zur Erlangung des akademischen Grades
„Doktor der Naturwissenschaften“
am Fachbereich Physik, Mathematik und Informatik (FB 08)
der Johannes Gutenberg-Universität Mainz

Simone Salvatore Li Muli

Born in Palermo, Italy
Mainz, den 31. Juli. 2023

Abstract

Muonic hydrogen-like atoms, bound systems of a muon and an atomic nucleus, are excellent probes for nuclear physics, because the muon is much heavier than the electron and its wavefunction overlaps significantly more with the nuclear charge distribution. This increased sensitivity to nuclear physics allows for precise extractions of nuclear charge radii by measuring the Lamb-shift. The precision of this extraction is currently limited by the uncertainty of nuclear structure effects, which are not known as precisely as quantum electrodynamics effects, due to the non-perturbative nature of the strong force at the low-energy scale relevant to muonic atoms. This work addresses the calculation of the nuclear structure corrections to the Lamb-shift of muonic helium and lithium atoms.

For muonic lithium, we calculate the nuclear structure corrections to the Lamb-shift using a simplified model of the nuclear force. This allows us to perform estimates, which are useful in view of the future planned experimental activities. For muonic helium, the novelty of this work comes from the use of nuclear interactions derived from the chiral effective field theory and of Bayesian inference for quantifying the uncertainties. This combination of techniques puts the problem of quantifying theoretical uncertainties in nuclear physics into a more solid statistical ground and defines a systematically improvable method for calculating observables. The main results of this work are new high-precision values for nuclear structure corrections in muonic atoms, which can be used to update the charge radii of ^{3}He and ^{4}He extracted from the recent muonic-atoms spectroscopy experiments in muonic helium.

Due to partial cancellation of uncertainties, the squared difference in the nuclear charge radii, $\delta r^2 = r_c^2(^3\mathrm{He}) - r_c^2(^4\mathrm{He})$ can be obtained with more precision than the nuclear charge radii itself. This quantity can also be precisely obtained from spectroscopy experiments in ordinary helium atoms, which allows to perform consistency checks between theory and experiments in electronic and muonic atoms. Two publications of δr^2, one using muonic atoms and the other using ordinary helium atoms, were recently published, which resulted in a disagreement at the level of 3.6 σ. Our updated theory of the nuclear structure effects supports the previous value of δr^2 coming from muonic atoms, and intensifies the current disagreement.

List of publications related to this thesis

The work presented in this thesis is based on published and unpublished material produced by the author Simone Salvatore Li Muli. The published parts of this work have appeared in the following references:

- [1] S. Li Muli, A. Poggialini, and S. Bacca. *Muonic Lithium atoms: nuclear structure corrections to the Lamb shift*, SciPost Phys. Proc., 3, 028, (2020).

  Here, we estimate the nuclear structure corrections to the Lamb-shift in muonic lithium atoms. I contributed by checking the previous preliminary calculation obtained by A. Poggialini and S. Bacca, by calculating further corrections, and by contributing to the paper writing.

- [2] S. S. Li Muli, S. Bacca, and N. Barnea. *Implementation of local chiral interactions in the hyperspherical harmonics formalism*. Frontiers in Physics, 9, (2021).

  Here, we write three nucleon forces derived from the chiral effective field theory as irreducible spherical tensors, and implement them in the few-body hyperspherical harmonics method. The spherical tensors were firstly derived by N. Barnea, and then checked by myself and S. Bacca. I then implemented these forces in the hyperspherical harmonics method, generated the results and contributed to the paper writing.

- [3] S. S. Li Muli, B. Acharya, O. J. Hernandez, and S. Bacca. *Bayesian analysis of nuclear polarizability corrections to the Lamb shift of muonic H-atoms and He-ions*. J. Phys. G, 49(10), 105101, (2022).

  Here, we analyze the uncertainties of the Lamb-shift in light muonic atoms due to the η-expansion method using Bayesian inference. The Bayesian theory and the analysis code was written by O.J. Hernandez and later checked and extended by myself. I then generated the results and contributed to the paper writing.

- [4] B. Acharya et. al. *Uncertainty quantification in electromagnetic observables on nuclei*. Frontiers in Physics, 10, (2023).

  This is a review paper that describes uncertainty quantifications in nuclear physics. I contributed by generating new results for the photoabsorption cross section of ^{4}He within the framework of chiral effective field theory, and wrote the relative part of the review.

- [5] K. Pachucki, V. Lensky, F. Hagelstein, S. S. Li Muli, S. Bacca, and R. Pohl. *Comprehensive theory of the Lamb shift in light muonic atoms*, arxiv: 2212.13782 (2023).

  This work is a review submitted to *Review of Modern Physics*. Here, we discuss the various atomic, nuclear and hadronic corrections to the Lamb-shift of muonic atoms in a unified framework. The main author of the review is K. Pachucki. I contributed by generating the results of the electron vacuum polarization correction to the leading nuclear polarizabilities in muonic helium atoms and wrote, in collaboration with S. Bacca, the nuclear theory part of the review.

- [6] S. S. Li Muli and S. Bacca, in preparation (2023).

  This work collects the final results of the PhD project discussed in this thesis. Here, we calculate the nuclear structure corrections in muonic helium atoms using interactions derived from chiral effective field theory and we analyze the uncertainties using Bayesian inference. This leads to new high-precision values for the charge radii of the ^{3}He and ^{4}He nuclei. I generated the results, performed the uncertainty quantification and wrote the first draft of the paper. The paper will be submitted soon.

Contents

List of Figures

List of Tables

1. Introduction

The hydrogen atom has historically been at the center of the development of modern physics. Explaining the gross features of its energy spectrum led Einstein, Bohr, Pauli, Heisenberg, Schrödinger and many others towards the development of quantum mechanics [7, 8]. The explanation of its fine structure inspired Dirac to generalize the theory for relativistic particles [9]. The experimental discovery of the Lamb shift [10] gave rise to the theory of quantum electrodynamics (QED) and its validation by the famous calculations of Feynman, Schwinger and Tomonaga proved that the world can be described in terms of quantum fields [11–13] at the energy scale accessible by our experiments. Currently, the hydrogen atom is still at the forefront of scientific research [14–16], given that its simplicity makes it an ideal ground for exploring the limits of predictions from bound state QED [17] and for determining the Rydberg constant, which is one of the most accurately known fundamental constants of nature and it is an important ingredient in the global adjustments of other fundamental constants [18].

The recent progress in trapping and studying simple atomic systems containing electrons or muons has opened a new frontier of precision physics searches aimed at discerning violations of lepton universality and possible interactions between leptons not yet included in the Standard Model [19, 20]. This can be achieved by comparing the high-precision spectroscopy experiments in positronium (Ps) [21], a bound state of an electron and a positron, and muonium (M) [22, 23], a bound state of a positive anti-muon and an electron, against the respective theory predictions based on the Standard Model. In comparison to purely leptonic systems, muonic atoms, bound states of a muon and an atomic nucleus, can hardly test lepton universality at the same level of significance, given that they suffer from the large uncertainties associated with the nuclear structure effects. However, this sensitivity to nuclear physics is not necessarily a negative feature. In fact, it allows to directly probe possible forces between leptons and hadrons not yet considered in the Standard Model and to establish new high-precision tests to nuclear physics.

Because the muon is roughly 200 times heavier than the electron, and accordingly the Bohr radii of muonic atoms are much smaller compared to Bohr radii of ordinary atoms, the wavefunction of the bound muon has a significant overlap with the nuclear charge distribution, which largely amplifies the corrections to the atomic spectra due to the nuclear structure. This argument inspired an experimental campaign aimed at extracting nuclear charge radii by performing spectroscopy experiments in light-muonic atoms, which led over the years to the

most precise determinations of the nuclear charge radii of the proton [24,25], alpha particle [26] and helion [27], while experiments in heavier muonic atoms such as muonic lithium [28] are planned for the future. The nuclear charge radii can be extracted form spectroscopy experiments in muonic atoms by comparing the result of the experiments with the theory prediction. In particular, for the Lamb-shift E_{LS}, the sensitivity to the nuclear charge radius can be parameterized as

$$E_{LS} = E_{QED} + \mathcal{C} r_c^2 + E_{NS} \,, \tag{1.1}$$

where E_{QED} comprises purely QED and nuclear recoil effects, while the other two terms are related to the structure of the nucleus. In the second term of Eq. (1.1), we made explicit the dependence over the nuclear charge radius r_c. This dependence allows for the extraction of nuclear charge radii by combining theory with laser spectroscopy of muonic atoms. The last term E_{NS} contains all the known nuclear structure effects that do not contribute to $\mathcal{C}$. For this extraction to be successful, both experiments and the theory predictions must reach a high level of precision. The most recent determinations of these factors are reported in Table 1.1, where the nuclear structure corrections are separated as $E_{NS} = E_{TPE} + E_{3PE}$, where E_{TPE} indicates the contribution from the two-photon-exchange diagrams and E_{3PE} is the contribution from the three-photon-exchange diagram.

	E_{LS} [meV]	E_{QED} [meV]	$\mathcal{C}$ [meV fm^{-2}]	E_{TPE} [meV]	E_{3PE} [meV]
μH	202.3706(23)	206.0344(3)	−5.2259	0.0292(25)	−0.0013(3)
μ^2H	202.8785(34)	228.7740(3)	−6.1074	1.718(20)	0.0022(9)
μ^3He$^+$	1258.598(48)	1644.348(8)	−103.383	15.370(310)	−0.214(214)
μ^4He$^+$	1378.521(48)	1668.491(7)	−106.209	9.224(400)	−0.165(165)

Table 1.1.: Experimental measurements (first column) of the Lamb-shift in muonic atoms and theoretical predictions (the other columns) of the terms on the right side of Eq. (1.1).

It is evident from Table 1.1 that the largest contribution to the Lamb-shift comes from the QED term. However, it is also clear that most of the uncertainty in Eq. (1.1) comes from nuclear structure effects. It is important to improve the calculation of the nuclear structure effects, since better calculations allow for a more precise extraction of the nuclear charge radii. This motivates the work of this thesis. Its scope is to re-examine the nuclear structure corrections in light-muonic atoms in view of recent progresses in nuclear theory, with the goal of better quantifying and possibly reducing the main sources of uncertainty. Our motivation for this work is directly related to a better determination of the charge radii of light nuclei, but it is not limited to this goal. A different approach is to experimentally measure the Lamb-shift in muonic atoms, and use an independent measurement

of the nuclear charge radii to extract a value for the nuclear corrections E_{NS}. This can be used as a benchmark to put our understanding of the nuclear interaction to the test [26, 27] and improve the description of the nuclear polarizability.

This thesis is structured as follows. In Chapter 2, we develop the atomic theory for calculating nuclear structure corrections to the Lamb-shift of hydrogen-like muonic atoms; the primary purpose of this theory is to identify the relevant nuclear matrix elements which must be obtained from nuclear physics. In Chapter 3, we discuss our strategy for calculating these matrix elements. This strategy is based upon deriving the interactions among nucleons as a low-energy effective representation of quantum chromodynamics, and then solving the nuclear Schrödinger equation numerically without making use of any uncontrolled approximations. In Chapter 4, we identify Bayesian statistics as the ideal framework for quantifying the uncertainties in the calculations. Accordingly, in this chapter the Bayesian methods are briefly described and adapted for the estimations of the most significant uncertainties associated to muonic atoms. Finally, in Chapter 5 we show the results of this work, while Chapter 6 is reserved for the concluding remarks and a discussion on the future prospects.

2. Atomic theory

In this chapter we derive a theory for calculating the nuclear structure corrections to the Lamb-shift [10] of hydrogen-like muonic atoms. These corrections are collected in the last two entries of Eq. (1.1) and their precise evaluation is crucial for enriching the significance of precision spectroscopy experiments in muonic ions, given that they currently dominate the uncertainty budget. Our definition of the Lamb-shift, which follows the definition used in the literature devoted to muonic atoms and that of CODATA [18], assumes no coupling between the total angular momentum of the orbiting muon and the nuclear spin. Accordingly, the Lamb-shift is defined as the difference between the $2P_{1/2}$ and $2S_{1/2}$ atomic energies, $E_{LS}= E(2P_{1/2}) - E(2S_{1/2})$.

In describing the spectral lines of muonic ions, we start from the solution of the Schrödinger equation for the muon bound by the Coulomb interaction to an infinitely massive and point-like nucleus standing at the origin of the coordinate system, see Figure 2.1 (left panel). The spectrum obtained from this theory differs from the experimental one. This is expected given that many physical effects are missing in such a model. However, the predicted and observed energy spectra are not profoundly different. This is mostly due to the perturbative nature of QED, the large separation of scales between nuclear and atomic physics, and the significant difference between the masses of the muon and of the lightest nuclei. The missing corrections can then be interpreted as refinements of the more basic picture obtained from the Schrödinger equation, and they can be included in perturbation theory. Nuclear structure effects originate from two distinct physical phenomena: the dominant one is due to the finite-size of the nucleus, while the sub-leading effect is due to the nuclear polarizability. This hierarchy is well explained by the evidence that nuclear finite-size effects originate from order $(Z\alpha)^4$, where Z is the nuclear charge and α the fine-structure constant, while the nuclear polarizabilities start from order $(Z\alpha)^5$. Our goal is to elaborate a theory for the calculation of these effects up to order $(Z\alpha)^5$, and also include selected corrections from higher orders. As a consequence, our theory includes the leading nuclear polarizabilities and the nuclear finite-size effects up to their sub-leading order. Unless otherwise specified, throughout this thesis we will be working in natural units $\hbar = c = 1$.

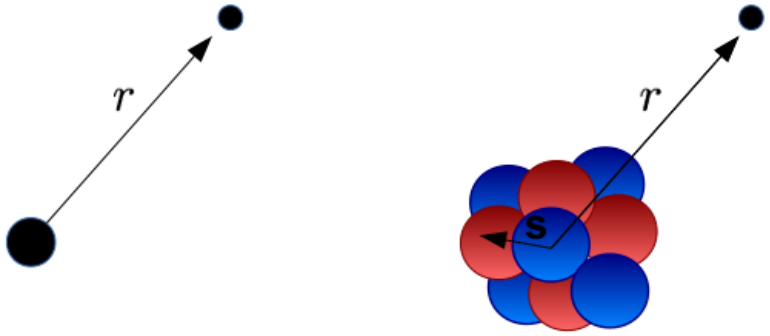

Figure 2.1.: Representation of the nuclear finite-size effects. Compared to the Coulomb interaction between point-like particles (left), the muon at position r interacts with the Coulomb field of the nuclear charge distribution $\rho_{\rm ch}(\mathbf{s})$ generated by the nucleons (right).

2.1. Nuclear finite-size

Nuclear finite-size corrections originate from the nuclear charge being distributed over a finite volume. Because the muon spends some time inside the nuclear charge cloud and experiences a smaller attraction compared to the case of a point-like nucleus, the qualitative effect of the nuclear finite-size is to increase the atomic energies. We define the unperturbed spectrum $\mathrm{E(nL)}$ and states $|\phi_{\rm nL}\rangle$ of hydrogen-like muonic atoms by the known solution of the Schrödinger equation in a Coulomb potential radiated by a point-like nucleus at the origin of the coordinate system. According to the discussion of the previous section, the nuclear finite-size effects can be included in perturbation theory. They arise from the following perturbative Hamiltonian [29]

$$\Delta V_c(r) = -(Z\alpha)\int d^3s\,\rho_{\rm ch}(s)\left(\frac{1}{|\mathbf{s}-\mathbf{r}|}-\frac{1}{r}\right) = -(Z\alpha)\int d^3s\,\rho_{\rm ch}(s)\left(\frac{1}{(r,s)_>}-\frac{1}{r}\right), \tag{2.1}$$

where $\mathbf{r}$ represents the coordinates of the muon, $r \equiv |\mathbf{r}|$, $s \equiv |\mathbf{s}|$ and $\rho_{\rm ch}(s)$ is the nuclear charge distribution, see Figure 2.1. The second equality holds if the charge density is a scalar under rotation. The symbol $(r,s)_>$ selects the largest between the norm of the two vectors. The Hamiltonian in Eq. (2.1) can be regarded as a perturbation because the term in the bracket is generally small compared to the point-like Coulomb interaction due to the large separation of scales between the size of the atom and the size of the nucleus.

Our goal is to calculate nuclear finite-size corrections to the Lamb-shift up to order $(Z\alpha)^5$. This means that we must calculate the nuclear finite-size corrections to the energies of the 2S-states only, given that corrections to the 2P-states are of higher orders. We expand the unperturbed $2S$-wavefunction in powers of $(Z\alpha)$ as

$$\phi_{2S}(r) = \phi_{2S}\Big(1 - mr(Z\alpha) + \frac{3}{8}(mr)^2(Z\alpha)^2 + \mathcal{O}(Z\alpha)^3\Big) \,, \tag{2.2}$$

where ϕ_{2S} is a shorthand for the value of the wavefunction at the origin of the coordinate system. The correction to the energies[1] of the 2S-states in first order perturbation theory reads

$$\Delta E^{(1)}_{2S} = \langle \phi_{2S}| \, \Delta V_c(r) \, |\phi_{2S}\rangle \ . \tag{2.3}$$

We calculate this expectation value up to order $(Z\alpha)^5$, obtaining

$$\Delta E^{(1)}_{2S} = \frac{2\pi}{3}(Z\alpha)\ \phi^2_{2S}\ \Big(\langle r_c^2\rangle - (Z\alpha)m\,\langle r_c^3\rangle + \mathcal{O}\big[(Z\alpha)^2\big]\Big) \,, \tag{2.4}$$

note that ϕ^2_{2S} is of order $(Z\alpha)^3$. Starting from order $(Z\alpha)^5$, we obtain further corrections to the energies of the 2S states from second-order perturbation theory. These corrections are expressed as

$$\Delta E^{(2)}_{2S} = \langle \phi_{2S}| \, \Delta V_c(r) G'(E_{2S}) \Delta V_c(r) \, |\phi_{2S}\rangle \ , \tag{2.5}$$

where

$$G'(E_n) = \sum_{k\neq n} \frac{|k\rangle\,\langle k|}{E_n - E_k} \,, \tag{2.6}$$

is the reduced Green's function for the Schrödinger equation of the muon in the Coulomb field generated by the nucleus. In coordinate space it is expressed as [29]

$$\begin{aligned} G'(r,r',E_n) \ &= \ -\frac{m}{2\pi}\frac{1}{r_>}\Big[1 - Z\alpha m(r+r') \\ &- \ 2Z\alpha m r_> \big(\log(\beta r_>) + \psi(n) + 2\gamma - 1/n - 3/2\big)\Big] + \mathcal{O}(Z\alpha)^2 \,, \end{aligned} \tag{2.7}$$

where $r = |\mathbf{r}|$ and $r' = |\mathbf{r}'|$ are coordinates in muon's space, $r_>$ selects the largest between r and r', $\beta = 2Z\alpha\pi/n$, γ is the Euler gamma constant, and $\psi(n)$ is the

[1] In what follows, $\Delta E^{(n)}_{2S}$ is one specific nuclear finite-size correction to the energy of the $2S$-state of the atom, $\mathrm{E}(2\mathrm{S}_{1/2})$. The superscript means that this correction originates from the n-th order perturbation theory of the interaction in Eq. (2.1).

digamma function. Keeping only terms contributing to order $(Z\alpha)^5$ we obtain

$$\Delta E_{2S}^{(2)} = \frac{2\pi}{3} m (Z\alpha)^2 \, \phi_{2S}^2 \, \langle r_c^3 \rangle - \frac{\pi}{3} m (Z\alpha)^2 \, \phi_{2S}^2 \int d^3s \, d^3t \, \rho_{\rm ch}(s) \, \rho_{\rm ch}(t) \, |\mathbf{s} - \mathbf{t}|^3 \, . \tag{2.8}$$

To summarize, the energy shift up to order $(Z\alpha)^5$ due to the finite-size of the nucleus is given by the sum of $\Delta E_{2S}^{(1)}$ and $\Delta E_{2S}^{(2)}$. We obtain

$$\begin{aligned} \Delta E_{2S} &= \frac{2\pi}{3} (Z\alpha) \, \phi_{2S}^2 \Big(\langle r_c^2 \rangle - (Z\alpha) m \, \langle r_c^3 \rangle + (Z\alpha) m \, \langle r_c^3 \rangle - \frac{m}{2} (Z\alpha) \, \langle r_c^3 \rangle_{(2)} + \mathcal{O}\big[(Z\alpha)^2\big] \Big) \\ &= \frac{2\pi}{3} (Z\alpha) \, \phi_{2S}^2 \Big(\langle r_c^2 \rangle - \frac{m}{2} (Z\alpha) \, \langle r_c^3 \rangle_{(2)} + \mathcal{O}\big[(Z\alpha)^2\big] \Big) \, , \end{aligned} \tag{2.9}$$

where

$$\langle r_c^3 \rangle_{(2)} = \int d^3s \, d^3t \, \rho_{\rm ch}(s) \, \rho_{\rm ch}(t) \, |\mathbf{s} - \mathbf{t}|^3 \tag{2.10}$$

is the third Zemach moment. Taking into account that $\mathrm{E_{LS}} = \mathrm{E}\big(2\mathrm{P}_{1/2}\big) - \mathrm{E}\big(2\mathrm{S}_{1/2}\big)$, the first term in Eq. (2.9) contributes to $\mathcal{C}$ in Eq. (1.1) as

$$\mathcal{C} = -\frac{2\pi}{3} (Z\alpha) \, \phi_{2S}^2 + \dots \, , \tag{2.11}$$

where the dots represent higher-order corrections which are not calculated in this thesis, they are presented in details in Ref. [5] and mostly include radiative corrections due to the electron-vacuum polarization.

The contribution to $\mathcal{C}$ derived in this section assumed a nucleus without spin. For a general nuclear spin the problem is more complicated and requires care in the definition of the nuclear charge radius. For instance, in the case of the proton one has that the photon-proton interaction is parameterized in terms of the Dirac $F_1(-\mathbf{q}^2)$ and Pauli $F_2(-\mathbf{q}^2)$ form factors, where $\mathbf{q}$ is the momentum transfer of the photon-proton interaction vertex. The general convention is to define the proton charge radius as the slope at $\mathbf{q}^2 = 0$ of the Sachs electric form factor $G_E(-\mathbf{q}^2)$, which is an appropriate combination of $F_1(-\mathbf{q}^2)$ and $F_2(-\mathbf{q}^2)$. If this definition of the proton charge radius is used, one sees that the correction to the Lamb-shift of muonic hydrogen takes the form in Eq. (2.11) with the dots representing also an effect coming from the Darwin-Foldy term [30], see for instance the discussion in Chapter 6 of Ref. [31].

The second term in Eq. (2.9) is referred to as the Zemach correction

$$\delta_{\rm Zem} = -\frac{\pi}{3} m (Z\alpha)^2 \phi_{2S}^2 \, \langle r_c^3 \rangle_{(2)} \, .$$

This correction does not effectively contribute to the Lamb-shift of muonic atoms, since it is analytically canceled by a term coming from the nuclear polarizabilities.

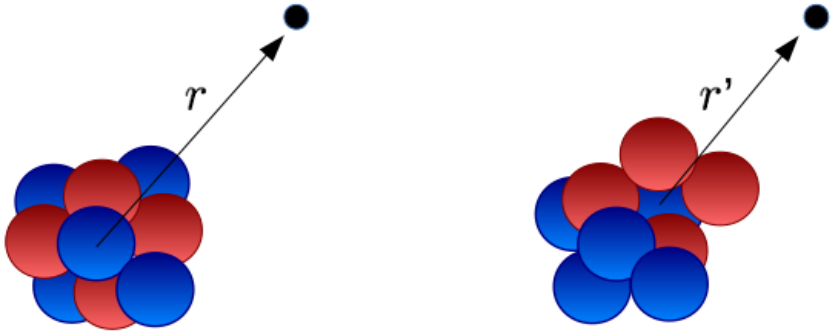

Figure 2.2.: Pictorial representation of the polarization effects. Due to the Coulomb attraction, the center of the nuclear charge distribution moves towards the orbiting muon. This increases the potential energy felt by the muon and lowers the energies of atomic states.

2.2. Nuclear polarizabilities

The energy spectrum of a bound muon is affected by the polarization of the nucleus. Polarizability effects are purely dynamical contributions which pictorially can be interpreted as due to the protons in the nucleus being pulled away from the nuclear center-of-mass due to the electromagnetic interaction with the orbiting lepton. The distorted charge distribution then follows the lepton in its orbit around the nucleus, lowering the energy levels of the atom [32], see representation in Fig. 2.2. The most complete derivation of this correction can be obtained by relating the energy shift to the forward Compton amplitude, Fig. 2.3. When the hadronic tensor is evaluated in the non-relativistic limit, the seagull correction needs to be introduced to make the amplitude gauge invariant. The seagull term effectively acts as a subtraction point that cancels an infrared divergence in the transverse part of the amplitude.

Below, we derive the energy correction to the Lamb-shift coming from the diagrams in Fig. 2.3. By making some simplifying assumptions that work very well in light-muonic atoms, we will express these corrections as sum rules or ground state expectation values over the nuclear Hilbert space, namely as quantities that can be either extracted from experiments or calculated from first principles using ab-initio nuclear theory. The derivation of the formula follows from a lengthy calculation. In the main part of the thesis we only describe the main results. The interested

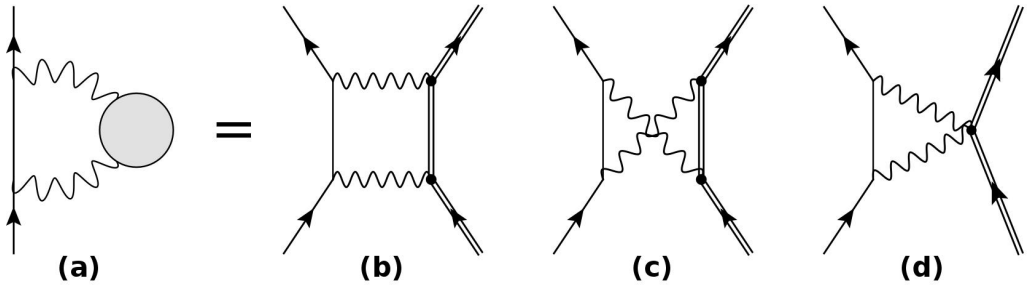

Figure 2.3.: (a): Self-energy correction to the bound muon spectrum due to the nuclear polarization. (b): ladder diagram. (c): crossed diagram. (d): seagull diagram.

reader can consult the Appendices A, and B where the derivation is reported in full.

The sum of the three Feynman diagrams in Fig. 2.3 is here expressed as a product of leptonic $L_{\mu\nu}(q,k)$, gauge $D_{\mu\nu}(q)$ and hadronic $H_{\mu\nu}(q,-q)$ tensors. Accordingly, the total amplitude reads

$$i\mathcal{M} = \int \frac{d^4q}{(2\pi)^4}\, L_{\mu\nu}(q,k)\; D^{\nu\sigma}(q)\; D^{\mu\rho}(-q)\; H_{\sigma\rho}(q,-q)\;, \tag{2.12}$$

where q denotes the 4-momentum of the photon loop and k denotes the 4-momentum of the bound lepton. In this section we discuss each of the tensors separately, and combine them together at the very end.

Leptonic tensor. We start with the evaluation of the leptonic tensor. As opposed to the notation in Eq. (2.12), here it is convenient to explicitly show the dependence of the leptonic tensor over the spin of the muon, namely $L_{\mu\nu}(q,k) \equiv L^s_{\mu\nu}(q,k)$. Since muons are structureless spin-1/2 particles, the leptonic tensor follows directly from the QED Lagrangian as

$$L^s_{\mu\nu}(q,k) = \left[-\frac{ie^2}{(k-q)^2 - m^2 + i\epsilon}\right] \bar{u}^s(k)\; \gamma_\mu \Big[(k-q)^\lambda \gamma_\lambda + m\Big] \gamma_\nu\; u^s(k)\;, \tag{2.13}$$

where $u^s(k)$ are the Dirac wavefunctions of the bound muon with spin s and 4-momentum k, while with m we denote the mass of the muon and with e the absolute value of its electric charge. In both the diagrams of Fig. 2.3 and in Eq. (2.13), we set the spins and the 4-momenta of the incoming and outgoing muons to be equal, this ensures that the amplitude of Eq. (2.12) includes processes affecting energy corrections of a specific atomic state. The internal leptonic line has been evaluated using the free Dirac propagator. This approximation allows us to ex-

tract the leading (in $Z\alpha$) correction to the energies due to the diagrams in Fig. 2.3, and later it will be relaxed with the inclusion of the so called Coulomb distortion effects.

Given our definition of the Lamb-shift, which assumes no coupling with the nuclear spin, the two states associated with the possible spin orientations of the muon are degenerate. This feature can be exploited to simplify the calculation of the amplitude in Eq. (2.12) by averaging the leptonic tensor over the spin. We further neglect the three momentum of the muon with respect to its rest mass. This approximation is motivated by the evidence that light hydrogen-like atoms are loosely bound systems, where the momentum of the bound lepton goes as $k \sim m(Z\alpha)$. For light atoms this means that $k \ll m$. We refer to this as the "wavefunction approximation" and since our derivations are entirely based on the applicability of this approximation, this means that our calculation works best in light systems where $(Z\alpha)$ is a small parameter. Finally, the hadronic tensor is generally written in a way that it obeys crossing symmetry $H_{\rho\sigma}(-q,q) = H_{\sigma\rho}(q,-q)$. The symmetries of the amplitude in Eq. (2.12) can then be exploited by writing the leptonic tensor in a way that it follows this symmetry as well. The full derivation of this symmetric leptonic tensor $L^{(S)}_{\mu\nu}(q,k)$ can be found in Appendix A. Here, we report only the final result

$$L^{(S)}_{\mu\nu} = -i2\pi\alpha\left[\frac{2m\delta_{\nu0}\delta_{\mu0} - q_\mu\delta_{\nu0} - q_\nu\delta_{\mu0} + q^0 g_{\mu\nu}}{q^2 - 2mq^0 + i\epsilon} + \frac{2m\delta_{\nu0}\delta_{\mu0} + q_\mu\delta_{\nu0} + q_\nu\delta_{\mu0} - q^0 g_{\mu\nu}}{q^2 + 2mq^0 + i\epsilon}\right], \tag{2.14}$$

where $g^{\mu\nu}$ is the Lorentz metric tensor, while $\delta_{\mu\nu}$ is the Kronecker delta function.

Gauge choice. As a next step, we specify a gauge for the photon propagators in Eq. (2.12). As long as we guarantee that the total amplitude is gauge invariant, the derived energy corrections will not depend on our arbitrary choice of gauge conditions. Our calculation is done in Coulomb gauge. This choice significantly simplifies the final expression for the amplitude, and allows for a much simpler numerical evaluation. The photon propagator in this gauge takes the following expression

$$D^{\mu\nu}(q) \;=\; \begin{cases} D^{00}(q) = \frac{1}{\mathbf{q}^2} \\ D^{i0}(q) = D^{0j}(q) = 0 \\ D^{ij}(q) = \frac{1}{q^2}\left(\delta^{ij} - \frac{q^i q^j}{\mathbf{q}^2}\right) \end{cases}, \tag{2.15}$$

where we follow the convention of using Greek letters for Lorentz vectors and Roman letters for denoting their space components. Bold variables denote spatial three-dimensional vectors. The simplifications from using the Coulomb gauge are immediately clear when performing the contractions with the symmetrized

leptonic tensor $L^{(S)}_{\mu\nu}$ of Eq. (2.14). Many contributions vanish and after a lengthy calculation ones is left with

$$L^{(S)}_{\mu\nu}\; D^{\nu\sigma}(q)\; D^{\mu\rho}(-q) = i(4\pi\alpha)\frac{2m}{(q^2+i\epsilon)^2 - 4m^2q_0^2}\left[\frac{g^{00}}{\mathbf{q}^2} + \frac{q_0^2}{(q^2+i\epsilon)^2}\; T^{nm}\right], \quad (2.16)$$

where $T^{nm} \equiv T^{nm}(\mathbf{q}) = \left(\delta^{nm} - (q^n q^m)/\mathbf{q}^2\right)$ defines the transverse-projector tensor and q_0 is the time component of the 4-vector q.

Hadronic Tensor. Lastly we discuss the structure of the hadronic tensor $H_{\mu\nu}(q,-q)$ that appears in Eq. (2.12). At present there are different approaches to derive this tensor, see for instance Refs. [33,34] and references therein.

In this work our approach is based on the calculation of this tensor from first principles, using ab-initio methods that will be described in Chapter 3. Defining with $J_\mu(\mathbf{q})$ the one-photon current operator and with $B_{\mu\nu}(\mathbf{q})$ the two-photon operator, we write the hadronic tensor as

$$\begin{aligned} H_{\mu\nu}(q,-q) &= \sum_N \left[\frac{\langle 0|\, J_\mu(\mathbf{q})\, |N\rangle\, \langle N|\, J_\nu(-\mathbf{q})\, |0\rangle}{E_0 - E_N + q_0 + i\epsilon} + \frac{\langle 0|\, J_\nu(-\mathbf{q})\, |N\rangle\, \langle N|\, J_\mu(\mathbf{q})\, |0\rangle}{E_0 - E_N - q_0 + i\epsilon}\right] \\ &+ B_{\mu\nu}(\mathbf{q})\,, \end{aligned} \quad (2.17)$$

where $|0\rangle$, $|N\rangle$ represent the nuclear ground and excited states with energies E_0, E_N respectively. Details regarding the derivation of the formula above can be found in Appendix A, while a discussion of the consequence of gauge invariance and the relations between the one-photon and two-photon operators can be found in Ref. [35]. It is easy to see that this tensor preserves crossing symmetry $H_{\rho\sigma}(-q,q) = H_{\sigma\rho}(q,-q)$ as anticipated.

For a relativistic Lagrangian of nucleons and photons $B_{\mu\nu}(\mathbf{q}) = 0$, since the electromagnetic coupling is derived from minimal substitution and the relativistic Dirac Lagrangian is linear with respect to the 4-momentum of the nucleons. When one performs a non-relativistic reduction of this Lagrangian, the kinetic energy becomes quadratic with respect to the momentum of the nucleons, this generates a coupling term with two-photon fields.

Total amplitude. The total amplitude follows from combining Eq. (2.16) and Eq. (2.17). We obtain

$$i\mathcal{M} = i(4\pi\alpha)^2 \int \frac{d^4q}{(2\pi)^4}\; \frac{2m}{(q^2+i\epsilon)^2 - 4m^2q_0^2}\left[\frac{1}{\mathbf{q}^2}\; H_L + \frac{q_0^2}{(q^2+i\epsilon)^2}\; H_T\right], \quad (2.18)$$

where we took a factor of $(4\pi\alpha)$ outside of the definition of $H_{\rho\sigma}$ and we defined the longitudinal H_L and transverse H_T parts of the hadronic tensors as

$$H_L = \sum_{N\neq 0} |\langle N|\, \rho_{\rm ch}(\mathbf{q})\, |0\rangle|^2 \left[\frac{1}{q_0-\omega_N+i\epsilon}-\frac{1}{q_0+\omega_N-i\epsilon}\right], \tag{2.19}$$

$$H_T = \sum_{N\neq 0} |\langle 0|\, \mathbf{J}_\perp\, |N\rangle|^2 \left[\frac{1}{q_0-\omega_N+i\epsilon}-\frac{1}{q_0+\omega_N-i\epsilon}\right] + B_\perp(\mathbf{q})\,, \tag{2.20}$$

where the symbol $(\perp)$ indicates contraction with the transverse-projector tensor T^{ij} defined after Eq. (2.16), while $\rho_{\rm ch}(\mathbf{q}) = J_0(\mathbf{q})$ and $\omega_N = E_N - E_0$. Note that, compared to Eq. (2.17), here we are taking only the inelastic part of the hadronic tensor, since we are interested in polarizability effects.

The energy corrections. The amplitude in Eq. (2.18) defines a complex potential that shifts the energies of the bound muon by $\Delta E_{\rm nL} = \langle\phi_{\rm nL}|\, {\rm Re}\big[i\mathcal{M}\big]\, |\phi_{\rm nL}\rangle$, where $|\phi_{\rm nL}\rangle$ is the eigenstate of the bound muon with principal quantum number n and orbital angular momentum L. An interesting derivation of the previous result applied to the radiative correction to the Lamb-shift in ordinary hydrogen due to the electron self-energy diagram can be found in Ref. [36]. According to this discussion, the energy shift due to the nuclear polarization reads

$$\Delta E_{nL} = (4\pi\alpha)^2\, \phi^2_{nL}\ {\rm Im}\int \frac{d^4q}{(2\pi)^4}\, \frac{2m}{(q^2+i\epsilon)^2-4m^2q_0^2}\left[\frac{1}{\mathbf{q}^2}\, H_L + \frac{q_0^2}{(q^2+i\epsilon)^2}\, H_T\right], \tag{2.21}$$

where to simplify the notation we introduced the shorthand for the modulus square of the muon's wavefunction at the origin $\phi^2_{nL} = |\phi_{nL}(0)|^2$. The functional dependence of Eq. (2.21) to ϕ^2_{nL} only is due to our approximation, introduced in the previous section, to completely neglect the three momentum of the bound muon compared to its rest mass. The energy correction is expressed in terms of the longitudinal and transverse parts of the hadronic tensors, which are defined in terms of the matrix elements of the nuclear electric charge, electromagnetic current and two-photon operators. Our strategy for calculating these matrix elements will be discussed in Chapter 3.

The expression in Eq. (2.21) can be further simplified by analytically performing the integration over the time-like component q_0. The calculation is a straightforward application of contour integration and it is reported in full in Appendix A

from which we only quote the final result [2]

$$\begin{aligned}\Delta E_{nL} &= -8\alpha^2 m\, \phi_{nL}^2 \int \frac{d^3\mathrm{q}}{4\pi} \left\{ \sum_{N\neq 0} |\langle N|\, \rho_{\mathrm{ch}}(\mathbf{q})\, |0\rangle|^2\, \frac{(2E_q+\omega_N)}{\mathrm{q}^4 E_q\left[(E_q+\omega_N)^2-m^2\right]} \right. \\ &+ \sum_{N\neq 0} |\langle 0|\, \mathbf{J}_\perp(\mathbf{q})\, |N\rangle|^2 \left[\frac{\mathrm{q}^2}{4m^2}\, \frac{(2E_q+\omega_N)}{\mathrm{q}^4 E_q\left[(E_q+\omega_N)^2-m^2\right]} - \frac{1}{4m^2\mathrm{q}^3}\, \frac{\omega_N+2\mathrm{q}}{(\omega_N+\mathrm{q})^2} \right] \\ &+ \left. B_\perp(\mathbf{q})\, \frac{1}{8m^2\mathrm{q}^2} \left(\frac{1}{\mathrm{q}} - \frac{1}{E_q} \right) \right\}, \end{aligned} \tag{2.22}$$

where $E_q = \sqrt{\mathbf{q}^2+m^2}$ and $\mathrm{q} = |\mathbf{q}|$. The previous equation is the leading correction to the non-relativistic energies in hydrogen-like atoms due to the polarization effects of the nucleus. The formula is derived in Coulomb gauge, but the correction is gauge invariant if the one-photon and two-photon operators are properly constructed. Due to the "wave-function approximation" (see discussion after Eq. (2.13)), and the use of the free Dirac propagator, the corrections to the 2S states are of order $(Z\alpha)^5$, while there is no correction to the energies of any state with orbital angular momentum greater than 0. In particular, nuclear polarizability corrections to 2P states are of order $(Z\alpha)^7$, whose precision is beyond the scope of this work.

The total sum in Eq. (2.22) is finite, but the individual terms are not. In fact both the electromagnetic current and seagull integrals are infrared divergent, but as we will see the divergence is canceled in the sum. Even though Eq. (2.22) is already well suited for numerical solutions, the equation has been directly applied only to the calculations of the nuclear structure effects in muonic deuterium [37, 38]. This is entirely due to the difficulties in calculating the matrix elements of the charge, current and two-photon operators for a comprehensive range of energy and momentum transfer in larger systems.

In this thesis a more sophisticated method is pursued, which allows to ease the numerical burden and extend the feasibility of the calculations to systems heavier than muonic hydrogen and deuterium. Unfortunately, this comes at the cost of introducing one further source of uncertainties, but we will prove in this thesis that such uncertainties can be both quantified and improved systematically. This method, sometimes referred to as the "η-expansion," is presented in the next sections of the thesis, first assuming non-relativistic kinematics for the muon and later in full relativistic form.

[2] Here, q is the magnitude of a three-dimensional vector and shall not be confused with q, which is a 4-vector.

The non-relativistic structure function

The integrals in Eq. (2.22) are generally peaked at small values of the momentum transfer. For muonic atoms most of the sensitivity of ΔE_{nL} is found in the non-relativistic region, where $\mathbf{q}^2 \ll m^2$. In this region, the longitudinal part of the equation dominates the transverse terms, which from Eq. (2.22) can be seen to be generally suppressed by further powers of $\mathbf{q}^2/m$. It is then clear that an approximate value for the nuclear polarizability correction can be obtained by considering only the contribution from the longitudinal hadronic tensor and reducing it to a non-relativistic form. Following this discussion, the non-relativistic approximation of the energy shift is written as

$$\Delta E_{nL}^{\mathrm{NR}} = -8\alpha^2\, \phi_{nL}^2 \sum_{N\neq 0} \int \frac{d^3\mathrm{q}}{4\pi}\, |\langle N|\, \rho_{\mathrm{ch}}(\mathbf{q})\, |0\rangle|^2 \frac{1}{\mathbf{q}^2\left(\frac{\mathbf{q}^2}{2m}+\omega_N\right)\mathbf{q}^2}\,. \tag{2.23}$$

An alternative derivation of the previous formula can be obtained from second-order perturbation theory in ordinary non-relativistic quantum mechanics, as shown in Ref. [39]. The matrix elements of the momentum-space charge-distribution operator are commonly defined in Fourier space from the definition of the coordinate space matrix elements. With the use of Eq. (B.2), we can express the previous equation in the following form

$$\Delta E_{nL}^{\mathrm{NR}} = -8\alpha^2\, \phi_{nL}^2 \sum_{N\neq 0} \int d^3x\, d^3y\ \langle 0|\, \rho_{\mathrm{ch}}^{\dagger}(\mathbf{y})\, |N\rangle\, \langle N|\, \rho_{\mathrm{ch}}(\mathbf{x})\, |0\rangle\ \mathrm{I}_{\mathrm{NR}}(z)\,, \tag{2.24}$$

where $\mathbf{z} = \mathbf{x} - \mathbf{y}$ and $z \equiv |\mathbf{z}|$. All of the coupling between the lepton and the nucleus is now contained within the structure function $\mathrm{I}_{\mathrm{NR}}(z)$, defined as

$$\mathrm{I}_{\mathrm{NR}}(z) = \int \frac{d^3\mathrm{q}}{4\pi} \frac{e^{i\mathbf{q}\cdot\mathbf{z}}}{\mathbf{q}^2\left(\frac{\mathbf{q}^2}{2m}+\omega_N\right)\mathbf{q}^2} = \frac{\lambda^2}{z\,\omega_N} \int \frac{d\mathrm{q}}{\mathrm{q}^3} \frac{\sin(\mathrm{q}z)}{(\mathbf{q}^2+\lambda^2)}\,, \tag{2.25}$$

where $\lambda^2 = 2m\omega_N$. The solution of the integral on the right-hand side of Eq. (2.25) is known, and an expression suitable for computation can be found by expanding it in terms of the small parameter $\eta = \lambda z$.

This parameter has been argued in previous literature [39–41] to hold an approximate value of ~ 0.3 in light-nuclear systems, which justifies the use of an expansion and allows us to obtain meaningful estimates of the non-relativistic correction by truncating an expansion to low orders. In Section 5.2 we will prove with the use of Bayesian techniques that η is indeed a small parameter in light-nuclear systems. We find

$$\mathrm{I}_{\mathrm{NR}}(z) = \frac{\pi}{2}\, \frac{1}{\lambda\,\omega_N} \left(-\frac{\lambda^2 z^2}{6} + \frac{\lambda^3 z^3}{24} - \frac{\lambda^4 z^4}{120} + \ldots \right)\,, \tag{2.26}$$

and inserting the expansion of $\mathrm{I}_{\mathrm{NR}}(z)$ back into Eq. (2.24) we obtain the following η-expansion expression for the nuclear polarizability corrections to the atomic energies

$$\begin{aligned}\Delta E^{\mathrm{NR}}_{nL} &= -\frac{4\pi}{3}\alpha^2\phi^2_{nL}\sum_{N\neq 0}\int d^3x\, d^3y\ \langle 0|\,\rho^\dagger_{\mathrm{ch}}(\mathbf{y})\,|N\rangle\,\langle N|\,\rho_{\mathrm{ch}}(\mathbf{x})\,|0\rangle \\ &\times \left[-\sqrt{\frac{2m}{\omega_N}}\frac{z^2}{2} + m\frac{z^3}{4} - m^2\sqrt{\frac{\omega_N}{2m}}\frac{z^4}{10} + \mathcal{O}(z^5)\right]. \end{aligned} \tag{2.27}$$

Relativistic effects

The formalism of the previous section was based on a non-relativistic approximation of the integration kernels in Eq. (2.22). Here we perform a similar derivation but without the non-relativistic reduction. Similarly to what was done for the non-relativistic derivation, we want to write the energy correction due to the nuclear polarizability in the following form

$$\begin{aligned}\Delta E_{nL} &= -8\alpha^2 m\,\phi^2_{nL}\left\{\sum_{N\neq 0}\int d^3x\, d^3y\ \langle 0|\,\rho^\dagger_{\mathrm{ch}}(\mathbf{y})\,|N\rangle\,\langle N|\,\rho_{\mathrm{ch}}(\mathbf{x})\,|0\rangle\ \mathrm{I}_{\mathrm{N}}(z)\right. \\ &+ \sum_{N\neq 0}\int d^3x\, d^3y\,\langle 0|\,J^\dagger_i(\mathbf{y})\,|N\rangle\,\langle N|\,J_j(\mathbf{x})\,|0\rangle\left[\delta_{ij}J_N(z) + z^i z^j \bar{J}_N(z)\right] \\ &+ \left.\int d^3x\, d^3y\ B^{ij}(\mathbf{x},\mathbf{y})\,\frac{1}{2}\left[\delta_{ij}K(z) + z_i z_j \bar{K}(z)\right]\right\}, \end{aligned} \tag{2.28}$$

where the problem of finding the structure function $\mathrm{I}_{\mathrm{NR}}(z)$ of the previous section now translates in finding the five relativistic structure functions $\mathrm{I}_{\mathrm{N}}(z)$, $J_N(z)$, $\bar{J}_N(z)$, $K(z)$ and $\bar{K}(z)$. The evaluation of the relativistic structure function is much more difficult than the non-relativistic case of the previous section, and it is best to address the longitudinal, transverse-current, and transverse-seagull terms separately, summing them together only at the very end. The details of the calculations are shown in Appendix B while in the main body of this thesis we describe only the crucial points.

Longitudinal term. From Eq. (2.22) we can extract the longitudinal part of the energy correction

$$\Delta E^{\mathrm{L}}_{nL} = -8\alpha^2 m\,\phi^2_{nL}\sum_{N\neq 0}\int\frac{d^3\mathrm{q}}{4\pi}\,|\langle N|\,\rho_{\mathrm{ch}}(\mathbf{q})\,|0\rangle|^2\,\frac{(2E_q+\omega_N)}{\mathrm{q}^4 E_q\left[(E_q+\omega_N)^2 - m^2\right]}\,. \tag{2.29}$$

Similarly to what was done in the non-relativistic section, we express the matrix elements of the nuclear charge-distribution operator in Fourier space, the integra-

tion over the angular part of the momentum transfer can easily be performed, leading to

$$\Delta E^{\mathrm{L}}_{nL} = -8\alpha^2 m\, \phi^2_{nL} \sum_{N\neq 0} \int d^3x\, d^3y\ \langle 0|\, \rho^{\dagger}_{\mathrm{ch}}(\mathbf{y})\, |N\rangle\, \langle N|\, \rho_{\mathrm{ch}}(\mathbf{x})\, |0\rangle\ \mathrm{I_N}(z)\ , \tag{2.30}$$

where the coupling between nucleus and lepton is now found within the relativistic structure function $\mathrm{I_N}(z)$

$$\mathrm{I_N}(z) = \frac{1}{\omega_N z} \int d\mathrm{q}\, \frac{\sin(\mathrm{q}z)}{\mathrm{q}^3}\, \frac{(2E_q\omega_N + \omega_N^2)}{E_q\left[(E_q+\omega_N)^2 - m^2\right]}\ . \tag{2.31}$$

There are some similarities between Eq. (2.25) and Eq. (2.31), but the solution for the latter one is much more difficult to find. Details of the calculation are shown in Appendix B, from which we merely quote the result of Eq. (B.24).

$$\begin{aligned} I_N(z) &= \frac{\mathcal{F}(\omega_N/m)}{6m} z^2 + \frac{\pi}{24} z^3 \\ &+ \left[\frac{m^2}{240\omega_N}\mathcal{D}^{(3)}(\mu,\nu',\beta) + \frac{\omega_N}{40}\left(\gamma + \ln(mz/2) - \frac{137}{60}\right)\right] z^4 \\ &+ \mathcal{O}(z^5)\ , \end{aligned} \tag{2.32}$$

where we defined two new structure functions

$$\mathcal{F}(\omega_N/m) = \frac{m}{2\omega_N} \begin{cases} \mu \sinh^{-1}(\mu) - \mu' \sinh^{-1}(\mu') & \omega_N > 2m \\ \mu \sinh^{-1}(\mu) + \nu' \sin^{-1}(\nu') & m \leq \omega_N \leq 2m \\ \mu \sinh^{-1}(\mu) + \nu' \left[\pi - \sin^{-1}(\nu')\right] & \omega_N < m \end{cases}\ , \tag{2.33}$$

and

$$\mathcal{D}^{(3)}(\mu,\nu',\beta) = \begin{cases} \mu^3 \sinh^{-1}(\mu) - \mu'^3 \sinh^{-1}(\mu') & \omega_N > 2m \\ \mu^3 \sinh^{-1}(\mu) - \nu'^3 \sin^{-1}(\nu') & m \leq \omega_N \leq 2m \\ \mu^3 \sinh^{-1}(\mu) - \nu'^3 \left[\pi - \sin^{-1}(\nu')\right] & \omega_N < m \end{cases}\ , \tag{2.34}$$

while the parameters are defined as

$$\mu^2 = \frac{\omega_N}{m}\left(\frac{\omega_N}{m}+2\right), \tag{2.35}$$

$$\mu'^2 = \frac{\omega_N}{m}\left(\frac{\omega_N}{m}-2\right), \tag{2.36}$$

$$\nu'^2 = -\mu'^2, \tag{2.37}$$

$$\beta = mz. \tag{2.38}$$

The result of Eq. (2.32) is obtained by using an expansion that is similar to the one used in the derivation of the non-relativistic structure functions of Eq. (2.26), which is truncated up to $\mathcal{O}(z^5)$. The first term in Eq. (2.32) generates energy corrections proportional to the nuclear electric dipole moment, by performing a low-energy expansion of the function

$$\mathcal{F}(\omega_N/m) \sim -\frac{\pi}{2}\sqrt{\frac{2m}{\omega_N}}\left(1-\frac{\omega_N}{4m}\right)+\frac{\omega_N}{3m}, \tag{2.39}$$

we see that the leading order generates the $\mathcal{O}(z^2)$ term that was found in the derivation of the non-relativistic structure function of Eq. (2.26), this leading-order term is of non-relativistic origin[3] and the rest can be regarded as a relativistic correction. The second term in Eq. (2.32) matches exactly the $\mathcal{O}(z^3)$ term found already in Eq. (2.26), and is thus of non-relativistic origin. By performing the non-relativistic expansion of

$$\mathcal{D}^{(3)}(\mu,\nu',\beta) \sim -4\pi\frac{\omega_N}{m}\sqrt{\frac{\omega_N}{2m}}+8\frac{\omega_N^2}{m^2}, \tag{2.40}$$

we recover from the leading order of the previous equation the previously found non-relativistic term of $\mathcal{O}(z^4)$ in Eq. (2.26), the rest can then be interpreted as a relativistic correction. In previous literature [32, 39, 40] it was argued that only the corrections related to the electric dipole response functions might give significant contributions at very high values of the energy transfer ω_N. We then retain the full expression of Eq. (2.33) but we write the longitudinal structure function by

[3]Non-relativistic origin is intended here, and below, as the leading order term in the low-momentum, $\mathbf{q}^2 \ll m^2$, expansion of Eq. (2.22).

performing the low-energy expansion of Eq. (2.40). We obtain

$$\begin{aligned} I_N(z) &= -\frac{\pi}{12m}\sqrt{\frac{2m}{\omega_N}}z^2 + \left[\frac{\mathcal{F}(\omega_N/m)}{6m} + \frac{\pi}{12m}\sqrt{\frac{2m}{\omega_N}}\right]z^2 \\ &+ \frac{\pi}{24}z^3 \\ &- \frac{m\pi}{60}\sqrt{\frac{\omega_N}{2m}}z^4 + \left[\frac{\omega_N}{40}\left(\gamma + \ln(mz/2) - \frac{57}{60}\right)\right]z^4 \\ &+ \mathcal{O}(z^5)\,, \end{aligned} \tag{2.41}$$

where we separated the relativistic terms (in square brackets) from the non-relativistic ones that were already found in Eq. (2.27).

Transverse-current term. The transverse-current corrections to the atomic energies read

$$\begin{aligned} \Delta E_{nL}^{(T)} &= -8\alpha^2 m\,\phi_{nL}^2 \sum_{N\neq 0}\int d^3x\, d^3y\ \langle 0|\, J_i^\dagger(\mathbf{y})\,|N\rangle\,\langle N|\, J_j(\mathbf{x})\,|0\rangle \\ &\times \int\frac{d^3\mathrm{q}}{4\pi}\left[\frac{\mathrm{q}^2}{4m^2}\,\frac{(2E_q+\omega_N)}{\mathrm{q}^4 E_q\left[(E_q+\omega_N)^2-m^2\right]} - \frac{1}{4m^2\mathrm{q}^3}\,\frac{\omega_N+2\mathrm{q}}{(\omega_N+\mathrm{q})^2}\right]\left(\delta_{ij}+\frac{\nabla_i^z\nabla_j^z}{q^2}\right)e^{i\mathbf{q}\cdot\mathbf{z}} \\ &\equiv -8\alpha^2 m\,\phi_{nL}^2 \sum_{N\neq 0}\int d^3x\, d^3y\,\langle 0|\, J_i^\dagger(\mathbf{y})\,|N\rangle\,\langle N|\, J_j(\mathbf{x})\,|0\rangle\left(\delta_{ij}J_N(z) + z^i z^j \bar{J}_N(z)\right). \end{aligned} \tag{2.42}$$

The two structure functions $J_N(z)$ and $\bar{J}_N(z)$ can be obtained from our solution of the longitudinal structure function $I_N(z)$ in Eq. (2.32), the derivation is done in Appendix B and in the following we only quote the main results

$$\bar{J}_N(z) = \frac{\mathcal{D}^{(3)}(\omega_N/m)}{120\omega_N} + \frac{\omega_N}{20m^2}\left[\ln\left(\frac{m}{2\omega_N}\right) - \frac{1}{3}\right], \tag{2.43}$$

$$J_N(z) = -\frac{1}{6m^3}\mathcal{F}(\omega_N/m) - \frac{1}{6\omega_N m^2}\left[1+\ln(\omega_N/\lambda)\right] - 2\bar{J}_N(z)z^2\,. \tag{2.44}$$

In Eq. (2.44) we wrote $2\lambda = m$ in the divergent logarithm. Although having a divergent structure function might seem surprising, we note that the divergence is removed by a similar divergence appearing in the seagull correction, which makes the total energy shift a finite quantity.

Transverse-seagull term. Similarly to the transverse-current term, we write the correction coming from the seagull diagram in the following form

$$\begin{aligned}\Delta E_{nL}^{(S)} &= -8\alpha^2 m\, \phi_{nL}^2 \int d^3x\, d^3y\, B^{ij}(\mathbf{x},\mathbf{y}) \\ &\times \int \frac{d^3q}{4\pi}\frac{1}{8m^2q^2}\left(\frac{1}{q}-\frac{1}{E_q}\right)\left(\delta_{ij}+\frac{\nabla_i^z\nabla_j^z}{q^2}\right)e^{i\mathbf{q}\cdot\mathbf{z}} \\ &\equiv -8\alpha^2 m\, \phi_{nL}^2 \int d^3x\, d^3y\, B^{ij}(\mathbf{x},\mathbf{y})\,\frac{1}{2}\Big[\delta_{ij}K(z)+z_iz_j\bar{K}(z)\Big]\,. \end{aligned} \tag{2.45}$$

The correction is defined in terms of the two structure functions $K(z)$ and $\bar{K}(z)$. Here we do not derive expression for these functions but quote the result in Refs. [32,42].

$$\bar{K}(z) = -\frac{1}{120}\Big[\gamma+\ln(\beta/2)-\frac{31}{30}\Big]+\mathcal{O}(z^2)\,, \tag{2.46}$$

$$K(z) = -\frac{\ln(2\lambda/m)}{6m^2}-2z^2\Big(\bar{K}(z)+\frac{1}{480}\Big)\,. \tag{2.47}$$

Note the logarithmic divergence in Eq. (2.47), when the total energy correction is evaluated this divergence cancels the one in Eq. (2.44).

2.2.1. Sum rules

In this section we write the corrections in Eq. (2.28) in terms of electromagnetic multipole sum rules. Our strategy is to evaluate the sum rules obtained from the longitudinal correction of Eq. (2.29) in full, while only the leading corrections are derived from the transverse terms of Eq. (2.42) and Eq. (2.45). This is justified by the evidence that the Lamb-shift of muonic atoms is mostly sensitive to the matrix elements of nuclear charge distribution, and not much to the matrix element of the electromagnetic current and seagull operators. As shown in Chapter 5, transverse corrections coming from the electromagnetic current and seagull operator contribute roughly 1% to the total nuclear nuclear structure effects. It is irrelevant at this point to look for small corrections of a 1% effect, given that we anticipate a relative uncertainty due to ab-initio nuclear physics at the few-percent level.

Electric-dipole corrections. Corrections related to the electric-dipole transitions of the nucleus are obtained by combining the z^2 terms of Eq. (2.30) with the z-independent corrections from Eq. (2.42) and Eq. (2.45). We obtain

$$\begin{aligned}
\Delta E_{nL} &= -8\alpha^2 m\, \phi_{nL}^2 \Bigg\{ \sum_{N\neq 0} \left[-\frac{\pi}{12m}\sqrt{\frac{2m}{\omega_N}} + \left(\frac{\mathcal{F}(\omega_N/m)}{6m} + \frac{\pi}{12m}\sqrt{\frac{2m}{\omega_N}} \right) \right] \\
&\times \int d^3x\, d^3y\ \langle 0|\, \rho_{\rm ch}^\dagger(\mathbf{y})\, |N\rangle\, \langle N|\, \rho_{\rm ch}(\mathbf{x})\, |0\rangle\, z^2 \\
&+ \sum_{N\neq 0} \left[-\frac{1}{6m^3}\mathcal{F}(\omega_N/m) - \frac{1}{6\omega_N m^2}\Big[1+\ln(\omega_N/\lambda)\Big] \right] \\
&\times \int d^3x\, d^3y\ \langle 0|\, J_i^\dagger(\mathbf{y})\, |N\rangle\, \langle N|\, J_i(\mathbf{x})\, |0\rangle - \frac{\ln(2\lambda/m)}{12m^2} \int d^3x\, d^3y\, B^{ii}(\mathbf{x},\mathbf{y}) \Bigg\} .
\end{aligned} \tag{2.48}$$

Let us consider the longitudinal part of the energy shift first. The electric dipole operator is defined as the first moment of the nuclear charge distribution, in spherical coordinates it is written as $\mathbf{D} = Z^{-1} \int \mathbf{Y}_1(\hat{x})\ x\ \rho_{\rm ch}(\mathbf{x})\ d^3x$, where $\mathbf{Y}_1(\hat{x})$ are the spherical harmonics functions with angular momentum equal to one and Z is the charge number of the nucleus. We expand $z^2 = \mathbf{x}^2 + \mathbf{y}^2 - 2\mathbf{x}\cdot\mathbf{y}$ and drop the first two terms, since they can not generate nuclear transitions, to obtain

$$\begin{aligned}
\Delta E_{nL}^{\rm L,E1} &= -\frac{16\pi^2}{9}(Z\alpha)^2\, \phi_{nL}^2 \sum_{N\neq 0} \sqrt{\frac{2m}{\omega_N}}\ |\langle N|\, \mathbf{D}\, |0\rangle|^2 \\
&+ \frac{32\pi}{9}(Z\alpha)^2\, \phi_{nL}^2 \sum_{N\neq 0} \left(\mathcal{F}(\omega_N/m) + \frac{\pi}{2}\sqrt{\frac{2m}{\omega_N}} \right) |\langle N|\, \mathbf{D}\, |0\rangle|^2 ,
\end{aligned} \tag{2.49}$$

where we have separated the correction into a non-relativistic part – quoted in the first line of the previous equation – and a purely relativistic correction.

We turn our attention to the transverse correction. We use the Siegert theorem to relate the matrix element of the electromagnetic current to the matrix element of the electric-dipole operator. Similarly, also the seagull correction can be related to matrix elements of the electric dipole operator by using one of the gauge conditions discussed in Refs. [35, 42]

$$\int d^3x\, d^3y\, B^{ii}(\mathbf{x},\mathbf{y}) = \frac{8\pi}{3} Z^2 \sum_{N\neq 0} \omega_N\ |\ \langle N|\, \mathbf{D}\, |0\rangle\ |^2 . \tag{2.50}$$

By making use of the previous relations, the transverse energy correction can be

written as

$$\Delta E_{nL}^{\mathrm{T},E1} = \frac{16\pi}{9}(Z\alpha)^2\,\phi_{nL}^2 \sum_{N\neq 0}\left\{\frac{\omega_N^2}{m^2}\,\mathcal{F}(\omega_N/m) + \frac{\omega_N}{m}\Big[1+\ln(2\omega_N/m)\Big]\right\}\,|\langle N|\,\mathbf{D}\,|0\rangle|^2\,. \tag{2.51}$$

Note that, as anticipated, this energy correction is finite and the divergences of Eq. (2.44) and Eq. (2.47) are removed.

At this point it is convenient to define the electric dipole response function

$$S_{\mathrm{D1}}(\omega) = \sum_{N\neq 0}|\langle N|\,\mathbf{D}\,|0\rangle|^2\,\delta(\omega-\omega_N)\,, \tag{2.52}$$

where ω is a energy variable, and divide the two corrections of Eq. (2.49) and Eq. (2.51) into three terms

$$\delta_{\mathrm{D1}} = -\frac{16\pi^2}{9}(Z\alpha)^2\,\phi_{nL}^2\int S_{\mathrm{D1}}(\omega)\,\sqrt{\frac{2m}{\omega}}\,d\omega\,, \tag{2.53}$$

$$\delta_{\mathrm{L}} = \frac{32\pi}{9}(Z\alpha)^2\,\phi_{nL}^2\int S_{\mathrm{D1}}(\omega)\left[\mathcal{F}(\omega_N/m)+\frac{\pi}{2}\sqrt{\frac{2m}{\omega}}\right]d\omega\,, \tag{2.54}$$

$$\delta_{\mathrm{T}} = \frac{16\pi}{9}(Z\alpha)^2\,\phi_{nL}^2\int S_{\mathrm{D1}}(\omega)\left[\frac{\omega_N^2}{m^2}\,\mathcal{F}(\omega_N/m)+\frac{\omega_N}{m}+\frac{\omega_N}{m}\,\ln(2\omega_N/m)\right]d\omega\,, \tag{2.55}$$

where Eq. (2.53) is the leading non-relativistic electric dipole correction while Eq. (2.54) and Eq. (2.55) are the relativistic corrections coming respectively from the longitudinal and transverse terms.

Zemach-like corrections. The only $\mathcal{O}(z^3)$ term comes from the longitudinal structure function of Eq. (2.41). The energy correction related to this term reads

$$\Delta E_{nL}^{z^3} = -\frac{\pi}{3}(Z\alpha)^2 m\,\phi_{nL}^2\sum_{N\neq 0}\int d^3x\,d^3y\,\langle 0|\,\rho_{\mathrm{ch}}^\dagger(\mathbf{y})\,|N\rangle\,\langle N|\,\rho_{\mathrm{ch}}(\mathbf{x})\,|0\rangle\,|\mathbf{x}-\mathbf{y}|^3\,. \tag{2.56}$$

It is well know [32,39,43] that this correction can be simplified by using closure on the nuclear states, which allows us to divide it in two terms

$$\delta_{\mathrm{R3}} = -\frac{\pi}{3}(Z\alpha)^2 m\,\phi_{nL}^2\int d^3x\,d^3y\,\langle 0|\,\rho_{\mathrm{ch}}^\dagger(\mathbf{y})\rho_{\mathrm{ch}}(\mathbf{x})\,|0\rangle\,|\mathbf{x}-\mathbf{y}|^3\,, \tag{2.57}$$

$$\delta_{\mathrm{Z3}} = \frac{\pi}{3}(Z\alpha)^2 m\,\phi_{nL}^2\int d^3x\,d^3y\,\langle 0|\,\rho_{\mathrm{ch}}^\dagger(\mathbf{y})\,|0\rangle\,\langle 0|\,\rho_{\mathrm{ch}}(\mathbf{x})\,|0\rangle\,|\mathbf{x}-\mathbf{y}|^3\,. \tag{2.58}$$

The advantage of splitting the correction of Eq. (2.56) is not limited to easing the computational costs. In fact, Eq. (2.58) analytically cancels the third Zemach moment of Eq. (2.9) contributing to the nuclear finite-size correction to the Lamb-shift. This means that only Eq. (2.57) effectively contributes to the Lamb-shift.

Electric monopole, quadrupole and retarded dipole corrections. The corrections of $\mathcal{O}(z^4)$ have both non-relativistic and relativistic origin, and come from both longitudinal, Eq. (2.29), and transverse, Eq. (2.42) and Eq. (2.45), electromagnetic transitions of the nucleus. Since these correction are already small we include only the leading longitudinal and non-relativistic term, which can be found in Eq. (2.41) (outside of the bracket). We get

$$\Delta E_{nL}^{z^4} = \frac{2\pi}{15}\alpha^2 m^2\, \phi_{nL}^2 \sum_{N\neq 0} \int d^3x\, d^3y\, \langle 0|\, \rho_{\rm ch}^\dagger(\mathbf{y})\, |N\rangle\, \langle N|\, \rho_{\rm ch}(\mathbf{x})\, |0\rangle \sqrt{\frac{\omega_N}{2m}}\, |\mathbf{x}-\mathbf{y}|^4 \,. \tag{2.59}$$

This expression can be simplified by performing the expansion $|\mathbf{x}-\mathbf{y}|^4 = x^4 + y^4 + \frac{10}{3}x^2y^2 - 4\mathbf{x}\cdot\mathbf{y}(y^2+x^2) + 4Q_{ij}^x Q_{ij}^y$, where $Q_{ij}^x = x_i x_j - \mathbf{x}^2\delta_{ij}/3$ is the irreducible quadrupole tensor written in Cartesian components. The first two terms in the expansion can be dropped because they can not generate nuclear transitions, the other three terms contribute with the following correction to the non-relativistic energies

$$\delta_{\rm R2} = \frac{4\pi}{9}(Z\alpha)^2 m^2\, \phi_{nL}^2 \int d\omega \sqrt{\frac{\omega}{2m}}\, S_{\rm R2}(\omega)\,, \tag{2.60}$$

$$\delta_{\rm Q} = \frac{64\pi^2}{225}(Z\alpha)^2 m^2\, \phi_{nL}^2 \int d\omega \sqrt{\frac{\omega}{2m}}\, S_{\rm Q}(\omega)\,, \tag{2.61}$$

$$\delta_{\rm D1D3} = -\frac{32\pi^2}{45}(Z\alpha)^2 m^2 \phi_{nL}^2 \int d\omega \sqrt{\frac{\omega}{2m}}\, S_{\rm D1D3}(\omega)\,, \tag{2.62}$$

where we introduced the monopole, $S_{\rm R2}(\omega)$, quadrupole $S_{\rm Q}(\omega)$ and retarded-dipole $S_{\rm D1D3}$ response functions. They are defined as

$$S_{\rm R2}(\omega) = \sum_{N\neq 0} |\langle N|\, r^2\, |0\rangle|^2\, \delta(\omega-\omega_N)\,, \tag{2.63}$$

$$S_{\rm Q}(\omega) = \sum_{N\neq 0} |\langle N|\, \mathbf{Q}\, |0\rangle|^2\, \delta(\omega-\omega_N)\,, \tag{2.64}$$

$$S_{\rm D1D3}(\omega) = \sum_{N\neq 0} \Big(\langle 0|\, \mathbf{D}^\dagger\, |N\rangle \cdot \langle N|\, \mathbf{O}\, |0\rangle\ + {\rm cc.}\Big)\, \delta(\omega-\omega_N)\,, \tag{2.65}$$

respectively. With the goal of exploiting standard angular momentum techniques, we write the monopole, quadrupole and retarded-dipole operators as irreducible spherical tensor operators of rank zero, two and one respectively.

Namely we have

$$\begin{aligned} r^2 &= Z^{-1} \int \rho_{\rm ch}(\mathbf{x})\; x^2\; d^3x \;, \\ \mathbf{O} &= Z^{-1} \int \rho_{\rm ch}(\mathbf{x})\; x^3\; \mathbf{Y}_1(\hat{x})\; d^3x \;, \\ \mathbf{Q} &= Z^{-1} \int \rho_{\rm ch}(\mathbf{x})\; x^2\; \mathbf{Y}_2(\hat{x})\; d^3x \;. \end{aligned}$$

Sub-sub-sub-leading non-relativistic term. It is straightforward to derive the term of $\mathcal{O}(z^5)$, at least for the non-relativistic structure functions. We obtain the following correction

$$\delta_{R^5} = -\frac{\pi}{45}\alpha^2 m^2\, \phi_{nL}^2 \sum_{N\neq 0} \int d^3x\, d^3y\, \langle 0|\, \rho_{\rm ch}^\dagger(\mathbf{y})\, |N\rangle\, \langle N|\, \rho_{\rm ch}(\mathbf{x})\, |0\rangle\; \omega_N\, |\mathbf{x}-\mathbf{y}|^5 \;. \quad (2.66)$$

We expect this correction to be more important than the relativistic correction to the $\mathcal{O}(z^4)$, since our analysis of the non-relativistic η-expansion uncertainty suggests that this correction is suppressed by roughly a factor of three compared to the sub-sub-leading term, whereas relativistic effects are suppressed by factors of $m/\omega_{\bar{N}} \sim 20$, where $\omega_{\bar{N}}$ represents the energy of the first nuclear excited state which in light-nuclei corresponds generally to the threshold energy of the first photo-dissociation channel. This term has not been calculated yet, and we are not including it in our results either.

2.2.2. Nucleon finite-size

The corrections to the Lamb-shift derived so far are model independent, in the sense that the nuclear charge $\rho_{\rm ch}(\mathbf{x})$, current $\mathbf{J}(\mathbf{x})$ and two-photon $B^{ij}(\mathbf{x},\mathbf{y})$ operator have been left unspecified, and the corrections do not change in form when a model for these operators is constructed. In nuclear physics it is common to express and calculate quantities in terms of point-nucleon electromagnetic operators. These operators are derived assuming that protons and neutrons are point-like particles, which is done with the scope of separating the nuclear dynamics with the sub-nuclear degrees of freedom. The internal degrees of freedom of the nucleons is generally taken into account by phenomenological models.

In this section, we re-define the previously derived corrections in terms of point-nucleon densities, and we derive the leading effects coming from the finite-size of the individual nucleons. We start by writing the charge operator in its impulse approximation form $\rho_p(\mathbf{x})$ – which assume point-like non-relativistic nucleons– plus a term $\rho_{\rm fs}(\mathbf{x})$ that corrects the charge distribution for the charge densities of

the individual nucleons. In this approximation we obtain

$$\rho_{\rm ch}(\mathbf{x}) = \rho_p(\mathbf{x}) + \rho_{\rm fs}(\mathbf{x}) \,, \tag{2.67}$$

$$\rho_p(\mathbf{x}) = \sum_{i=1}^{A} e\, \delta(\mathbf{x}-\mathbf{x}_i)\, \hat{e}_i^p \,, \tag{2.68}$$

$$\rho_{\rm fs}(\mathbf{x}) = \sum_{i=1}^{A} e \left[\Big(\eta_p(\mathbf{x}-\mathbf{x}_i) - \delta(\mathbf{x}-\mathbf{x}_i) \Big)\, \hat{e}_i^p + \eta_n(\mathbf{x}-\mathbf{x}_i)\, \hat{e}_i^n \right] , \tag{2.69}$$

where $\hat{e}_i^p$ and $\hat{e}_i^n$ are isospin projector operators on the proton and neutron state respectively, $\eta_p(\mathbf{x}-\mathbf{x}_i)$ is the charge distribution of the proton while $\eta_n(\mathbf{x}-\mathbf{x}_i)$ is the charge distribution of the neutron and with $\rho_p(\mathbf{x})$ we defined the point-proton charge density. In Fourier space this distribution reads

$$\begin{aligned} \rho_{\rm ch}(\mathbf{q}) &= \rho_p(\mathbf{q}) + \left[\Big(\eta_p(\mathbf{q}) - 1 \Big) \rho_p(\mathbf{q}) + \eta_n(\mathbf{q}) \rho_n(\mathbf{q}) \right] \\ &= \rho_p(\mathbf{q}) + \rho_{\rm fs}(\mathbf{q}). \end{aligned} \tag{2.70}$$

The proton and neutron form factors are parametrized using a phenomenological-dipole model. With the scope of simplifying the derivation, we proceed by approximating this model by its leading low-$\mathbf{q}$ expansion

$$\eta_p(\mathbf{q}) = \frac{1}{(1+\mathbf{q}^2/\beta^2)^2} \sim 1 - 2\,\frac{\mathbf{q}^2}{\beta^2} \,, \tag{2.71}$$

$$\eta_n(\mathbf{q}) = \frac{\lambda q^2}{(1+\mathbf{q}^2/\beta^2)^3} \sim \lambda\, \mathbf{q}^2 \,, \tag{2.72}$$

where λ and β are related to the charge radii of the neutron and proton respectively. This expansion creates a further source of uncertainty which might be improved at a later stage by extending the expansion to more orders or making use of other parametrizations of the form factors, similarly to what was done in Ref. [38]. In this work we use the value of the proton radius obtained from muonic atoms [25] and the value of the neutron radius taken from [44]. Using Eq. (2.71) and Eq. (2.72), the relevant matrix element of the charge operator can be written as

$$\begin{aligned} |\langle N|\, \rho_{\rm ch}(\mathbf{q})\, |0\rangle|^2 &= \int d^3x d^3y\, \langle 0|\, \rho_p^\dagger(\mathbf{y})\, |N\rangle\, \langle N|\, \rho_p(\mathbf{x})\, |0\rangle \left[1 + \frac{2}{\beta^2}\nabla_x^2 + \frac{2}{\beta^2}\nabla_y^2 \right] e^{i\mathbf{q}\cdot\mathbf{z}} \\ &+ \int d^3x d^3y\, \langle 0|\, \rho_p^\dagger(\mathbf{y})\, |N\rangle\, \langle N|\, \rho_n(\mathbf{x})\, |0\rangle\ \lambda \nabla_x^2\, e^{i\mathbf{q}\cdot\mathbf{z}} \\ &+ \int d^3x d^3y\, \langle 0|\, \rho_n^\dagger(\mathbf{y})\, |N\rangle\, \langle N|\, \rho_p(\mathbf{x})\, |0\rangle\ \lambda \nabla_x^2\, e^{i\mathbf{q}\cdot\mathbf{z}} + \mathcal{O}(q^4) \,. \end{aligned} \tag{2.73}$$

The first term in the square bracket of the previous equation generates the point-nucleon sum rules. The other terms proportional to q^2 are the leading nucleon finite-size corrections. With the insertion of Eq. (2.73) into Eq. (2.23) we obtain the leading correction to the non-relativistic polarizabilities due to the finite-size of the nucleons. After some lengthy manipulation we extract the three following corrections

$$\delta_{\rm R1} = -8\pi\alpha^2 m\ \phi_{nL}^2 \int d^3x d^3y \Big[\frac{2}{\beta^2}\ \rho_{pp}(\mathbf{x},\mathbf{y}) - \lambda\ \rho_{np}(\mathbf{x},\mathbf{y})\Big] |\mathbf{x}-\mathbf{y}|\ , \quad (2.74)$$

$$\delta_{\rm Z1} = 8\pi\alpha^2 m\ \phi_{nL}^2 \int d^3x d^3y \rho_p(\mathbf{x})\ \Big[\frac{2}{\beta^2}\ \rho_p(\mathbf{y}) - \lambda\ \rho_n(\mathbf{y})\Big] |\mathbf{x}-\mathbf{y}|\ , \quad (2.75)$$

$$\delta_{\rm NS} = -\frac{128}{9}\pi^2 (Z\alpha)^2 m^2\ \phi_{nL}^2 \Big[\frac{2}{\beta^2} + \lambda\Big] \int d\omega\ \sqrt{\frac{\omega}{2m}}\ S_{\rm D1}(\omega)\ , \quad (2.76)$$

where $\rho_{pp}(\mathbf{x},\mathbf{y})$ and $\rho_{np}(\mathbf{x},\mathbf{y})$ are two-body proton-proton and proton-neutron densities, defined as

$$\rho_{pp}(\mathbf{x},\mathbf{y}) = \frac{1}{Z^2}\sum_{i,j}^{A} \langle 0|\ \delta(\mathbf{x}-\mathbf{x_i})\ \delta(\mathbf{y}-\mathbf{y_j}) \hat{e}_i^p \hat{e}_j^p\ |0\rangle\ , \quad (2.77)$$

$$\rho_{np}(\mathbf{x},\mathbf{y}) = \sum_{i,j}^{A} \langle 0|\ \delta(\mathbf{x}-\mathbf{x_i})\ \delta(\mathbf{y}-\mathbf{y_j}) \hat{e}_i^p \hat{e}_j^n\ |0\rangle\ . \quad (2.78)$$

2.3. Higher-order nuclear polarizabilities

So far, the derived nuclear polarizabilities are of order $(Z\alpha)^5$. Most of the higher-order corrections are usually neglected, since they are suppressed by more powers of α or $(Z\alpha)$. There are however some exceptions, which were calculated within the scope of solving previous discrepancies between experiment and theory, or because the corrections were expected to be unnaturally large. One example is the three-photon-exchange correction, which is of order $(Z\alpha)^6$ and is included in the theory of muonic deuterium [45]. Other examples are Coulomb distortion effects, of order $(Z\alpha)^6$, and nuclear polarizabilities with electron vacuum polarization effects, which are of order $(Z\alpha)^5\alpha$. The Coulomb distortion was calculated in the past by many authors [40,41,43,46] and it is also included in our calculations. The electron-vacuum polarization was included in the theory of muonic deuterium in Ref. [47] and we included this effect in the theory of muonic helium for the first time in Ref. [5]. This section is devoted to the description of these two higher-order corrections.

2.3.1. Coulomb distortion

Coulomb distortion effects originate as corrections of the lepton propagator in Fig. 2.3 due to intermediate Coulomb interactions with the nucleus. The leading effect is of order $\mathcal{O}(Z\alpha)^6$ and is calculated in the leading electric dipole approximation. The derivation of this correction was performed by many authors, one example can be found in Ref. [39], from which we only quote the final result

$$\delta_{\rm C} = -\frac{16\pi^2}{9}(Z\alpha)^3\,\phi_{nL}^2 \int d\omega\,\frac{m}{\omega}\,\ln\left(\frac{2(Z\alpha)^2 m}{\omega}\right) S_{D1}(\omega)\,. \tag{2.79}$$

Although this correction is formally of order $(Z\alpha)^6$, it is logarithmically enhanced and previous numerical calculations have shown [39–41, 43] that this term is large and can not be neglected.

2.3.2. Electron vacuum polarization

The electron-vacuum polarization (eVP) is a radiative correction to the leading nuclear polarizability that originates from the intermediate creation of electron-positron pairs in the interaction between the muon and the nucleus. This effect modifies the Coulomb interaction by charged particles as

$$V_{vp} = -\frac{\alpha}{r}\left(1 + \frac{2\alpha}{3\pi}\int_1^\infty d\xi\,\rho(\xi)\,e^{-2rm_e\xi}\right)\,, \tag{2.80}$$

As shown in [47], in the electric dipole approximation and neglecting Coulomb distortion effects, the correction is expressed in terms of the following sum rule

$$\begin{aligned}\delta_{\rm eVP1} &= \frac{32\pi}{27}(Z\alpha)^2\alpha\,\phi_{nL}^2 \\ &\times \int d\omega\,|\,\langle 0|\,\mathbf{D}\,|N\rangle\,|^2\sqrt{\frac{2m}{\omega}}\left(\ln\frac{E}{2m} + 2\ln\frac{2m}{m_e} - \frac{5}{3} + \frac{3\pi m_e}{4m}\sqrt{\frac{2m}{\omega}}\right) \\ &+ \frac{\alpha}{\pi}\,C_{2S}\,\delta_{D1}\,,\end{aligned} \tag{2.81}$$

where the second term in Eq. (2.81) comes from the modification of the wave function of the muon at the origin of coordinate system. In fact, following [48] this modification is expressed for the 2S-state in terms of the original wave function as

$$\tilde{\phi}^2(0) = \left(1 + \frac{\alpha}{\pi}\,C_{2S}\right)\phi^2(0)\,, \tag{2.82}$$

where some notable values for the coefficients are $C_{2S}(\mathrm{D}) = 1.4523$, $C_{2S}(\mathrm{3He}) = 2.1818$ and $C_{2S}(\mathrm{4He}) = 2.1920$. The correction in Eq. (2.81) is the eVP-correction to the leading electric-dipole polarizabilities, another correction of similar order

is included in Ref. [5]. It comes from an eVP correction to the sub-leading non-relativistic structure function of $\mathcal{O}(z^3)$. The correction is

$$\delta_{eVP2} = \delta_{\rm R3}\left[\frac{\alpha}{\pi}\, C_{2S} - \frac{\alpha}{\pi}\frac{4}{3}\Big(\frac{5}{12} + \ln(m_e r_L) + \gamma\Big)\right] , \tag{2.83}$$

where r_L is defined as

$$\sum_{i,j} \langle 0|\, |\mathbf{r}_i - \mathbf{r}_j|^3 \ln(|\mathbf{r}_i - \mathbf{r}_j|)\, |0\rangle = \sum_{i,j} \langle 0|\, |\mathbf{r}_i - \mathbf{r}_j|^3\, |0\rangle \ln(r_L) , \tag{2.84}$$

where $\mathbf{r}_i$ and $\mathbf{r}_j$ are the coordinates of nucleon i and nucleon j, respectively. In Ref. [5] it was assumed $r_L \sim 2r_c$, where r_c is the charge radius of the nucleus, and we follow the same assumption in this work.

2.4. Summary

We write the nuclear structure corrections, $\delta_{\rm NS}$, to the energies of muonic atoms as

$$\delta_{\rm NS} = \delta_{\rm TPE} + \delta^N_{\rm TPE} + \delta_{\rm 3PE} + \delta_{\rm eVP} + \delta_{\mu\rm SEVP} ,$$

where $\delta^N_{\rm TPE}$, is the two-photon exchange correction on individual nucleons, $\delta_{\rm 3PE}$ is the three-photon nuclear structure correction, $\delta_{\rm eVP}$ is the nuclear polarizability with electron vacuum polarization and $\delta_{\mu\rm SEVP}$ is the nuclear polarizability with muon self-energy and muon vacuum polarization [5]. At our level of precision, corrections to the Lamb-shift differ from corrections to the $2S_{1/2}$ energy by a factor of (-1). This means that $\rm E_{NS}$ of Eq. (1.1) is obtained as $\rm E_{NS} = -\delta_{NS}(2S_{1/2})$, where the notation highlights that the nuclear structure corrections are calculated for the $2S$-state.

This work concerns with the calculation of the two-photon nuclear structure correction, $\delta_{\rm TPE}$. This term is obtained as

$$\delta_{\rm TPE} \;=\; \delta_{\rm Zem} + \delta_{\rm pol} ,$$

where $\delta_{\rm Zem}$ is the elastic part of the two-photon exchange and $\delta_{\rm pol}$ is the nuclear polarizability. These effects are defined as

$$\begin{aligned} \delta_{\rm Zem} &= -\delta_{\rm Z3} - \delta_{\rm Z1} , \\ \delta_{\rm pol} &= \Big[\delta_{\rm D1} + \big(\delta_{\rm Z3} + \delta_{\rm R3}\big) + \big(\delta_{\rm R2} + \delta_{\rm Q} + \delta_{\rm D1D3}\big)\Big] \\ &+ \delta_{\rm C} + \Big[\big(\delta_{\rm L} + \delta_{\rm T}\big)\Big] + \Big[\big(\delta_{\rm Z1} + \delta_{\rm R1} + \delta_{\rm NS}\big)\Big] . \end{aligned}$$

The terms are:

$$\delta_{\rm D1} = -\frac{16\pi^2}{9}(Z\alpha)^2\,\phi_{nL}^2\int S_{\rm D1}(\omega)\,\sqrt{\frac{2m}{\omega}}\,d\omega\,, \tag{2.85}$$

$$\delta_{\rm L} = \frac{32\pi}{9}(Z\alpha)^2\,\phi_{nL}^2\int S_{\rm D1}(\omega)\,\left[\mathcal{F}(\omega_N/m)+\frac{\pi}{2}\sqrt{\frac{2m}{\omega}}\right]d\omega\,, \tag{2.86}$$

$$\delta_{\rm T} = \frac{16\pi}{9}(Z\alpha)^2\,\phi_{nL}^2\int S_{\rm D1}(\omega)\,\left[\frac{\omega_N^2}{m^2}\mathcal{F}(\omega/m)+\frac{\omega}{m}+\frac{\omega}{m}\ln(2\omega/m)\right]d\omega\,, \tag{2.87}$$

$$\delta_{\rm R3} = -\frac{\pi}{3}(Z\alpha)^2 m\,\phi_{nL}^2\int d^3x\,d^3y\,\langle 0|\,\rho_{\rm ch}^\dagger(\mathbf{y})\rho_{\rm ch}(\mathbf{x})\,|0\rangle\,|\mathbf{x}-\mathbf{y}|^3\,, \tag{2.88}$$

$$\delta_{\rm Z3} = \frac{\pi}{3}(Z\alpha)^2 m\,\phi_{nL}^2\int d^3x\,d^3y\,\langle 0|\,\rho_{\rm ch}^\dagger(\mathbf{y})\,|0\rangle\,\langle 0|\,\rho_{\rm ch}(\mathbf{x})\,|0\rangle\,|\mathbf{x}-\mathbf{y}|^3\,, \tag{2.89}$$

$$\delta_{\rm R2} = \frac{4\pi}{9}(Z\alpha)^2 m^2\,\phi_{nL}^2\int d\omega\,\sqrt{\frac{\omega}{2m}}\,S_{\rm R2}(\omega)\,, \tag{2.90}$$

$$\delta_{\rm Q} = \frac{64\pi^2}{225}(Z\alpha)^2 m^2\,\phi_{nL}^2\int d\omega\,\sqrt{\frac{\omega}{2m}}\,S_{\rm Q}(\omega)\,, \tag{2.91}$$

$$\delta_{\rm D1D3} = -\frac{32\pi^2}{45}(Z\alpha)^2 m^2\phi_{nL}^2\int d\omega\,\sqrt{\frac{\omega}{2m}}\,S_{\rm D1D3}(\omega)\,, \tag{2.92}$$

$$\delta_{\rm R1} = -8\pi\alpha^2 m\,\phi_{nL}^2\int d^3x d^3y\,\left[\frac{2}{\beta^2}\,\rho_{pp}(\mathbf{x},\mathbf{y})-\lambda\,\rho_{np}(\mathbf{x},\mathbf{y})\right]|\mathbf{x}-\mathbf{y}|\,, \tag{2.93}$$

$$\delta_{\rm Z1} = 8\pi\alpha^2 m\,\phi_{nL}^2\int d^3x d^3y\,\rho_p(\mathbf{x})\,\left[\frac{2}{\beta^2}\,\rho_p(\mathbf{y})-\lambda\,\rho_n(\mathbf{y})\right]|\mathbf{x}-\mathbf{y}|\,, \tag{2.94}$$

$$\delta_{\rm NS} = -\frac{128}{9}\pi^2(Z\alpha)^2 m^2\,\phi_{nL}^2\left[\frac{2}{\beta^2}+\lambda\right]\int d\omega\,\sqrt{\frac{\omega}{2m}}\,S_{\rm D1}(\omega)\,, \tag{2.95}$$

$$\delta_{\rm C} = -\frac{16\pi^2}{9}(Z\alpha)^3\,\phi_{nL}^2\int d\omega\,\frac{m}{\omega}\,\ln\left(\frac{2(Z\alpha)^2 m}{\omega}\right)S_{D1}(\omega)\,, \tag{2.96}$$

$$\begin{aligned}\delta_{\rm eVP1} &= \frac{32\pi}{27}(Z\alpha)^2\alpha\,\phi_{nL}^2\\ &\times\int d\omega\,|\,\langle 0|\,\mathbf{D}\,|N\rangle\,|^2\sqrt{\frac{2m}{\omega}}\left(\ln\frac{E}{2m}+2\ln\frac{2m}{m_e}-\frac{5}{3}+\frac{3\pi m_e}{4m}\sqrt{\frac{2m}{\omega}}\right)\\ &+\frac{\alpha}{\pi}\,C_{2S}\,\delta_{D1}\,,\end{aligned} \tag{2.97}$$

$$\delta_{eVP2} = \delta_{\rm R3}\left[\frac{\alpha}{\pi}\,C_{2S}-\frac{\alpha}{\pi}\frac{4}{3}\Big(\frac{5}{12}+\ln(m_e r_L)+\gamma\Big)\right]. \tag{2.98}$$

Values for C_{2S} are given after Eq. (2.82) and the response functions are defined as

$$S_{\mathrm{D1}}(\omega) = \sum_{N\neq 0} |\langle N|\,\mathbf{D}\,|0\rangle|^2\,\delta(\omega-\omega_N)\,, \tag{2.99}$$

$$S_{\mathrm{R2}}(\omega) = \sum_{N\neq 0} |\langle N|\,r^2\,|0\rangle|^2\,\delta(\omega-\omega_N)\,, \tag{2.100}$$

$$S_{\mathrm{Q}}(\omega) = \sum_{N\neq 0} |\langle N|\,\mathbf{Q}\,|0\rangle|^2\,\delta(\omega-\omega_N)\,, \tag{2.101}$$

$$S_{\mathrm{D1D3}}(\omega) = \sum_{N\neq 0} \Big(\langle 0|\,\mathbf{D}^\dagger\,|N\rangle\cdot\langle N|\,\mathbf{O}\,|0\rangle\ + \mathrm{cc.}\Big)\,\delta(\omega-\omega_N)\,, \tag{2.102}$$

and the operators are the electromagnetic moments of the nuclear charge distribution. They are written as irreducible spherical tensors as

$$\mathbf{D} = Z^{-1}\int \rho_{\mathrm{ch}}(\mathbf{x})\; x\; \mathbf{Y}_1(\hat{x})\; d^3x\,, \tag{2.103}$$

$$r^2 = Z^{-1}\int \rho_{\mathrm{ch}}(\mathbf{x})\; x^2\; d^3x\,, \tag{2.104}$$

$$\mathbf{O} = Z^{-1}\int \rho_{\mathrm{ch}}(\mathbf{x})\; x^3\; \mathbf{Y}_1(\hat{x})\; d^3x\,, \tag{2.105}$$

$$\mathbf{Q} = Z^{-1}\int \rho_{\mathrm{ch}}(\mathbf{x})\; x^2\; \mathbf{Y}_2(\hat{x})\; d^3x\,. \tag{2.106}$$

Important remarks. We have constructed two approaches for calculating the nuclear structure corrections to the Lamb-shift of muonic ions. The first one, summarized in Eq. (2.22) is formulated in terms of the matrix elements of the nuclear charge density, electromagnetic current and two-photon operators. Apart for the expansion in $(Z\alpha)$, this method does not use any further approximation, it is model independent and allows for a calculation of the complete nuclear structure corrections. However, the difficulties in evaluating the nuclear matrix elements for a comprehensive range of energy and momentum transfers has so far limited its applications to the lightest muonic ions [37, 38]. The need to extend the calculation to heavier systems has led to the development of the η-expansion method [32, 39, 43, 46, 49], which is summarized by the list of corrections written in this section. This method, at the cost of introducing a further source of uncertainty from the truncation of the expansion of the nuclear structure functions $I_{\mathrm{NR}}(z)$, $I_{\mathrm{N}}(z)$, $J(z)$, $\bar{J}(z)$, $K(z)$ and $\bar{K}(z)$, expresses the nuclear structure corrections in terms of matrix elements that can be more easily calculated, since they involve only multipole expansions of the nuclear charge distribution. Here, we make use of the η-expansion method, given that our goal is to extend the calculation of the nuclear structure corrections to muonic helium and lithium ions. In the next chapter we describe our strategy for calculating the nuclear matrix elements.

3. Nuclear theory

In this thesis, we describe the atomic nuclei as systems of non-relativistic and point-like nucleons bound by the nuclear force. The nuclear force is an effective picture of the more fundamental interaction among quarks mediated by the gluons, the gauge bosons of Quantum Chromodynamics (QCD). It is well known that to describe results of low-energy experiments one does not need to know the details of high energy physics. The classical example is the applicability of the multipole expansion of the electric field generated by a localized charge distribution. At large distances the exact details of the distribution are not needed and a simplified description of the physics can be obtained by the only use of its multipole moments. The partial decoupling between high- and low-energy physics allows us to construct a robust picture of the atomic nuclei without the explicit introduction of the sub-nuclear degrees of freedom.

In this work, the relevant degrees of freedom are identified with the nucleons and the pions, and our picture of the nuclear dynamics will then be given by the so called chiral effective field theory (ChEFT). Being an effective theory, the chiral Lagrangian contains an infinite number of operators, which need to be classified according to a power counting scheme. From the series of Lagrangians at different chiral orders, a series of nuclear Hamiltonians can be derived, which are then iterated in the Schrödinger equation to obtain the nuclear wavefunctions and to calculate the relevant electromagnetic matrix elements. The electromagnetic operators must be derived consistently with the nuclear Hamiltonians, since they are related by a gauge transformation. It is clear that the process of calculating any observable in low-energy nuclear physics can be separated in two complex, but partially independent, steps. One deals with the systematic construction of the Hamiltonians of interacting nucleons and electromagnetic (or electroweak) operators via which nucleons couple to external fields [50, 51], the other deals with the solution of the nuclear few-body problem and with the calculation of the observables, assuming that Hamiltonians and operators were previously derived.

This chapter is organized as follows. First we discuss the solution of the nuclear few-body problem and the calculation of the nuclear wavefunctions. Our method of choice is based on the effective interaction hyperspherical harmonics (EIHH) method, which we explain in detail. In the second part of the chapter we describe the construction of the nuclear Hamiltonians.

3.1. Few-body methods

The quantum few-body problem appeared in the scientific practice right at the birth of modern physics. After the finding that quantum mechanics was able to predict the spectrum of the hydrogen atom, the next validation test for the theory was the description of the second-simplest atomic system, the helium atom. The problem captured the attention of many leading scientists, including Max Born, who soon gave it to one of his young collaborator, Egil Hylleraas, which solved it by an early application of the variational principle [52]. After this early success, research in few-body physics extended its range of applicability both towards heavier atomic systems and to the study of physics at disparate energy scales.

Few-body methods are nowadays applied to studies in molecular [53,54], atomic [55], nuclear and hadronic [4,56] and even condensed-matter physics [57]. This work focuses on the application of these methods to the description of the lightest atomic nuclei. There are several reasons that make nuclear physics a challenge for few-body methods. The strong repulsion of the nuclear force at short distances creates short-distance correlations that are difficult to capture with ordinary basis expansions. The presence of the long-distance Coulomb force creates distortion effects, which make it difficult to accurately describe scattering processes, or absorption and dissociation reactions. Depending on the computational method, even the anti-symmetrization of the nuclear wavefunction might be a challenging task. On top of this the nuclear interaction is not exactly known, which requires us to solve the few-body problem while learning about the structure of the Hamiltonian at the same time.

Several methods have been successfully applied to the study of nuclear systems, most notably we quote the hyperspherical harmonics [2,58,59], the no-core-shell-model [60], the direct solution of the Faddeev [61] and Faddeev-Yakubovsky [62] equations, various formulations of the stochastic variational method [57] and Quantum Monte-Carlo methods, like the Green's function Monte Carlo (GFMC) [63] etc. Each of these methods has both advantages and disadvantages when compared to the others. The work presented in this thesis made use of the hyperspherical harmonics method, which is described in the following section.

3.1.1. The hyperspherical harmonics

This section is devoted to the description of hyperspherical harmonics method. The algorithm was in large part developed by other authors and successfully applied for studying the structure of light nuclei, see for instance Ref. [64]. In describing the method of hyperspherical harmonics, we follow closely Refs. [65,66].

The algorithm solves the time-independent many-body Schrödinger equation

for the A-nucleon system

$$H_N \left|\Psi\right\rangle = E_N \left|\Psi\right\rangle \ , \tag{3.1}$$

with the nuclear Hamiltonian, H_N, being the sum of the non-relativistic kinetic energy operator and of the forces among nucleons, V and W, as

$$\begin{aligned} H_N &= T + V + W \\ &= \sum_i^A T_i + \sum_{i<j}^A V_{ij} + \sum_{i<j<k}^A W_{ijk} \ . \end{aligned} \tag{3.2}$$

Here, T_i is the kinetik energy operator associated with the i^{th} nucleon, while V_{ij} and W_{ijk} are two-body (NN) and three-body (3N) nuclear forces, respectively. In principle, the sum in Eq. (3.2) should include also four-body and, in general, many-body nuclear forces. In fact, as it is discussed in Section 3.2, these forces arise naturally in chiral effective field theory. However these terms are expected to give contributions that are much smaller than the precision of our calculation, and they have not been considered in this work.

The method is based upon an expansion of the internal wavefunction of the A-nucleons system in terms of the eigenstates of the hyper-angular part of the Laplace operator in $3A-3$ dimensions, namely the hyperspherical harmonics functions. It was firstly introduced in 1935 by Zernike and Brinkman [67], reintroduced later in the 60's by Delves [68], Simonov [69], Zickendraht [70] and Smith [71] and it is widely applied nowadays to the study of few-body systems. Recent reviews with applications to nuclear physics can be found in Refs. [59,72].

In this work, the hyperspherical harmonic functions are constructed to form irreducible representations of the $SO(3)$ group of space rotations, the S_A permutation group of the A-particle system and the dynamical $O(N)$ group of rotations in the space of the $N = A-1$ Jacobi vectors. There are many reasons to motivate the construction of basis functions that fill irreducible representations of these symmetries.

The nuclear Hamiltonian is symmetric under rotations of the coordinate system, nuclear states then populate the corresponding irreducible representations of the $SO(3)$ group identified by their total angular momentum. If one neglects the electromagnetic interaction and the isospin symmetry breaking part of the nuclear force, nuclei can be considered as bound states of identical particles which populate the totally antisymmetric irreducible representation of the permutation group S_A. Finally, two reasons motivate the construction of a basis populating irreducible representations of the dynamical $O(N)$ group. The first comes from noting that $S_A \subset O(N)$, namely that the permutation group of A particles is a sub-group of the dynamical $O(N)$ group. The irreducible representations of S_A can then be con-

structed from the reduction $O(N) \downarrow S_A$. Secondly, in the hyperspherical harmonics method the nuclear wavefunctions are written in terms of Jacobi coordinates, but the nuclear interaction is generally expressed in terms of the relative coordinates of the nucleons. The calculation of the matrix elements of the nuclear interaction then follows the transformation of Jacobi vectors into relative coordinates, this is generally accomplished by several $O(N)$ rotations, and the rotations are more easily implemented in the wavefunction if the basis functions have well defined transformation properties under $O(N)$.

Jacobi coordinates. In physical applications, the Hamiltonian operator generally factorizes out the time evolution of the center of mass (c.o.m.) from the internal dynamic of the system. This is a welcomed feature, since several times one is not interested in studying the time-evolution of the c.o.m. and the study of its internal structure can be formalized as a problem in lower dimensions. This separation can best be achieved by writing the internal wavefunction of the system in terms of Jacobi coordinates.

The most general method of defining the set of Jacobi coordinates is done through a recursive splitting of the A particles into sub-groups. The method can best be described with an example. Starting by writing the A particles in any order, a possible splitting might be

$$
\begin{aligned}
&(1234\ ...\ 789\ ...\ A-1\ A)\\
&(1234\ ...\ 789\ ...\ A-1)(A)\\
&(1234\ ...\ 789\ ...\ )(A-1)(A)\\
&(1234)(\ ...\ 789\ ...\ )(A-1)(A)\\
&...\\
&...\\
&(12)(3)(4)\ ...\ (7)(8)(9)\ ...\ (A-1)(A)\\
&(1)(2)(3)(4)\ ...\ (7)(8)(9)\ ...\ (A-1)(A)\ .
\end{aligned}
$$

We clearly need $N = A - 1$ steps to completely divide the particles into the A sub-groups. The construction follows by associating a Jacobi vector connecting the c.o.m. of the two fragments created at each steps.

The division of the A particles into sub-groups can be done in several ways.

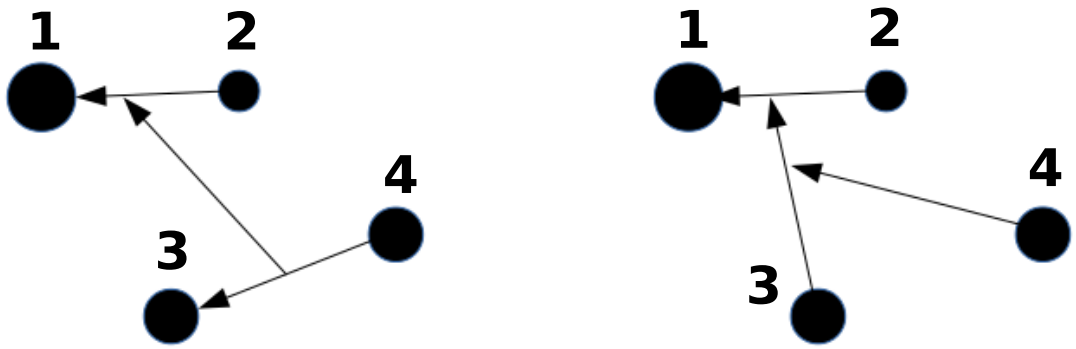

Figure 3.1.: Two possible definition of Jacobi vectors for describing the internal motion of a four-body system with different masses. The recursive 'K' splitting on the right is compared with another possible definition of Jacobi vectors on the left.

However, In the general case, it is best to work with the recursive 'K' splitting

$$
\begin{aligned}
&(1234\ ...\ 789\ ...\ A-1\ A)\\
&(1234\ ...\ 789\ ...\ A-1)(A)\\
&(1234\ ...789\ ...)(A-1)(A)\\
&...\\
&...\\
&(1234)\ ...\ (7)(8)(9)\ ...\ (A-1)(A)\\
&(123)(4)\ ...\ (7)(8)(9)\ ...\ (A-1)(A)\\
&(12)(3)(4)\ ...\ (7)(8)(9)\ ...\ (A-1)(A)\\
&(1)(2)(3)(4)\ ...\ (7)(8)(9)\ ...\ (A-1)(A)\ .
\end{aligned}
$$

This splitting defines a set of $N = A - 1$ Jacobi coordinates, $\{\boldsymbol{\eta}_i\}$ with $i = 1, ..., N$, which together with the coordinate of the c.o.m. $\boldsymbol{\eta}_0 = \mathbf{R}_{cm}$ completely identifies the configuration of the system. An example of the recursive splitting applied to the four-body system with different masses is shown in Figure 3.1.

By following this scheme the Jacobi coordinates of a system made of particles with different masses are written as [73]

$$\boldsymbol{\eta}_{k-1} = \sqrt{\frac{M_{k-1}m_k}{M_k\bar{m}}}\left(\boldsymbol{r}_k - \frac{1}{M_{k-1}}\sum_{i=1}^{k-1} m_i\boldsymbol{r}_i\right); \quad k = 2, ..., A. \tag{3.3}$$

where $\{m_i\}$ is the set of masses of the particles, $M_k = \sum_{i=1}^{k} m_i$ and $\bar{m}$ identifies an arbitrary mass scale. It is possible to rewrite this linear transformation by defining

an orthogonal matrix S_{ij} [74]

$$\boldsymbol{\eta}_{k-1} = \sum_{i=1}^{A} S_{ki} \sqrt{\frac{m_i}{\bar{m}}}\, \boldsymbol{r}_i \,, \tag{3.4}$$

$$\boldsymbol{r}_i = \frac{1}{\sqrt{m_i/\bar{m}}} \sum_{k=1}^{A} S_{ki}\, \boldsymbol{\eta}_{k-1} \,, \tag{3.5}$$

where S_{ij} has the following form

$$S_{ij} = \begin{cases} \sqrt{\frac{m_j}{M_A}} & i = 1 \\ -\sqrt{\frac{m_i m_j}{M_i M_{i-1}}} & i > 1 \\ \sqrt{\frac{M_{i-1}}{M_i}} & i = j \\ 0 & j > i \end{cases} . \tag{3.6}$$

The gradient and momentum operators are transformed as

$$\frac{\partial}{\partial \boldsymbol{r}_i} = \sum_{k=1}^{A} \sqrt{m_i/\bar{m}}\, S_{ki}\, \frac{\partial}{\partial \boldsymbol{\eta}_{k-1}} \,, \tag{3.7}$$

$$\mathbf{p}_i = \sum_{k=1}^{A} \sqrt{m_i/\bar{m}}\, S_{ki}\, \mathbf{q}_{k-1} \,, \tag{3.8}$$

where $\mathbf{q}_k = -i\partial/\partial\boldsymbol{\eta}_k$. The bilinear combinations are given by

$$\mathcal{I}_{\alpha,\beta} = \sum_{i=1}^{A} m_i (\mathbf{r}_i)_\alpha (\mathbf{r}_i)_\beta = \bar{m} \sum_{i=1}^{A} (\boldsymbol{\eta}_{i-1})_\alpha (\boldsymbol{\eta}_{i-1})_\beta \,, \tag{3.9}$$

$$\mathcal{T}_{\alpha,\beta} = \sum_{i=1}^{A} \frac{1}{2m_i} (\mathbf{p}_i)_\alpha (\mathbf{p}_i)_\beta = \frac{1}{2\bar{m}} \sum_{i=1}^{A} (\mathbf{q}_{i-1})_\alpha (\mathbf{q}_{i-1})_\beta \,, \tag{3.10}$$

$$\mathcal{L}_{\alpha,\beta} = \sum_{i=1}^{A} m_i (\mathbf{r}_i)_\alpha (\mathbf{p}_i)_\beta = \bar{m} \sum_{i=1}^{A} (\boldsymbol{\eta}_{i-1})_\alpha (\mathbf{q}_{i-1})_\beta \,, \tag{3.11}$$

and finally the volume elements are expressed as

$$\prod_{i=1}^{A} d\boldsymbol{r}_i = \frac{1}{\mu} \prod_{i=1}^{A} d\boldsymbol{\eta}_{i-1} \,, \tag{3.12}$$

$$\prod_{i=1}^{A} d\mathbf{p}_i = \mu \prod_{i=1}^{A} d\mathbf{q}_{i-1} \,, \tag{3.13}$$

where $\mu = \prod_{i=1}^{N} \sqrt{m_i}$.

Hyperspherical coordinates. From a given choice of Jacobi coordinates, the hyperspherical coordinates $\{\rho_N, \varphi(N), \Omega(N)\}$ can be introduced. In this notation, ρ_N is the hyper-radius, $\Omega(N) \equiv \{\Omega_1, ..., \Omega_N\}$ where $\Omega_j = (\theta_j, \phi_j)$ gathers the angular coordinates of the Jacobi vectors , and $\varphi(N) \equiv \{\varphi_2, ..., \varphi_N\}$ is a set of hyper-angles. The hyper-radial coordinates $\rho_1, ..., \rho_N$ and the hyper-angular coordinates $\varphi_2, ..., \varphi_N$ are constructed recursively. The transformation law for the first two Jacobi coordinates is

$$\begin{aligned} \eta_1 &= \rho_1 = \rho_2 \cos\varphi_2 \ , \\ \eta_2 &= \rho_2 \sin\varphi_2 \ . \end{aligned} \tag{3.14}$$

Assuming that we obtained already the hyper-radial coordinates $\rho_1, ..., \rho_{j-1}$ and the hyper-angular coordinates $\varphi_2, ..., \varphi_{j-1}$, the transformation law for ρ_j and φ_j reads in analogy to Eq. (3.14) as

$$\begin{aligned} \rho_{j-1} &= \rho_j \cos\varphi_j \ , \\ \eta_j &= \rho_j \sin\varphi_j \ . \end{aligned} \tag{3.15}$$

This iterative procedure defines the full set of hyperspherical coordinates from the Jacobi vectors.

The internal kinetic energy operator for the A-body system is given by the $3N$-dimensional Laplace operator $\Delta(N)$, which in terms of the hyperspherical coordinates it is written as

$$\Delta(N) = \Delta_\rho - \frac{1}{\rho^2}\widehat{K}_N^2(\varphi(N), \Omega(N)) \ . \tag{3.16}$$

In the previous equation we simplified the notation by writing $\rho \equiv \rho_N$. The hyper-radial part is

$$\Delta_\rho = \frac{\partial^2}{\partial\rho^2} + \frac{3N-1}{\rho}\frac{\partial}{\partial\rho} \ , \tag{3.17}$$

where $\widehat{K}_N^2$ is the grand-angular momentum operator[1]. Denoting with $\hat{l}_j$ the angular momentum operator related to the Jacobi vector $\boldsymbol{\eta}_j$, and with $\hat{L}_j^2$ and $\hat{M}_j$ the total orbital angular momentum operator and z-projection of the system identified by the first j Jacobi coordinates, it is possible to define the grand-angular momentum operator $\widehat{K}_N^2$ of the system recursively in terms of $\widehat{K}_{N-1}^2$ and $\hat{l}_N$ as [75]

$$\widehat{K}_N^2 = -\frac{\partial^2}{\partial\varphi_N^2} + \frac{3N-6-(3N-2)\cos(2\varphi_N)}{\sin(2\varphi_N)}\frac{\partial}{\partial\varphi_N} + \frac{1}{\cos^2\varphi_N}\widehat{K}_{N-1}^2 + \frac{1}{\sin^2\varphi_N}\hat{l}_N^2 \tag{3.18}$$

where $\widehat{K}_1^2 = \hat{l}_1^2$. The operators $\widehat{K}_N^2, ..., \widehat{K}_2^2$, $\hat{L}_N^2, ..., \hat{L}_2^2$, $\hat{l}_N^2, ..., \hat{l}_1^2$ and $\widehat{M}_N$ commute with each others. As a consequence, it is possible to label hyperspherical states using the set of $3N-1$ quantum numbers $\{K_N\} \equiv \{K_N, ..., K_2, L_N, ..., L_2, l_N, ..., l_1, M_N\}$.

[1]Here we put hats on the operators to avoid confusion with the related quantum numbers.

Hyperspherical Harmonics functions. The hyperspherical harmonics functions $\mathcal{Y}_{\{K_N\}}$ are the eigenfunctions of the grand-angular momentum operator with eigenvalues $K_N(K_N+3N-2)$. The explicit expression for the hyperspherical harmonics functions is given by [76]

$$\begin{aligned}\mathcal{Y}_{\{K_N\}} = &\left[\sum_{m_1,\ldots,m_N} C^{L_2M_2}_{l_1m_1,l_2m_2} C^{L_3M_3}_{L_2M_2,l_3m_3} \times \ldots \times C^{L_NM_N}_{L_{N-1}M_{N-1},l_Nm_N} \prod_{j=1}^{N} Y_{l_jm_j}(\Omega_j)\right] \times \\ &\times \left[\prod_{j=2}^{N} \mathcal{N}_j (\sin\varphi_j)^{l_j} (\cos\varphi_j)^{K_{j-1}} P_{n_j}^{\left[l_j+\frac{1}{2},K_{j-1}+\frac{(3j-5)}{2}\right]}(\cos 2\varphi_j)\right],\end{aligned} \tag{3.19}$$

where $C^{LM}_{l_im_i,l_jm_j}$ are the Clebsch-Gordan coefficients, $Y_{l_jm_j}(\Omega_j)$ are the spherical harmonics associated with the Jacobi coordinate $\boldsymbol{\eta}_j$, $P_n^{\left[\alpha,\beta\right]}$ are Jacobi polynomials, and

$$\mathcal{N}_j = \left[\frac{(3K_j+3j-2)n_j!\Gamma(n_j+K_{j-1}+l_j+\frac{3j-2}{2})}{\Gamma(n_j+l_j+\frac{3}{2})\Gamma(n_j+K_{j-1}+\frac{3j-3}{2})}\right]^{\frac{1}{2}} \tag{3.20}$$

is a normalization constant with $2n_j = K_j - K_{j-1} - l_j$. The hyperspherical harmonics form a complete orthogonal set so that

$$\begin{aligned}\langle \mathcal{Y}_{\{K_N\}} | \mathcal{Y}_{\{K'_N\}} \rangle &= \delta_{K_N,K'_N}\, \delta_{L_N,L'_N}\, \delta_{M_N,M'_N}\, \delta_{\ell_N,\ell'_N} \\ &\times \delta_{K_{N-1},K'_{N-1}}\, \delta_{L_{N-1},L'_{N-1}}\, \delta_{M_{N-1},M'_{N-1}}\, \delta_{\ell_{N-1},\ell'_{N-1}} \\ &\times \ \ldots \\ &\times \delta_{K_2,K'_2}\, \delta_{L_2,L'_2}\, \delta_{M_2,M'_2}\, \delta_{\ell_1,\ell'_1}\ .\end{aligned} \tag{3.21}$$

Anti-symmetrization. The hyperspherical functions of Eq. (3.19) do not have well defined transformation properties under the permutation group S_A. As required by Fermi statistics, the nuclear wavefunction must belong to the total anti-symmetric irreducible representation of S_A, at least in the limit where we can ignore any isospin symmetry breaking effects in the nuclear Hamiltonian. The complete algorithm that generates the symmetry-adapted hyperspherical harmonics was developed in Ref. [65], from which we just quote the main findings. The main idea is to first construct functions populating the irreducible representations of the dynamical $O(N)$ group, and then use that $S_A \subset O(N)$, to reduce to the irreducible representations of S_A. These symmetry-adapted hyperspherical harmonics, $\mathcal{Y}_{[K_N]}$, are uniquely identified by the set of quantum numbers $[K_N] \equiv \{K_N, L_N, M_N, \boldsymbol{\lambda}_N, \alpha_N\, Y_A, \beta_A\}$, where $\boldsymbol{\lambda}_N$ identifies the irreducible representation of $O(N)$, Y_A is the Yamanouchi symbol which specifies the irreducible

representations of the group-subgroup chain $S_1 \subset ... \subset S_A$ presented by the appropriate Young diagrams $\Gamma_1, ..., \Gamma_A$, while α_N and β_A are additional quantum numbers needed to remove further degeneracies. The $O(N)$ and S_A symmetry-adapted hyperspherical harmonics $\mathcal{Y}_{[K_N]}$ are constructed recursively. Assuming that $\mathcal{Y}_{[K_{N-1}]}$ have been already constructed, the Nth Jacobi coordinate is then coupled to this system, so that a state with total angular momentum L_N and grand-angular momentum K_N is formed. Let us call this state $\mathcal{Y}_{[K_{N-1}],K_N L_N M_N}$. Note that $\mathcal{Y}_{[K_{N-1}],K_N L_N M_N}$ is a irreducible tensor under $O(N-1)$ and S_{A-1} but not under $O(N)$ and S_A. The states $\mathcal{Y}_{[K_N]}$ are obtained as linear combinations of the states $\mathcal{Y}_{[K_{N-1}],K_N L_N M_N}$, where the coefficients of the linear combinations are labeled as $\Big[\big(K_{N-1}, L_{N-1}, \boldsymbol{\lambda}_{N-1}, \alpha_{N-1}; l_N\big) K_N L_N | \} K_N L_N \boldsymbol{\lambda}_N \alpha_N\Big]$, $\Big[\big(\boldsymbol{\lambda}_{N-1} \Gamma_N \beta_N\big) \boldsymbol{\lambda}_N | \} \boldsymbol{\lambda}_N \Gamma_A \beta_A\Big]$ and are known as hyperspherical orthogonal group parentage coefficients (hsopcs) and orthogonal group coefficients of fractional parentage (ocfps) respectively. The final expression of the symmetry-adapted hyperspherical harmonics reads

$$\begin{aligned} \mathcal{Y}_{[K_N]} &= \sum_{\boldsymbol{\lambda}_{N-1}\beta_N} \Big[\big(\boldsymbol{\lambda}_{N-1}\Gamma_N\beta_N\big)\boldsymbol{\lambda}_N|\}\boldsymbol{\lambda}_N\Gamma_A\beta_A\Big] \\ &\times \sum_{K_{N-1},L_{N-1},\alpha_{N-1},l_N} \Big[\big(K_{N-1}, L_{N-1}, \boldsymbol{\lambda}_{N-1}, \alpha_{N-1}; l_N\big) K_N L_N | \} K_N L_N \boldsymbol{\lambda}_N \alpha_N\Big] \\ &\times \mathcal{Y}_{[K_{N-1}],K_N L_N M_N}. \end{aligned} \tag{3.22}$$

Spin-isospin degrees of freedom. In Eq. (3.22), we have constructed hyperspherical harmonics functions belonging to irreducible representations of the dynamical orthogonal $O(N)$ and permutation S_A groups. Nucleons possess also spin and isospin degrees of freedom, which slightly complicate the construction of the hyperspherical basis with the proper transformation properties. In particular, the rotational symmetry of the nuclear Hamiltonian requires us to couple the spin and configuration part of the nuclear wavefunction into a state that has the total angular momentum J as good quantum number. On the other hand, isospin is an approximate symmetry for the nuclear interaction with the consequence that the total isospin T of the system is (almost) conserved. On top of this, the complete basis function in configuration, spin and isospin space must belong to the total anti-symmetric irreducible representation of the permutation group S_A, as required by Fermi statistics. All of this can be achieved by coupling the configuration, $\mathcal{Y}_{[K_N]}$, and spin-isospin wavefunction, $\chi_{[S_A]}$, of the A-nucleon system as [77]

$$H_{(K_N)} = \sum_{Y_N} \frac{\Lambda_{\Gamma_A, Y_N}}{\sqrt{|\Gamma_A|}} \sum_{M_N S_z} C^{JJ_z}_{L_N M_N, S S_z} \mathcal{Y}_{[K_N]}\, \chi_{[S_A]}\,, \tag{3.23}$$

where $\mathcal{Y}_{[K_N]}$ is defined in Eq. (3.22), while $\chi_{[S_A]}$ is the spin-isospin wavefunction of the A-nucleon system populating irreducible representations of the permuta-

tion group. Above, we defined $(K_N) \equiv \{K_N, L_N, S_N, J_N, (J_N)_z, \boldsymbol{\lambda}_N, \alpha_N^{ST}, Y_A, \beta_A\}$, $[S_A] \equiv \{S, S_z, T, T_z, Y_A, \alpha_A^{ST}\}$, while Λ_{Γ_A, Y_N} is a phase factor, and $|\Gamma_A|$ is the dimension of the irreducible representation Γ_A. The construction of the A-nucleon symmetrized spin-isospin wavefunction $\chi_{[S_A]}$ is done, similarly with the construction of the configuration part of the basis functions, recursively. As explained for instance in Ref. [77].

The Schrödinger equation. The symmetry-adapted hyperspherical harmonics form a complete and orthogonal basis in the hypersphere spanned by the Jacobi vectors. This allows us to expand the internal wavefunction of the many-body system as

$$\Psi_{\text{in}}(\boldsymbol{\eta}_1, ..., \boldsymbol{\eta}_N) = \sum_{(K_N)}^{K_{\max}} \mathcal{R}_{(K_N)}(\rho)\ H_{(K_N)}\big(\varphi(N), \Omega(N)\big)\ , \tag{3.24}$$

where the radial part $\mathcal{R}_{(K_N)}(\rho)$ is a function of the hyper-radius only, and $K_{\max}$ is the maximum grand-angular momentum quantum number. Using Eq. (3.10), Eq. (3.16), Eq. (3.17) and the orthogonality of the hyperspherical functions we see that the Schrödinger equation for the internal wavefunction of the many-body system generates the following coupled system of eigenvalue problems for the hyper-radial wavefunction

$$\begin{aligned} -\frac{1}{2m}\left(\frac{\partial^2}{\partial\rho^2} + \frac{3N-1}{\rho}\frac{\partial}{\partial\rho} - \frac{K(K+3N-2)}{\rho^2}\right) \mathcal{R}_{(K_N)}(\rho) \\ + \sum_{(K'_N)}^{K_{\max}} V_{(K'_N),(K_N)}(\rho)\mathcal{R}_{(K'_N)}(\rho) = E\ \mathcal{R}_{(K_N)}(\rho)\ . \end{aligned} \tag{3.25}$$

Here, $V_{(K'_N),(K_N)}(\rho)$ are matrix elements of the nuclear many-body interactions among hyperspherical states

$$\begin{aligned} V_{(K'_N),(K_N)}(\rho) &= \langle (K'_N)| \left(\sum_{i<j} V_{ij} + \sum_{i<j<k} W_{ijk} + ...\right) |(K_N)\rangle \\ &= \int d\Omega\ H^*_{(K'_N)}(\Omega) \left(\sum_{i<j} V_{ij} + \sum_{i<j<k} W_{ijk} + ...\right) H_{(K_N)}(\Omega)\ , \end{aligned} \tag{3.26}$$

where we simplified the notation with the definition $\Omega \equiv \big(\varphi(N), \Omega(N)\big)$. We see that, with the expansion of the internal wavefunction in hyperspherical harmonics, the solution of the Schrödinger equation is obtained in two steps. The first involves the calculation of the matrix elements of the potential in Eq. (3.26), the second requires the solution of the hyperradial equation in Eq. (3.25). The latter is generally obtained by expanding the hyper-radial wavefunction in terms of a

further complete set of state. In the work described in this thesis, the expansion is done in terms of the generalized Laguerre polynomials $L_n^v(\rho_N)$

$$\mathcal{R}_{(K_N)}(\rho) = \sum_{n=0}^{n_{max}} C^n_{(K_N)} L^v_n(\rho). \tag{3.27}$$

The hyperspherical harmonics method is very powerful and allows for precise solutions of the Schrödinger equation in three- and four-body systems, but unfortunately the numerical cost scales very quickly with the mass number A, see Figure 3.2.

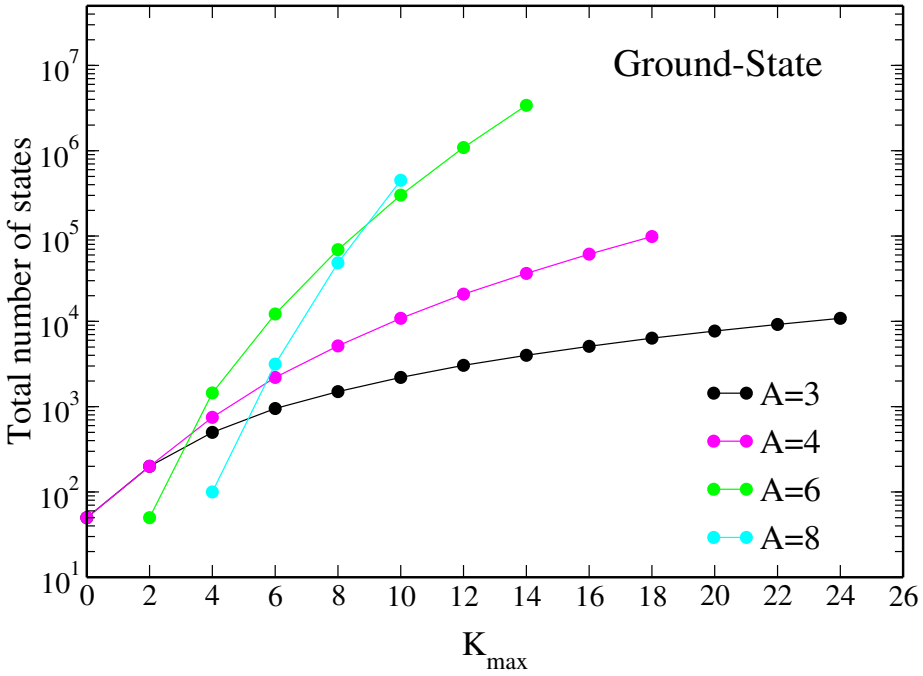

Figure 3.2.: Total number of states (HH states $\times$ hyperradial states) as a function of the maximum grand-angular momentum quantum number $K_{\max}$ and of the number, A, of particles in the system. Figure taken from Ref. [78].

Since the dimension of the basis becomes untreatable as we go to large value of $K_{\max}$, to accelerate the convergence of the hyperspherical harmonics expansion, we substitute the bare nucleon-nucleon interaction with an effective interaction, using the so called effective interaction hyperspherical harmonics (EIHH) method [79]. To derive the effective interaction, the Hilbert space of the A-body Hamiltonian $H_N = T + V + W + ...$ is divided into a model space and a residual space, defined by the projectors operators P and Q of T,

$$\begin{aligned} \left[T, P\right] &= \left[T, Q\right] = 0\,; \\ Q\,T\,P &= P\,T\,Q = 0\,; \\ P + Q &= \mathbb{1}\,. \end{aligned}$$

The Hamiltonian is then replaced by the effective model space Hamiltonian

$$H_N^{\text{eff}} = P\ T\ P + P\ V^{\text{eff}}\ P + P\ W^{\text{eff}}\ P + \dots\ ,$$

that by construction has the same energy levels as the low-lying spectrum of the bare Hamiltonian. In general, finding the complete many-body effective interaction is a problem that is numerically as complicate as finding the full-space solution with the bare interaction. However, for the case of the hyperspherical harmonics expansion, we can easily construct the two-body effective interaction, $V_{[2]}^{\text{eff}}$. In this work we truncate the generation of the effective interaction at the two-body level, and work then with bare three-nucleon forces. Despite the truncation of the effective interaction, observable in three- and four- body nuclei converge relatively fast, see for instance Ref. [2].

Important remarks. In essence, the hyperspherical harmonics method is a powerful technique and for many years it has been applied to the study of few-body systems. In the limit of infinite model space the solution converges to the exact solution of the Schrödinger equation, however in common practice one will always truncate the expansion at some point. While we observe that good convergence can be reached with $n_{max} \leq 50$, the convergence in terms of K_{max} is more problematic, and requires careful investigations. The uncertainty related to these truncations can be estimated by looking at the convergence pattern of the observables of interest, as will be shown in Chapter 5 of this thesis. Because the formulation presented here is developed in coordinate space, the method benefits from having local forces, such as the AV18 nucleon-nucleon potential. While one can formulate hyperspherical harmonics also in momentum space [58], the goal of this work is to focus on the coordinate space representation and implement local-chiral interactions.

3.2. The nuclear interaction

In 1935 Yukawa laid the foundation to the theory of the nuclear forces by considering an interactions among nucleons mediated by pions [80]. His one-pion exchange term is nowadays known as an important contribution to the interaction among nucleons in the long-distance range and is implemented in many nuclear interaction models. In the mid 1990s and early years of the next decade the first high-precision nucleon-nucleon potentials able to reproduce at the same time the deuteron properties, the proton-proton, and the proton-neutron scattering data were released. Some notable examples of these interactions are the above mentioned AV18 [81], the Nijmegen (Nijm93) [82], and the charge-dependent Bonn (CD-Bonn) [83]. The subsequent development of three-nucleon interactions, see

for instance Refs. [84, 85], improved the description of the $A > 2$ nuclear dynamics, initiating a successful theoretical campaign of nuclear structure and reaction predictions, see e.g., Refs. [86–88] and references therein. Despite the great success of the phenomenological interactions, there were still open questions to address, including the estimation of the uncertainties due to the modeling of the forces, the lack of connection between the NN and 3N interactions and the missing direct link to quantum chromodynamic.

An important step forward to address these issues was made when the concept of effective field theory (EFT) was introduced and applied to low-energy QCD. As suggested by Weinberg [89–92], the low-energy nuclear dynamic can be described by a Lagrangian written in terms of pions and nucleons fields and consistent with all the commonly accepted symmetries of QCD, including the (explicitly and spontaneously broken) chiral symmetry which strongly constrains the pion dynamics. The proposed Lagrangian contains an infinite number of terms and a systematic expansion must be introduced to make the theory applicable. Following Weinberg's proposal, in the early 2000s modern versions of chiral-inspired nuclear interactions were released by many groups – for a compilation of results, see for instance Refs. [50, 51, 93] and references therein – each interaction being different by the truncation order of the chiral expansion, by the inclusion or exclusion of the Δ-isobar, by the fitting procedure or by the regularization scheme used. Given that these interactions are derived in field theories written in momentum space, they are highly non-local. One of the consequences is that they are difficult to implement in some of the few- and many-body techniques which are developed in coordinate-space representation.

In recent years a set of local nuclear interactions derived from chiral effective field theory at the next-to-next-to-leading order (N2LO) has become available [63, 94–96]. This interaction has a series of properties which make it interesting for our computations. It is formulated in coordinate space and contains only one non-local operator. Furthermore, the two-body and three-body forces are regularized consistently, in the sense that the same regulator form and cut-off is used. Given that the hyperspherical harmonics method takes advantage in working with local interactions in coordinate space, this interaction is extensively used in the work described in this thesis.

Below, we highlight how the nuclear interactions originate from an effective field theory of the QCD Lagrangian. We start our discussion by describing the symmetries of QCD in the chiral limit, these symmetries are then used as a guiding point in constructing the leading order effective Lagrangians describing the dynamics of pions and nucleons, and finally we show how the nuclear force can be obtained from the calculation of the few-nucleon scattering amplitudes in the effective theory.

3.2.1. The symmetries of the QCD Lagrangian

The dynamics of the hadrons is described by QCD, a field theory based on the gauge $SU(3)_{\text{color}}$ group. The fundamental degrees of freedom for the theory are the quark and gluon fields. Here, we limit the discussion to the part of the QCD Lagrangian that is more strongly related to nuclear physics. Accordingly, our Lagrangian contains only two species of quarks: the "up" and "down" flavours. These quarks live in the fundamental representation of color $SU(3)$ and populate the spinor representation of the Poincaré group. Their interaction is mediated by the exchange of gluons, which are the gauge fields of the theory and are introduced in order to make the QCD Lagrangian invariant under a local $SU(3)_{\text{color}}$ transformation. The Lagrangian reads

$$\mathcal{L}_{\text{QCD}} = \bar{q}\Big(i\not{D} - \mathcal{M}\Big)q - \frac{1}{4}F_{\mu\nu,a}F_a^{\mu\nu} \ , \tag{3.28}$$

with

$$\not{D} \equiv \gamma^\mu D_\mu = \gamma^\mu\partial_\mu - ig\gamma^\mu\frac{\lambda_a}{2}G_{\mu,a} \ , \tag{3.29}$$

$$F_{\mu\nu,a} = \partial_\mu G_{\nu,a} - \partial_\nu G_{\mu,a} + g f_{abc} G_{\mu,b} G_{\mu,c} \ . \tag{3.30}$$

Here $\mathcal{M}$ is the quark mass matrix, λ_a $\{a = 1, ..., 8\}$ are the eight Gell-Mann matrices operating in color space, f_{abc} are the structure constants of $SU(3)_{\text{color}}$ and g is the strong coupling. In the notation of Eq. (3.28), the quark field is represented as a collection of column vectors in Dirac, color and flavour spaces as

$$q = \begin{pmatrix} \phi \\ \chi \end{pmatrix} \otimes \begin{pmatrix} q_r \\ q_g \\ q_b \end{pmatrix} \otimes \begin{pmatrix} u \\ d \end{pmatrix} \ ,$$

where ϕ and χ are the large and small components of the Dirac field, q_r, q_g, q_b represent the three different colors of quarks, while the remaining two dimensional column vector collects the flavours. The quark mass matrix takes the following form

$$\mathcal{M} = \mathbb{1}_{\text{Dirac}} \otimes \mathbb{1}_{\text{color}} \otimes \begin{pmatrix} m_u & 0 \\ 0 & m_d \end{pmatrix} \ .$$

Given the previous form of the quark mass matrix, the Lagrangian in Eq. (3.28) is both Lorentz and local $SU(3)_{\text{color}}$ invariant. It is also invariant under independent $U(1)_u \otimes U(1)_d$ global transformations, which implies flavour conservation of the strong force. This Lagrangian exhibits also a larger approximate symmetry in flavour space, known as isospin symmetry. It can be seen by noting that the mass of the lightest quarks $m_u \sim 2.5$ Mev, $m_d \sim 5$ MeV are much smaller than the typical masses of the hadrons $m_h \sim 1$ GeV. As a first approximation, the lightest quarks

can then be considered as having identical masses. We seek the description of an even larger approximate flavour symmetry, which arises when $m_u = m_d = 0$. In this approximation the QCD Lagrangian reads

$$\begin{aligned}\mathcal{L}^{(0)}_{\text{QCD}} &= \bar{q} i \not{D} q - \frac{1}{4} F_{\mu\nu,a} F^{\mu\nu}_a \\ &= \bar{q}_R i \not{D} q_R + \bar{q}_L i \not{D} q_L - \frac{1}{4} F_{\mu\nu,a} F^{\mu\nu}_a \ , \end{aligned} \tag{3.31}$$

where

$$q_R = \frac{1}{2}(1+\gamma_5) q \ , \tag{3.32}$$

$$q_L = \frac{1}{2}(1-\gamma_5) q \ . \tag{3.33}$$

This Lagrangian is invariant under the chiral transformation $U(1)_L \otimes U(1)_R \otimes SU(2)_L \otimes SU(2)_R$. Without any loss of generality the chiral transformations can be expressed in terms of vector and axial-vectors transformations $U(1)_V \otimes U(1)_A \otimes SU(2)_V \otimes SU(2)_A$. Noether's theorem then predicts the existence of 8 conserved currents

$$V^\mu_i = \bar{q} \gamma^\mu \frac{\tau_i}{2} q \ , \tag{3.34}$$

$$A^\mu_i = \bar{q} \gamma^\mu \gamma_5 \frac{\tau_i}{2} q \ , \tag{3.35}$$

$$V^\mu = \bar{q} \gamma^\mu q \ , \tag{3.36}$$

$$A^\mu = \bar{q} \gamma^\mu \gamma_5 q \ , \tag{3.37}$$

and eight corresponding conserved charges, which are the generators of the chiral transformation in the hadronic Hilbert space. In the previous equations τ_i $\{i = 1,2,3\}$ are Pauli matrices in flavour space. The singlet axial-vector current, A^μ, is only conserved at the classical level, i.e., quantum corrections break the current conservation [97,98]. Furthermore there is strong evidence that the chiral symmetry group of the Lagrangian $G = U(1)_V \otimes SU(2)_V \otimes SU(2)_A$ is spontaneously broken into $H = U(1)_V \otimes SU(2)_V$ by the ground state of QCD. This implies the existence of three massless Goldstone bosons with the same quantum numbers of the broken generators. These Goldstone bosons are nowadays associated with the pions, which is not massless because the chiral group is not only spontaneously but also explicitly broken.

3.2.2. Chiral effective field theory

Starting from the symmetries of QCD, in this section we construct an EFT that describes the properties of the atomic nuclei at low energies. Accordingly, only

pions and nucleons are explicitly included in the theory. This theory is known as chiral effective field theory (ChEFT). The structure of the chiral Lagrangian is strongly constrained by the symmetries and symmetry breaking pattern of QCD.

Given that the chiral Lagrangian contains an infinite number of terms, it is important to start by structuring a classification scheme. As a first approach we classify the operators in the Lagrangian as

$$\begin{aligned}\mathcal{L}_{\chi EFT} &= \mathcal{L}_{\pi}^{(2)}(m_\pi, f_\pi) + \mathcal{L}_{\pi}^{(4)}(l_1, ..., l_7) \\ &+ \mathcal{L}_{\pi N}^{(1)}(g_A) + \mathcal{L}_{\pi N}^{(2)}(M_N, c_1, ..., c_7) + \mathcal{L}_{\pi N}^{(3)}(d_1, ..., d_{23}) + \mathcal{L}_{\pi N}^{(4)}(e_1, ..., e_{118}) + ... \\ &+ \mathcal{L}_{NN}^{(0)}(C_S, C_T) + \mathcal{L}_{NN}^{(2)}(C_1, ..., C_7) + \mathcal{L}_{NN}^{(4)}(D_1, ..., D_{12}) + ... \\ &+ \mathcal{L}_{3N}^{(0)}(E) + \mathcal{L}_{3N}^{(2)}(E_1, ..., E_{10}) + ... \,, \end{aligned} \tag{3.38}$$

where m_π and f_π are the pion mass and decay constant, M_N is the nucleon mass, and $\{l_1, ..., l_7\}$, $\{g_A, c_1, ..., c_7, d_1, ..., d_{23}, e_1, ..., e_{118}\}$, $\{C_S, C_T, C_1, ..., C_7, D_1, ..., D_{12}\}$ and $\{E, E_1, ..., E_{10}\}$ are low-energy constants (LECs). These constants multiply the operators, and since they are not constrained by the symmetries of QCD, they need to be first fitted to the experimental data, or matched to lattice QCD, before making the theory predictive. The generally accepted rule is to indicate with lower case letters the constants that set the strength of the operators in the meson or single barion sector, while with capital case letters the constants that multiply short-range interactions between (and among) nuclei. The first row of Eq. (3.38) describes the dynamics and interaction of the pion fields, the second row describes the interaction between pion and nucleon fields, the third row describes short-range interactions between two nucleons and so on. The superscript counts the number of derivatives or pion mass insertions.

The group-theoretical foundations for the non-linear realization of the spontaneously broken chiral symmetry was developed in Refs. [99–101]. The crucial point is that the fields entering the Lagrangian are assumed to transform under irreducible representations of the subgroup H which leaves the vacuum invariant, whereas the chiral symmetry group G of the Lagrangian is non-linearly realized. We start by constructing the chiral Lagrangians in the purely mesonic sector. Accordingly, the non-linear realization of chiral symmetry is realized by introducing the operator $U(x)$, which collects the goldstone bosons, $\{\phi_1(x), \phi_2(x), \phi_3(x)\}$, and transforms under $G = SU(2)_L \otimes SU(2)_R$ as

$$G = SU(2) \otimes SU(2) = \{(L, R) | L \in SU(2), R \in SU(2)\} \,, \tag{3.39}$$

$$U(x) \overset{G}{\Rightarrow} RU(x)L^\dagger \,. \tag{3.40}$$

A widely used representation of this operator is the exponential one

$$U(x) = \exp\left[i\frac{\phi(x)}{f_\pi}\right], \tag{3.41}$$

$$\phi \equiv \phi_i\tau_i = \begin{pmatrix} \phi_3 & \phi_1 - i\phi_2 \\ \phi_1 + i\phi_2 & -\phi_3 \end{pmatrix} = \begin{pmatrix} \pi^0 & \sqrt{2}\pi^+ \\ \sqrt{2}\pi^- & -\pi^0 \end{pmatrix}, \tag{3.42}$$

where $\{\pi^0, \pi^+, \pi^-\}$ are the physical pion fields and for convenience, in Eq. (3.42), we have suppressed the dependence over the Minkowski variables. It is easy to prove [102] that a $SU(2)_V$ transformation leaves the vacuum ($\phi(x) = 0$) invariant and that the pion fields transform according to the adjoint representation. On the other hand, under the spontaneously broken $SU(2)_A$ transformation, the fields $\phi_i(x)$ do not have a simple transformation behaviour. In other words, the commutation relations of the pion fields with the axial charges are complicated nonlinear functions of the fields. This is the origin for the terminology *nonlinear realization of chiral symmetry* [99–101].

The most general Lagrangian with the least number of derivatives with respect to the exponential operator, $U(x)$, reads [103]

$$\begin{aligned} \mathcal{L}_\pi^{(2)} &= \frac{f_\pi^2}{4}\mathrm{Tr}\left[\partial_\mu U\, \partial^\mu U^\dagger + m_\pi^2(U + U^\dagger)\right], \\ &= \frac{1}{2}\partial_\mu\boldsymbol{\phi}\partial^\mu\boldsymbol{\phi} - \frac{1}{2}m_\pi^2\boldsymbol{\phi}^2 + \ldots \end{aligned} \tag{3.43}$$

where the missing terms contain operators with three or more pion fields. We note that the second term in Eq. (3.43) explicitly breaks chiral symmetry and its origin can be traced back to the quark mass matrix in the QCD Lagrangian, see for instance Chapter 3 of Ref. [102].

We now generalize the previous discussion to the baryon sector. We start by defining the nucleon field $\Psi(x)$ as

$$\Psi = \begin{pmatrix} \phi \\ \chi \end{pmatrix} \otimes \begin{pmatrix} p \\ n \end{pmatrix},$$

namely as a collection of Dirac fields for the proton, p, and neutron, n. We denote the unitary square root of $U(x)$ by $u(x)$, $u^2(x) = U(x)$ and define the $SU(2)$ valued function $K(L, R, U)$ by

$$u(x) \overset{G}{\Rightarrow} \sqrt{RUL^\dagger} \equiv RuK^{-1}(L, R, U), \tag{3.44}$$

$$K(L, R, U) = \sqrt{RUL^\dagger}\, R\, \sqrt{U}\,. \tag{3.45}$$

The following homomorphism defines an operation of G on the set $\{(U, \Psi)\}$

$$\varphi(g) : \begin{pmatrix} U \\ \Psi \end{pmatrix} \to \begin{pmatrix} U' \\ \Psi' \end{pmatrix} = \begin{pmatrix} RUL^\dagger \\ K(L,R,U)\Psi \end{pmatrix} , \tag{3.46}$$

where $g \in G$. Under the isospin transformation $H = SU(2)_V$ the field Ψ transform as an isospin doublet [102].

We are now in a position to introduce the most general chiral baryonic Lagrangian at lowest order. We demand the effective chiral Lagrangian to be invariant under a *local* $G = SU(2)_L \otimes SU(2)_R \otimes U(1)_V$ flavor transformation. The transformation behavior of the nucleon and pion fields reads

$$\begin{pmatrix} U(x) \\ \Psi(x) \end{pmatrix} \xrightarrow{G} \begin{pmatrix} R(x)U(x)L^\dagger(x) \\ \exp\Big[-i\theta(x)\Big]K\Big(L(x),R(x),U(x)\Big)\Psi(x) \end{pmatrix} , \tag{3.47}$$

where the phase factor is responsible for the $U(1)_V$ transformation of the nucleon field, the pions transform trivially under this transformation since they have baryon number $B = 0$. The local character of the transformation means that one needs to introduce a covariant derivative $D_\mu\Psi$, with the property that it transform in the same way as Ψ. It can be proven that the covariant derivative

$$D_\mu = \partial_\mu + \Gamma_\mu , \tag{3.48}$$

$$\Gamma_\mu = \frac{1}{2}[u^\dagger, \partial_\mu u] , \tag{3.49}$$

has the right transformation properties. The most general Lagrangian that preserves the *local* symmetry G contains also another building block, the so called chiral *vielbein*

$$u_\mu \equiv i\{u^\dagger, \partial_\mu u\} , \tag{3.50}$$

which under parity transforms as an axial vector. The most general pion-nucleon Lagrangian with the least number of derivative reads [104]

$$\mathcal{L}^{(1)}_{\pi N} = \bar{\Psi}\Big(i\gamma^\mu D_\mu - M_N + \frac{g_A}{2}\gamma^\mu\gamma_5 u_\mu\Big)\Psi , \tag{3.51}$$

by expanding D_μ and u_μ, in terms of the pion fields, the previous Lagrangian reads

$$\mathcal{L}^{(1)}_{\pi N} = \bar{\Psi}\Big(i\gamma^\mu\partial_\mu - M_N - \frac{1}{4f_\pi^2}\gamma^\mu\boldsymbol{\tau}\cdot(\pi\times\partial_\mu\pi) - \frac{g_A}{2f_\pi}\gamma^\mu\gamma_5\boldsymbol{\tau}\cdot\partial_\mu\pi + ...\Big)\Psi , \tag{3.52}$$

where $\boldsymbol{\tau}$ is the vector of Pauli matrixes in isospin space, the term proportional to g_A is the axial-vector coupling of the pion and the nucleus fields and the term with two pion fields is known as the Weinberg-Tomozawa coupling.

Heavy baryon formalism. The Lagrangian in Eq. (3.51) leads to power counting problems. The reason is that the time-derivative $\partial_0\Psi$ generates a factor $E \approx M_N$ which is not small as compared to the chiral symmetry breaking scale $\Lambda_\chi \approx 1$ GeV. A solution to the problem has been proposed in [105], using an effective field theory technique originally developed in [106] for the study of heavy quark systems. The idea is to treat the baryons as heavy static sources such that the momentum transfer between baryons due to the pion exchanges is small as compared to the baryon mass. The expansion is performed in terms of these small momenta over the baryon mass and has become known as heavy baryon chiral perturbation theory (HBChPT). We parameterize the four-momentum of the nucleon field as $p^\mu = M_N v^\mu + l^\mu$, with v^μ being the four-velocity and l^μ a small residual momentum. By defining the operators

$$P_v^\pm = \frac{\mathbb{1} \pm \gamma_\mu v^\mu}{2} , \tag{3.53}$$

$$P_v^+ + P_v^- = \mathbb{1} , \tag{3.54}$$

we can introduce the so-called velocity-dependent fields

$$N(x) = \exp\Big[iM_N v_\mu x^\mu\Big] P_v^+ \, \Psi(x) , \tag{3.55}$$

$$h(x) = \exp\Big[iM_N v_\mu x^\mu\Big] P_v^- \, \Psi(x) , \tag{3.56}$$

so that the nucleon field can be expressed as

$$\Psi(x) = \exp\Big[-iM_N v_\mu x^\mu\Big] \Big(N(x) + h(x)\Big) . \tag{3.57}$$

The point that makes the redefinition in Eq. (3.55) and Eq. (3.56) useful is that when considering a static nucleon field $v^\mu \equiv (1,0,0,0)$ the projectors $P_v^\pm$ select the large and small component of the Dirac field, furthermore the phase redefinition of Eq. (3.55) removes the large M_N dependence in the chiral Lagrangian for the nucleon field $N(x)$. Accordingly, inserting Eq. (3.57) back into the relativistic pion-nucleon Lagrangian of Eq. (3.51), we obtain the following heavy-baryon Lagrangian describing the leading order pion-nucleon interaction

$$\widehat{\mathcal{L}}_{\pi N}^{(1)} = \bar{N}\Big(iD_0 - \frac{g_A}{2}\boldsymbol{\sigma}\cdot\mathbf{u}\Big)N + \mathcal{O}(h) \tag{3.58}$$

$$= \bar{N}\Bigg\{ i\partial_0 - \frac{1}{4f_\pi^2}\boldsymbol{\tau}\cdot(\boldsymbol{\phi}\times\partial_0\boldsymbol{\phi}) - \frac{g_A}{2f_\pi}\boldsymbol{\tau}\cdot(\boldsymbol{\sigma}\cdot\nabla)\boldsymbol{\phi}$$

$$- \frac{g_A}{12f_\pi^3}(\boldsymbol{\tau}\cdot\boldsymbol{\phi})\big[\boldsymbol{\phi}\cdot(\boldsymbol{\sigma}\cdot\nabla)\boldsymbol{\phi}\big] + \frac{g_A}{12f_\pi^3}\boldsymbol{\phi}^2\big[\boldsymbol{\tau}\cdot(\boldsymbol{\sigma}\cdot\nabla)\boldsymbol{\phi}\big] \Bigg\} N + \ldots , \tag{3.59}$$

where the missing terms in Eq. (3.59) contains more pion or $h(x)$ fields, while σ is a vector of Pauli matrices in spin space.

The pion-nucleon Lagrangian of Eq. (3.51) and Eq. (3.58) is responsible for generating the leading long-range part of the nuclear interactions. In conventional meson exchange models, the short-range nuclear force is described by the exchange of heavy mesons. Qualitatively, the short-range behavior of the NN interaction is obtained by Fourier transforming the propagator of heavy mesons

$$\int d^3q \frac{e^{i\mathbf{q}\cdot\mathbf{r}}}{m_\omega^2 + \mathbf{q}^2} \sim \frac{e^{-m_\omega r}}{r} \,. \tag{3.60}$$

ChEFT is an expansion in small momenta of order $q \sim m_\pi$, which are too small to resolve the structure of the lightest mesons, like $\rho(770)$ or $\omega(782)$, because $q \ll \Lambda_\chi \approx m_{\rho,\omega}$. This means that it is possible to obtain an approximate treatment of the propagator in Eq. (3.60) by expanding it for small momenta

$$\frac{1}{m_\omega^2 + \mathbf{q}^2} \approx \frac{1}{m_\omega^2}\left(1 - \frac{\mathbf{q}^2}{m_\omega^2} + \frac{\mathbf{q}^4}{m_\omega^4} + ...\right) \,, \tag{3.61}$$

which generate contact interactions with an increasing number of derivatives. The contact operators do not break the chiral symmetry, so they must be included in the effective Lagrangian. They mimic the effects of heavy boson exchanges and are important for the renormalization of the theory. In the heavy-baryon formalism, the nucleon-nucleon Lagrangian consistent with the symmetries of ChEFT and with the minimal number of derivatives can be written as [90,91]

$$\widehat{\mathcal{L}}_{NN}^{(0)} = -\frac{1}{2}C_S(\bar{N}N)(\bar{N}N) - \frac{1}{2}C_T(\bar{N}\sigma N)\cdot(\bar{N}\sigma N) \,. \tag{3.62}$$

Power Counting. The operators in the chiral Lagrangian have been organized by counting the powers of derivatives or pion mass. This approach can be successfully applied in the mesonic or single baryon sector but it is insufficient in describing the interactions among nucleons. Furthermore, as noted by Weinberg in the early 90s [90,91], there are large terms in the scattering series associated with the nucleon propagators in the intermediate states which explicitly break the perturbative convergence of the scattering series. To overcome this problem, Weinberg suggestion was to generate a potential from the amplitudes not containing these large terms, and then iterate the interaction in the Schrödinger or Lippmann-Schwinger equation to generate the complete scattering series. The Feynman diagrams, given that they do not contain the large terms, can be organized by simply counting the powers, v, of the associated small external momenta Q, which are assumed to be much smaller than the breakdown scale of ChEFT, $Q \ll \Lambda_\chi$. Using naive dimensional

	Diagram	Expression
π propagator	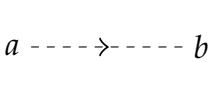	$\frac{i\delta_{ab}}{q^2 - m_\pi^2 + i\epsilon}$
NN vertex	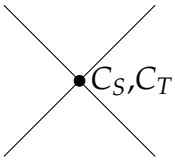	$C_S, C_T(\sigma_1 \cdot \sigma_2)$
Nπ vertex	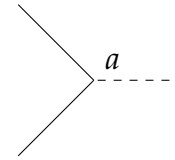	$-\frac{g_A}{2f_\pi}\tau^a \boldsymbol{\sigma} \cdot \mathbf{q}$

Table 3.1.: The relevant Feynman rules for calculating the leading order chiral nuclear potential in Weinberg power counting.

analysis, Weinberg derived the following power counting scheme

$$v = 2 - \frac{1}{2}E_n + 2L + \sum_i V_i \left[\tilde{d}_i + \frac{1}{2}\tilde{n}_i - 2\right], \tag{3.63}$$

where E_n counts the number of external nucleon lines, L counts the number of loops, $\tilde{n}_i$ counts the internal nucleon lines associated with each interaction vertex, $\tilde{d}_i$ is the number of derivative of the interaction while V_i counts the number of interactions of the type associated with the square bracket.

Feynman rules. The relevant terms of the pion-nucleon Lagrangian which generate the Feynman diagrams with the least power of v is [50]

$$\begin{aligned}\widehat{\mathcal{L}}_{\chi EFT} &= \frac{1}{2}\partial_\mu \boldsymbol{\phi}\partial^\mu \boldsymbol{\phi} - \frac{1}{2}m_\pi^2 \boldsymbol{\phi}^2 \\ &+ \bar{N}\left[i\partial_0 - \frac{1}{4f_\pi^2}\boldsymbol{\tau}\cdot(\boldsymbol{\phi}\times\partial_0\boldsymbol{\phi}) - \frac{g_A}{2f_\pi}\boldsymbol{\tau}\cdot(\boldsymbol{\sigma}\cdot\nabla)\boldsymbol{\phi}\right]N \\ &- \frac{1}{2}C_S(\bar{N}N)(\bar{N}N) - \frac{1}{2}C_T(\bar{N}\boldsymbol{\sigma}N)\cdot(\bar{N}\boldsymbol{\sigma}N)\,,\end{aligned} \tag{3.64}$$

from which the Feynman rules that are relevant for deriving the leading-order nuclear potential in Weinberg power counting can be derived, and are shown in Table. 3.1.

3.2.3. Nuclear Hamiltonians

In the modern view of nuclear physics, nuclear Hamiltonians are derived from ChEFT or an alternative EFT. Nuclear forces can be either formulated in coordinate or in momentum space. In this work we prefer a coordinate space formulation, given that the hyperspherical harmonics method is better suited to work in this framework. There are many important details that must be considered when deriving nuclear forces from the chiral Lagrangian, such as the choices of power counting and regulator schemes and the renormalization of the few-nucleon amplitudes obtained from the interaction. These important points will not be addressed in this thesis, given that they were not the main focus of this work, and that there are already some very well written reviews on the subject. The interested reader can consult for instance Refs. [50, 51] and references therein for more details.

In what follows, we start our derivation of the nuclear interaction by organizing the NN potential as

$$V_{12} = V_{12}^{ct} + V_{12}^{\pi} \,, \tag{3.65}$$

where the indexes $1/2$ refers to the two nucleons taking part in the interaction. In Eq. (3.65) we explicitly separate the pion-exchange diagrams from the contact terms. The operator structure of the contact terms is the most general one allowed by the symmetries of QCD in the chiral limit. These operators are then multiplied by their respective LECs which must be fitted to $A \geq 2$ nucleon observables before making the theory predictive. The structure of V_{12}^{π} is completely determined by the spontaneously broken approximate chiral symmetry of QCD and the experimental information on the πN system. This means that there are no free parameters in V_{12}^{π}, the most general structure of this interaction up to N2LO is given by [94]

$$\begin{aligned} V_{12}^{\pi} = & V_C(\boldsymbol{r}_{12}) + W_C(\boldsymbol{r}_{12})\boldsymbol{\tau}_1 \cdot \boldsymbol{\tau}_2 \\ & + \left[V_S(\boldsymbol{r}_{12}) + W_S(\boldsymbol{r}_{12})\boldsymbol{\tau}_1 \cdot \boldsymbol{\tau}_2\right]\boldsymbol{\sigma}_1 \cdot \boldsymbol{\sigma}_2 \\ & + \left[V_T(\boldsymbol{r}_{12}) + W_T(\boldsymbol{r}_{12})\boldsymbol{\tau}_1 \cdot \boldsymbol{\tau}_2\right] S_{12} \,, \end{aligned} \tag{3.66}$$

where S_{12} is the well-known tensor operator, defined as

$$S_{12} = 3(\boldsymbol{\sigma}_1 \cdot \hat{\boldsymbol{r}}_{12})(\boldsymbol{\sigma}_2 \cdot \hat{\boldsymbol{r}}_{12}) - (\boldsymbol{\sigma}_1 \cdot \boldsymbol{\sigma}_2) \,. \tag{3.67}$$

Here $\hat{\boldsymbol{r}}_{12}$ is the unit vector related to the relative distance, $\boldsymbol{r}_{12}$, between the two nucleons. The local functions $V_C(\boldsymbol{r}_{12})$, $W_C(\boldsymbol{r}_{12})$, $V_S(\boldsymbol{r}_{12})$, $W_S(\boldsymbol{r}_{12})$, $V_T(\boldsymbol{r}_{12})$ and $W_T(\boldsymbol{r}_{12})$ change form at each order in ChEFT. In the discussion that follows, we discuss the structure of the nuclear interactions up to the next-to-next-to-leading order in Weinberg's power counting.

Leading order nuclear force. The leading order (LO) interaction in Weinberg power counting is derived in Appendix. C. It consists of two contact terms and a static pion-exchange diagram. Using the Fierz rearrangement, see for instance Ref. [94], the contact terms can be written with the following operator structure

$$V_{12}^{ct,LO} = (C_S + C_T \sigma_1 \cdot \sigma_2)\delta(\boldsymbol{r}_{12}), \tag{3.68}$$

where $\delta(\boldsymbol{r}_{12})$ is the Dirac delta function, while C_S and C_T are two low-energy constants. Following Eq. (C.5), and according to Eq. (3.66), we parameterize the pion exchange interaction as

$$W_S^{\rm LO}(\boldsymbol{r}_{12}) = \left(\frac{g_A}{2f_\pi}\right)^2 \frac{m_\pi^2}{12\pi}\, Y(r_{12})\,, \tag{3.69}$$

$$W_T^{\rm LO}(\boldsymbol{r}_{12}) = \left(\frac{g_A}{2f_\pi}\right)^2 \frac{m_\pi^2}{12\pi}\, T(r_{12})\,, \tag{3.70}$$

and with all the other functions in Eq. (3.66) identically zero. For convenience in the previous equations we have defined the two functions

$$Y(r_{12}) = \frac{e^{-m_\pi r_{12}}}{r_{12}}\,, \tag{3.71}$$

$$T(r_{12}) = \left(1 + \frac{3}{m_\pi r_{12}} + \frac{3}{(m_\pi r_{12})^2}\right) Y(r_{12})\,. \tag{3.72}$$

Next-to-leading-order nuclear force. At the next-to-leading order (NLO) there are contributions coming from the leading two-pion exchange diagrams, which greatly improves the description of the intermediate-range part of the nuclear interaction. In this work, we follow Refs. [94,107] where the loop diagrams are regularized using the spectral-function-regularization (SFR). Given that the calculation is quite technical, we will not evaluate the NLO diagrams here, but refer to the relevant literature [50,94]. For the scope of this thesis, it is important to only note that the NLO diagrams modify the values of the local functions $V_S(\boldsymbol{r}_{12})$, $V_T(\boldsymbol{r}_{12})$ and $W_C(\boldsymbol{r}_{12})$, which with respect to the leading-order case are not identically zero anymore. Furthermore, the strength of the one-pion-exchange (OPE) diagram is slightly modified because of the Goldberger-Treiman discrepancy (GTD) [108]

$$g_{\pi N} = \frac{g_A m_N}{f_\pi}\left(1 - \frac{2m_\pi^2 \bar{d}_{18}}{g_A}\right)\,, \tag{3.73}$$

where $g_{\pi N}$ is the coupling constant in the pion-nucleus vertex and $\bar{d}_{18}$ is a LEC from the third-order pion-nucleon effective Lagrangian, see Eq. (3.38). At NLO there are also 7 new independent LECs coming from the short-distance part of the interaction, using Fierz rearrangement, the operator structure of the contact interaction can be written as

$$\begin{aligned} V_{12}^{ct,NLO} &= -\Big[C_1 + C_2(\boldsymbol{\tau}_1 \cdot \boldsymbol{\tau}_2)\Big]\Delta\delta(\boldsymbol{r}_{12}) - \Big[C_3 + C_4(\boldsymbol{\tau}_1 \cdot \boldsymbol{\tau}_2)\Big](\boldsymbol{\sigma}_1 \cdot \boldsymbol{\sigma}_2)\Delta\delta(\boldsymbol{r}_{12}) \\ &+ \frac{C_5}{2}\frac{\partial_{r_{12}}\delta(\boldsymbol{r}_{12})}{r_{12}}\Big(\mathbf{L}\cdot\mathbf{S}\Big) + \Big[C_6 + C_7(\boldsymbol{\tau}_1 \cdot \boldsymbol{\tau}_2)\Big] \\ &\cdot \left[(\boldsymbol{\sigma}_1 \cdot \hat{\boldsymbol{r}}_{12})(\boldsymbol{\sigma}_2 \cdot \hat{\boldsymbol{r}}_{12})\left(\frac{\partial_{r_{12}}\delta(\boldsymbol{r}_{12})}{r_{12}} - \partial^2_{r_{12}}\delta(\boldsymbol{r}_{12})\right) - (\boldsymbol{\sigma}_1 \cdot \boldsymbol{\sigma}_2)\frac{\partial_{r_{12}}\delta(\boldsymbol{r}_{12})}{r_{12}}\right], \end{aligned} \tag{3.74}$$

where Δ is the Laplace operator, while $\mathbf{L}$ and $\mathbf{S}$ are the total orbital angular momentum and spin operator in the two-body system represented by the two interacting nucleons. The $\{C_1, ..., C_7\}$ is the set of new low energy constants (LECs). In this version of the nuclear interaction, the term proportional to C_5 is the only non-local operator.

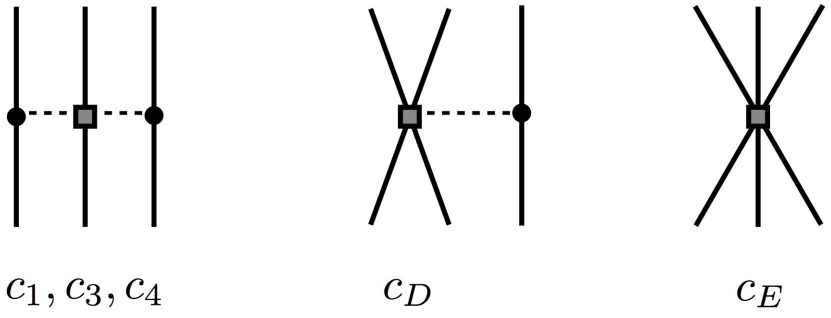

Figure 3.3.: Feynman diagrams of the chiral 3N force at N2LO, from the left to the right: 2π-term, 1π-term and ct-term.

N2LO nuclear force. At this order there are sub-leading two-pion-exchange diagrams which modify the values of $V_C(\boldsymbol{r}_{12})$, $W_S(\boldsymbol{r}_{12})$ and $W_T(\boldsymbol{r}_{12})$ [94]. There are no new contact diagrams, however the first non-zero three-nucleon (3N) forces, see the diagrams shown in Figure 3.3, arise at this order. The 3N force is composed of a two-pion (2π) exchange, a one-pion (1π) exchange and a 3N contact (ct) interaction. The 2π-term comes with the LECs c_1, c_3, and c_4 that already appear in the subleading two-pion-exchange interaction at the NN level at the same chiral order, while the one-pion exchange and the 3N contact diagrams introduce two new LECs, c_D and c_E, which must be fitted on $A \geq 3$ observables. In writing the

3N forces we follow Ref. [63]. The 3N interaction reads

$$W_{123} = \sum_{\text{cyc}} W_{1,23} = \sum_{\text{cyc}} \left[W_{1,23}^{2\pi,c_1} + W_{1,23}^{2\pi,c_3} + W_{1,23}^{2\pi,c_4} + W_{1,23}^{1\pi,c_D} + W_{1,23}^{ct,c_E} \right] , \tag{3.75}$$

where the sum runs over the cyclic permutations of the particle triplet and the notation has the intention to highlight the symmetry of the interaction over the exchange of particles 2 and 3. Each term is denoted with a label that includes the associated LEC. The 2π exchange $3N$ terms are given by

$$\begin{aligned} W_{1,23}^{2\pi,c_1} &= A\, U_{12} Y_{12} U_{13} Y_{13}\, (\boldsymbol{\tau}_2 \cdot \boldsymbol{\tau}_3)\, (\boldsymbol{\sigma}_2 \cdot \hat{\mathbf{r}}_{12})\, (\boldsymbol{\sigma}_3 \cdot \hat{\mathbf{r}}_{13}) , & (3.76)\\ W_{1,23}^{2\pi,c_3} &= B\, \{\boldsymbol{\tau}_1 \cdot \boldsymbol{\tau}_2, \boldsymbol{\tau}_1 \cdot \boldsymbol{\tau}_3\}\, \{\chi_{12}, \chi_{13}\} , & (3.77)\\ W_{1,23}^{2\pi,c_4} &= -C\, [\boldsymbol{\tau}_1 \cdot \boldsymbol{\tau}_2, \boldsymbol{\tau}_1 \cdot \boldsymbol{\tau}_3]\, [\chi_{12}, \chi_{13}] , & (3.78) \end{aligned}$$

where we have defined the coupling constants A, B and C as

$$\begin{aligned} A &= c_1 \frac{g_A^2 m_\pi^4 (\hbar c)^2}{16\pi^2 F_\pi^4} , & (3.79)\\ B &= c_3 \frac{g_A^2 m_\pi^4 (\hbar c)^2}{1152\pi^2 F_\pi^4} , & (3.80)\\ C &= c_4 \frac{g_A^2 m_\pi^4 (\hbar c)^2}{2304\pi^2 F_\pi^4} , & (3.81) \end{aligned}$$

while the other functions and operators are

$$\begin{aligned} U_{12} &\equiv U(r_{12}) = 1 + \frac{1}{m_\pi r_{12}} , & (3.82)\\ \chi_{12} &\equiv \chi(r_{12}) = X_{12} - \frac{4\pi}{m_\pi^2}\, \delta(r_{12})\, (\boldsymbol{\sigma}_1 \cdot \boldsymbol{\sigma}_2) \\ &= T(r_{12}) S_{12} + \tilde{Y}_{12}\, (\boldsymbol{\sigma}_1 \cdot \boldsymbol{\sigma}_2) , & (3.83)\\ X_{12} &\equiv X(r_{12}) = T(r_{12}) S_{12} + Y(r_{12}) (\boldsymbol{\sigma}_1 \cdot \boldsymbol{\sigma}_2) , & (3.84)\\ \tilde{Y}_{12} &\equiv \tilde{Y}(r_{12}) = Y(r_{12}) - \frac{4\pi}{m_\pi^2}\, \delta(r_{12}) \quad . & (3.85) \end{aligned}$$

Finally $Y(r_{12})$, $T(r_{12})$ are defined in Eq. (3.71) and Eq. (3.72) respectively. The 1π-interaction and contact terms used in this work read

$$\begin{aligned} W_{1,23}^{1\pi,c_D 2} &= D (\boldsymbol{\tau}_2 \cdot \boldsymbol{\tau}_3)\, \chi_{23}\, [\delta(r_{12}) + \delta(r_{13})] , & (3.86)\\ W_{1,23}^{ct,c_E \tau} &= E (\boldsymbol{\tau}_2 \cdot \boldsymbol{\tau}_3)\, \delta(r_{12})\, \delta(r_{13}) & (3.87) \end{aligned}$$

with

$$D = c_D \frac{g_A m_\pi^2 (\hbar c)^4}{96\pi \Lambda_\chi F_\pi^4} , \tag{3.88}$$

$$E = c_E \frac{(\hbar c)^6}{\Lambda_\chi F_\pi^4} . \tag{3.89}$$

In addition to the isospin-symmetric interactions described so far, there are also isospin symmetry breaking effects, which originate from the mass splitting between the pion triplet and nucleon doublet and from the electromagnetic interaction. We will not describe these effect here, but refer directly to Ref. [94], where more details can be found.

The NN forces derived so far are already written as irreducible spherical tensors, in fact they follow the same structure of the AV18 [81] interaction. However, the same does not apply for the 3N forces, an important work of this thesis was the re-formulation of the three-nucleon forces as spherical tensors, and their implementation in the hyperspherical harmonics formalism. Given that this part of the work is quite technical, it is described in Appendix D.

Important remarks. Given that the chiral Lagrangian contains an infinite number of operators, the ChEFT expansion must be truncated at a certain order. In this work, we choose to truncate the expansion at N2LO. This is motivated by the evidence that starting from N3LO there are sub-leading three-body forces that have not yet been derived consistently with the other forces [109, 110]. Furthermore, at N3LO, ChEFT predicts the existence of four-body forces [50], which complicate even further the solution of the many-body Schrödinger equation. Nevertheless, in Chapter 5 we include a partial N3LO calculation, which is done by truncating the expansion of the 3N forces at N2LO while the NN forces are truncated at N3LO. We expect this to improve our results, but it is difficult to quantify what could be the effect of the missing N3LO operators.

It is important that we find methods to estimate the uncertainties of our results due to truncations of the ChEFT expansion. We have achieved this by the use of Bayesian methods, which are briefly introduced in the next Chapter.

4. Bayesian uncertainty quantification

In the previous two chapters, we described the relevant theory for the calculation of the nuclear structure effects on the spectra of muonic hydrogen-like atoms. As the importance of our theoretical result is closely tied to the expected precision, it becomes crucial to devise methods that quantify the uncertainties inherent in our predictions. In this chapter, we illustrate how the Bayesian analysis provides an optimal tool to achieve this goal, enabling us to estimate the ChEFT truncation error that predominantly influences the uncertainty of the calculation.

The Bayesian interpretation of probability was originally introduced by the Reverend Thomas Bayes in the latter half of the 18th century. It was later independently reformulated in the early 19th century by Laplace, who made significant contributions in advancing the theory during its early stages. Notably, one of the most remarkable applications of Bayesian inference at that time was Laplace's prediction of the mass of Saturn. Given the experimental data of its orbit $\{\mathbf{D}\}$ and the theory of celestial mechanics available at that time, which is denoted here with the label I, Laplace employed Bayes' theorem to extract a probability density function (pdf) of the mass of Saturn $\mathrm{pr}\big(M_s|\mathbf{D}, I\big)$ which has remarkably withstood the test of time. Despite its early successes, the Bayesian approach faced significant opposition from the scholars throughout the 19th and early 20th centuries, who favored the more objective definition of probability advocated by the classical frequency school. Various criticisms emerged, ranging from the interpretation of probabilistic thinking to the meaning of the so-called Bayesian priors. These led to the overall disguise of the Bayesian approach, until in modern years the works of Cox [111], Jeffrey [112] and Jaynes [113] rescued and revitalized the Bayesian school by establishing the theory on solid mathematical foundations. Presently, Bayesian statistics is extremely popular in frontier science, due to its capacity to extract the maximum amount of information from limited data sets while providing a systematic framework to confront theory against data.

This chapter is structured as follows. In Section 4.1 we introduce the fundamentals of Bayesian statistics, in Section 4.2 we apply the method to the problem of quantifying truncation uncertainties, and finally in section 4.3 we present a discussion on the derivation of the Bayesian priors.

4.1. Fundamentals of Bayesian statistics

The work of Richard Cox [111] laid the mathematical ground for interpreting the Bayesian perspective on probability. He started by considering how we can represent our belief in the truth of various propositions. As a minimum requirement, he assumed that our beliefs in various statement can be ranked in a transitive manner. If we believe in X more than Y, and if we believe that Y is more likely to be true than Z, then necessarily we have to believe in X more than Z. This transitive ranking can be obtained if we assign a real number to each statement according to our belief, where the number 1 (0) represents absolute certainty that the statement is true (false). Starting from this obvious point, Cox derived the rules that these numbers have to satisfy in order to meet some requirement of logical consistency. He started from two axioms:

- If we specify our belief in X, then we indirectly specify our belief in $\bar{X}$, the opposite of X.

- If we specify our belief in (X and Y assuming X), this uniquely identifies our belief in (X and Y).

Starting from these two axioms, Cox derived the following two relations

$$\mathrm{pr}(X|I) + \mathrm{pr}(\bar{X}|I) = 1\,, \tag{4.1}$$
$$\mathrm{pr}(X, Y|I) = \mathrm{pr}(Y|X, I)\ \mathrm{pr}(X|I)\,, \tag{4.2}$$

which take the name of sum rule and product rule, respectively. In Eq. (4.1) and Eq. (4.2), I represents the background information relevant in assessing the probability of X and Y. Among the most useful consequences of the previous rules, one can prove the following corollaries

$$\mathrm{pr}(X|Y, I) = \frac{\mathrm{pr}(Y|X, I)\ \mathrm{pr}(X|I)}{\mathrm{pr}(Y|I)}\,, \tag{4.3}$$
$$\mathrm{pr}(X|I) = \int \mathrm{pr}(X, Y|I)\ dY = \int \mathrm{pr}(X|Y, I)\ \mathrm{pr}(Y|I)\ dY\,. \tag{4.4}$$

Eq. (4.3) is known as Bayes' theorem, it follows directly from the product rule and it is invaluable in daily scientific practice. It allows us to turn things around and relate the probability of X given Y to the probability of Y given X. Its advantages are evident if we write it with $X \equiv$ Hypothesis and $Y \equiv$ Data then Eq. (4.3) becomes

$$\mathrm{pr}(\mathrm{Hyp}|\mathbf{D}, I) = \frac{\mathrm{pr}(\mathbf{D}|\mathrm{Hyp}, I)\ \mathrm{pr}(\mathrm{Hyp}|I)}{\mathrm{pr}(\mathbf{D}|I)}\,. \tag{4.5}$$

The theorem allows us to extract the probability distribution of hypothesis (related to some underlying theory) being true given the observed experimental data $\{\mathbf{D}\}$. Each term in Eq. (4.5) has a name. We call the term on the left-hand side of the equation "posterior probability distribution" (ppd). On the right-hand side, $\mathrm{pr}(\mathbf{D}|\mathrm{Hyp}, I)$ is known as the "likelihood" since it represents how likely it is to obtain the data given that the hypothesis is true and $\mathrm{pr}(\mathrm{Hyp}|I)$ is the "prior probability distribution" or simply "prior" since it represent our belief in the hypothesis being true even before acquiring the experimental data $\{\mathbf{D}\}$. Finally $\mathrm{pr}(\mathbf{D}|I)$ takes the name of "evidence". In some situation it is omitted, since it effectively acts as a normalization constants. Eq. (4.4) goes with name of marginalization and it is of great importance in scientific practice because it allows integrating out of nuisance parameters that enter the analysis but with no intrinsic interest.

There are many other corollaries that can be derived from Eq. (4.1) and Eq. (4.2), but they will not be needed for the applications of Bayesian statistics described in this thesis. In our work, we are focusing on applying Bayesian statistic to study the truncation uncertainties of the EFT expansion which is, described in the next section.

4.2. Estimating truncation uncertainties

The goal of this chapter is to develop a general method to give uncertainty estimates of truncation errors. In physics, truncations arise from various sources each with their own distinct nature. One example is the truncation of the Hamiltonian operator, which in ChEFT is expanded in different terms with small parameters. Another example might be the truncations of the Taylor series, as those made in Chapter 2 to derive closed expressions for the nuclear polarizability effects on the spectrum of muonic atoms. While the specific details of each truncation may vary depending on the particular expansion being employed, we can still highlight certain general principles that remain unchanged across most applications.

Problem statement. Our goal is to study the convergence pattern of an observable X which is calculated in terms of the following expansion

$$X = \sum_{n=0}^{k} D_n + \sum_{n=k+1}^{\infty} D_n \,, \tag{4.6}$$

the observable could be, e.g, the binding energy of a system, while the terms denoted by $\mathbf{D} \equiv \{D_0, ..., D_k, ...\}$ correspond to the partial calculations of that observable at different orders in the underlying expansion. This expansion is meaningful only under the assumption that there exists a hierarchy among the partial correc-

tions, that is $|D_0| > |D_1| > |D_2| > ...$, and that the series converges towards the real value of the observable X. To provide further specificity, it is often anticipated that each term in the series is suppressed by a factor of Q compared to the previous one, where $Q < 1$ is referred to as the expansion parameter of the series. With these considerations, we then rewrite Eq. (4.6) as

$$\begin{aligned} X &= \sum_{n=0}^{k} D_n + \sum_{n=k+1}^{\infty} D_n \\ &= X_{\text{ref}} \left[\sum_{n=0}^{k} c_n \, Q^n + \sum_{n=k+1}^{\infty} c_n \, Q^n \right] , \end{aligned} \tag{4.7}$$

where X_{ref} sets the natural scale of the observable X and the coefficients $\mathbf{c} \equiv \{c_0, ...c_k, ...\}$[1] are dimensionless and parameterize the converging pattern of the series. In an ideal case, where each term in Eq. (4.6) is exactly suppressed by a factor of Q compared to the previous one, all the coefficients in Eq. (4.7) can be taken as $\mathbf{c} = \mathbf{1}$ by an appropriate choice of the reference scale. One could argue that this ideal case is meaningless, since it reduces the expansion in Eq. (4.6) to a geometric series which can be analytically summed to all order. However it makes the idea that, in a properly converging series for the observable X, it is generally expected that the expansion coefficients are of $\mathcal{O}(1)$ through an appropriate choice of reference.

Our goal has two aspects. First, if the expansion parameter Q is unknown, we would like to make an optimal estimation for its value. Second, assuming that the expansion in Eq. (4.6) and Eq. (4.7) are truncated to the order $n = k$, we seek to guess the extent of the un-calculated corrections at higher orders, namely to estimate the size of dimensionless quantity

$$\Delta_k = \left[\sum_{n=k+1}^{\infty} c_n \, Q^n \right] , \tag{4.8}$$

which, after multiplication with X_{ref}, gives the uncertainty of the truncation in Eq. (4.7) at order $n = k$.

Learning the expansion parameter. Given the most general dataset of partial corrections $\{D_m, ..., D_k\}$, Bayes' theorem allows us to obtain a posterior probability distribution for the expansion parameter Q as

$$\text{pr}(Q|D_m, ..., D_k) = \frac{\text{pr}(D_m, ..., D_k|Q) \; \text{pr}(Q)}{\text{pr}(D_m, ..., D_k)} . \tag{4.9}$$

[1] These coefficients shall not be confused with the sub-leading pion-nucleon coupling constants defined in Chapter 3.

In Eq. (4.9) the evidence $\mathrm{pr}(D_m, ..., D_k)$ effectively enters the analysis as a normalization constant. The quantity $\mathrm{pr}(Q)$ is the prior which summarizes our expectations for the value of the expansion parameter before performing the Bayesian analysis, and the likelihood $\mathrm{pr}(D_m, ..., D_k|Q)$ is specified by the series of assumptions made in the previous paragraph, which define the relations between the dataset **D** and the expansion parameter as $D_n = X_{\mathrm{ref}}\, c_n\, Q^n$. We further assume that the expansion coefficients are uncorrelated among each other and their scale is set by a single scale parameter $\bar{c}$ through a probability distribution $\mathrm{pr}(c_n|\bar{c})$ for $n = m, ..., k$. We then eliminate the dependence on this "nuisance" parameter $\bar{c}$ by marginalizing over it as

$$\begin{aligned}\mathrm{pr}(D_m, ..., D_k|Q) &= \int dc_m ... dc_k\ \mathrm{pr}(D_m, ..., D_k|c_m, ..., c_k, Q)\mathrm{pr}(c_m, ..., c_k|Q) \\ &= \int d\bar{c}\ dc_m ... dc_k\ \mathrm{pr}(D_m, ..., D_k|c_m, ..., c_k, Q)\ \mathrm{pr}(c_m, ..., c_k|\bar{c}, Q)\ \mathrm{pr}(\bar{c}|Q)\,. \end{aligned} \tag{4.10}$$

Following Eq. (4.7) and the assumption that the dimensionless coefficients c_i are uncorrelated, we have

$$\begin{aligned}&\mathrm{pr}(D_m, ..., D_k|c_m, ..., c_k, Q) = \prod_{n=m}^{k} \mathrm{pr}(D_n|c_n, Q) = \prod_{n=m}^{k} \delta\Big(D_n - X_{\mathrm{ref}} c_n Q^n\Big) \\ = &\prod_{n=m}^{k} \frac{1}{X_{\mathrm{ref}}\, Q^n} \delta\Big(D_n/(X_{\mathrm{ref}} Q^n) - c_n\Big) = \frac{\mathcal{N}}{Q^{(k-m+1)(k+m)/2}} \prod_{n=m}^{k} \delta\Big(D_n/(X_{\mathrm{ref}} Q^n) - c_n\Big)\,, \end{aligned} \tag{4.11}$$

Here, the dependence on X_{ref} has been absorbed in the normalization constant $\mathcal{N}$. Using the delta functions to analytically perform the integrals over the dimensionless coefficients in Eq. (4.10), we obtain

$$\begin{aligned}&\mathrm{pr}(D_m, ..., D_k|Q) = \\ = &\frac{\mathcal{N}}{Q^{(k-m+1)(k+m)/2}} \int \mathrm{pr}\Big(c_m = \frac{D_m}{X_{\mathrm{ref}} Q^m}\,, ...,\ c_k = \frac{D_k}{X_{\mathrm{ref}} Q^k}\ \Big|\ \bar{c}, Q\Big)\ \mathrm{pr}(\bar{c})\ d\bar{c}\,, \end{aligned} \tag{4.12}$$

where we further assumed that the scale-parameter $\bar{c}$ is independent of Q. The posterior probability distribution for the expansion parameter $\mathrm{pr}(Q|D_m, ..., D_k)$ can then be written as

$$\begin{aligned}&\mathrm{pr}(Q|D_m, ..., D_k) = \\ = &\mathcal{N} \frac{\mathrm{pr}(Q)}{Q^{(k-m+1)(k+m)/2}} \int \mathrm{pr}\Big(c_m = \frac{D_m}{X_{\mathrm{ref}} Q^m}\,, ...,\ c_k = \frac{D_k}{X_{\mathrm{ref}} Q^k}\ \Big|\ \bar{c}, Q\Big)\ \mathrm{pr}(\bar{c})\ d\bar{c}\,, \end{aligned} \tag{4.13}$$

where this equation is well specified once we define the priors $\text{pr}(Q)$, $\text{pr}(\bar{c})$ and give the probability distribution $\text{pr}(c_n|\bar{c})$. The definition for these quantities will be specified in the result section of this thesis, since their optimal choice depends on the individual features of the series to be studied.

Estimating the truncation uncertainty. Assuming that we already know the expansion parameter Q, or that we have previously obtained its probability distribution by following the analysis indicated in the previous paragraph, our next goal is to obtain a probability distribution for the truncation error in Eq. (4.8). We will work in the approximation that this uncertainty is dominated by the first omitted term, $\Delta_k \approx \Delta_k^{(1)} = c_{k+1}\, Q^{k+1}$. Given the data set $\{D_m, ..., D_k\}$, we begin by expressing the Bayesian posterior for the truncation error $\text{pr}(\Delta_k^{(1)} \mid D_m, ..., D_k, Q)$, as an integrated likelihood over the first omitted coefficient c_{k+1},

$$\begin{aligned}
&\text{pr}(\Delta_k^{(1)} \mid D_m, ..., D_k, Q) = \\
&= \int dc_{k+1}\, \text{pr}(\Delta_k^{(1)} \mid D_m, ..., D_k, Q, c_{k+1})\, \text{pr}(c_{k+1} \mid D_m, ..., D_k, Q) \\
&= \int dc_{k+1}\, \delta(\Delta_k^{(1)} - c_{k+1}\, Q^{k+1})\, \text{pr}(c_{k+1} \mid D_m, ..., D_k, Q) \\
&= \frac{1}{Q^{k+1}}\, \text{pr}\Big(c_{k+1} = \frac{\Delta_k^{(1)}}{Q^{k+1}} \mid D_m, ..., D_k, Q\Big)\,. \qquad (4.14)
\end{aligned}$$

From the assumptions introduced in our Bayesian analysis of the expansion parameter, the coefficient c_{k+1} is only related to the scale parameter $\bar{c}$, which we explicitly introduce in the previous equation by marginalizing over it

$$\begin{aligned}
&\text{pr}(\Delta_k^{(1)} \mid D_m, ..., D_k, Q) \\
&= \frac{1}{Q^{k+1}} \int d\bar{c}\, \text{pr}\Big(c_{k+1} = \frac{\Delta_k^{(1)}}{Q^{k+1}} \mid D_m, ..., D_k, Q, \bar{c}\Big)\, \text{pr}(\bar{c} \mid D_m, ..., D_k, Q)\,. \qquad (4.15)
\end{aligned}$$

Eq. (4.15) expresses the truncation error in terms of the probability distribution of the coefficient c_{k+1}. Our analysis uses the calculated partial corrections $\{D_m, ..., D_k\}$ to learn about the probability distribution of $\bar{c}$ and then folds it with $\text{pr}(c_{k+1}|\bar{c})$ to obtain our estimate of the truncation uncertainty. Applying Bayes' theorem on the last term of Eq. (4.15), we arrive at the expression

$$\text{pr}(\Delta_k^{(1)}|\, D_m, ..., D_k, Q) = \frac{\int d\bar{c}\, \text{pr}\big(c_{k+1} = \frac{\Delta_k^{(1)}}{Q^{k+1}} \mid \bar{c}\,\big) \Big[\prod_{n=m}^{k} \text{pr}\big(c_n = \frac{D_n}{Q^n} \mid \bar{c}\,\big)\Big]\, \text{pr}(\bar{c})}{Q^{k+1} \int d\bar{c} \Big[\prod_{n=m}^{k} \text{pr}\big(c_n = \frac{D_n}{Q^n} \mid \bar{c}\,\big)\Big] \text{pr}(\bar{c})}. \qquad (4.16)$$

Since we are not interested in the explicit dependence of the truncation error over the expansion parameter Q, we marginalize over it to obtain

$$\text{pr}(\Delta_k^{(1)}|\ D_m, ..., D_k) = \int dQ\ \text{pr}(\Delta_k^{(1)}|\ D_m, ..., D_k, Q)\ \text{pr}(Q|\ D_m, ..., D_k)\,, \tag{4.17}$$

with $\text{pr}(Q|\ D_m, ..., D_k)$ given either by Eq. (4.13) or, if Q is already known, expressed in terms of a delta distribution $\text{pr}(Q|\ D_m, ..., D_k) = \delta(Q - \bar{Q})$, with $\bar{Q}$ being the known value of the expansion parameter.

4.3. Assigning probabilities

In the previous sections, limited discussion was given upon the selection of Bayesian priors. The basic premise is that these prior probability distributions should summarize the available information about the related quantities *prior* to the Bayesian analysis. However, the practical question remains: How do we choose the prior? Again, we can offer a few general principles.

First of all, given that the dataset **D** is informative enough, any reasonable choice of the priors will converge to the same posterior. In other words, the result is independent of the (reasonable) prior choice in the case of a very large and informative dataset **D** [2]. In this ideal case, we do not need a particularly informative prior to get a narrow posterior probability distribution, since all the information needed for the statistical inference is provided by the dataset. However, since in practice one has to work with a limited dataset, it is important that we implement all the available information on the system in our choice of priors, since this will be crucial in obtaining posterior probability distributions that are statistically meaningful. The question at hand is how one can summarize all the available information and, at the same time, make the most unbiased choices for the Bayesian priors. The assignments of probabilities that make use of the minimum amount of information are commonly called *Least Informative Probabilities* (LIP). A variety of methods have been invented to construct priors free of inconsistencies and at the same time capable of conveying the information we have on the problem at hand.

Invariance for transformation groups. Assume that our problem concerns over a bounded parameter, whose scale is not known. One example might be the mass of a heavy particle beyond the Standard Model, which could be anywhere from $M \sim 10^5$ GeV to the Planck mass. Consistency demands that the LIP should remain invariant when the scale is changed, $M \to k \cdot M$,

[2] The notation for the dataset shall not be confused with the electric dipole operator defined in Chapter 2.

$$\mathrm{pr}(M|I)dM = \mathrm{pr}(k \cdot M|I)d(k \cdot M) = k\,\mathrm{pr}(k \cdot M|I)dM \tag{4.18}$$

hence

$$\mathrm{pr}(M|I) \propto \frac{1}{M}\,. \tag{4.19}$$

This is known as Jeffreys' prior [112], and it represents the least informative prior for a scale parameter.

If a parameter θ is unbounded and our interest lies in its location, then the LIP should be invariant under the transformation $\theta \to \theta + a$, with a being a constant. This means

$$\mathrm{pr}(\theta|I)d\theta = \mathrm{pr}(\theta + a|I)d(\theta + a) = \mathrm{pr}(\theta + a|I)d\theta\,, \tag{4.20}$$

hence

$$\mathrm{pr}(\theta|I)d\theta = \text{const}\,, \tag{4.21}$$

and we obtain the uniform distribution.

The Maximum Entropy principle. Given the availability of more detailed information, the *Principle of Maximum Entropy* states that the probability distribution that most accurately represents our state of knowledge is the one that maximizes the Shannon information entropy [113]

$$S = -\int \mathrm{pr}(x) \cdot \log\Big[\mathrm{pr}(x)\Big]\; dx \tag{4.22}$$

under the constraints posed by the problem. There are numerous reasons that make the maximization of the Shannon information entropy desirable. However, we will not dive into discussions and instead focus on the application of this principle. For instance, using the principle of maximum entropy one obtains that the LIP of a positive definite quantity with mean μ is given by the exponential distribution, namely

$$\mathrm{pr}(x) = \frac{1}{\mu}\, e^{-x/\mu}\,, \tag{4.23}$$

which can easily be proven by the use of the Lagrange multipliers. The prior in Eq. (4.23) will be used as the optimal prior for the analysis of the η-expansion uncertainty in Chapter 5 of this thesis.

5. Results

In the last three chapters we introduced the relevant theory for calculating the nuclear structure corrections to the Lamb-shift in muonic ions. The theory is based on a $(Z\alpha)$ expansion, in which the nuclear finite-size effects start at order $(Z\alpha)^4$ while nuclear polarizabilities begin at order $(Z\alpha)^5$. The most important corrections found at order $(Z\alpha)^5$ are summarized in Section 2.4, Eqs. (2.85–2.95). Higher-order corrections are suppressed by further powers of α or $(Z\alpha)$, and are expected to be small. However, there are two high-order effects that have been found unexpectedly large which cannot be neglected: the Coulomb distortion shown in Eq. (2.96) and the electron-vacuum polarization correction to the leading polarizabilities shown in Eq. (2.97) and Eq. (2.98), which are of order $(Z\alpha)^6 \log(Z\alpha)$ and $(Z\alpha)^5\alpha$, respectively.

In this Chapter, this theory is applied to calculate the nuclear structure corrections to the Lamb-shift in muonic helium and lithium ions. For muonic helium ions, the corrections are calculated with the highest possible precision and uncertainties originating from the ChEFT truncation of the nuclear interaction are quantified with Bayesian inference. For muonic lithium ions, instead, we just aim at an estimate of the two-photon-exchange correction using simple NN potentials.

The present Chapter is organized as follows: Section 5.1 presents our study of the nuclear structure effects in $\mu^6\mathrm{Li}^{2+}$ and $\mu^7\mathrm{Li}^{2+}$ ions; Section 5.2 gives the quantification of the truncation uncertainties of the Taylor expansions of the structure functions $I_{\mathrm{NR}}(z)$, $I_{\mathrm{N}}(z)$, $J(z)$, $\bar{J}(z)$, $K(z)$ and $\bar{K}(z)$ (derived in Section 2.2); Section 5.3 shows the benchmark tests of our implementation, and finally Section 5.4 provides the calculations of the nuclear structure corrections in muonic helium ions with uncertainty estimations using Bayesian statistics.

5.1. Estimates of the nuclear structure effects in muonic lithium atoms

In this section we describe how we estimated the nuclear structure effects to the Lamb-shift of muonic lithium. The work described below is published in *SciPost Phys. Proc.* [1].

In order to calculate the nuclear structure corrections shown in Section 2.4, one needs to obtain both the ground-state wavefunction of the nucleus and the relevant nuclear response functions. For lithium such calculations are challenging and we are not yet able to perform them with realistic Hamiltonian. Our strategy for estimating the nuclear structure effects in muonic lithium ions is to extract them from the photoabsorption cross-sections $\sigma_\gamma(\omega)$, of lithium nuclei at low energies. From the photoabsorption cross-section, one can get the electric dipole response function $S_{\mathrm{D1}}(\omega)$, in fact in the unretarded-dipole approximation they are related by the following equation [4]

$$\sigma_\gamma(\omega) = 4\pi^2 \alpha\omega \; S_{\mathrm{D1}}(\omega) \; . \tag{5.1}$$

We perform the extraction using the cross-section calculated in Refs. [114–116] with the semi-realistic AV4′ nucleon-nucleon interaction [117], which is a simplified version of the realistic AV18 interaction [81]. Compared to the AV18, the AV4′ interaction has only central terms and its parameters have been refitted to reproduce the deuteron binding energy.

In Figure 5.1, the corrections are shown as functions of the final integration point of the sum rules. From the plots it is evident that the most important sum rules, namely δ_{D1} and δ_{C} are well converged at 100 MeV. The same applies for the small electron-vacuum polarization correction, δ_{eVP}. Other corrections, such as δ_{L}, δ_{T} and δ_{NS} are close to but yet not fully convergent, especially for the $\mu^7\mathrm{Li}^{2+}$ system.

To complete the estimates, it is necessary to evaluate the remaining terms. Based on our experience [5, 39], we are aware that, in addition to the electric-dipole corrections, there are other important terms, namely δ_{R3} and δ_{R1} which are shown in Eq. (2.88) and Eq. (2.93), respectively, which we cannot easily calculate. Our strategy to estimate these terms is the following. First, using the calculated proton and neutron distribution in lithium nuclei [118] with the AV18+UIX, we compute δ_{Z3} and δ_{Z1} which are strongly correlated with δ_{R3} and δ_{R1}. Second, we assume that the ratios $\delta_{\mathrm{R3}}/\delta_{\mathrm{Z3}}$ and $\delta_{\mathrm{R1}}/\delta_{\mathrm{Z1}}$ in lithium ions are the same as the ratios observed in helium ions with the AV18+UIX interaction [39].

The remaining corrections are related to the electric monopole, retarded dipole and quadrupole response functions, which are expected to be small. However, for the sake of completeness, we estimate these terms as well assuming that their ratios

	μ^6Li [meV]	μ^7Li [meV]
δ_{D1}	-41	-51
δ_C	8	10
δ_L	2	2
δ_T	-1	-1
δ_{R3}	-155	-118
δ_{Z3}	165	126
δ_{R2}	4	5
δ_Q	6	8
δ_{D1D3}	-5	-7
δ_{R1}	-12	-11
δ_{Z1}	24	22
δ_{NS}	-1	-2
δ_{eVP}	-1	-1
δ_{pol}	-7	-18
δ_{Zem}	-189	-148
δ_{TPE}	-196	-166

Table 5.1.: Nuclear structure corrections to the Lamb-shift in muonic lithium ions

with the related terms in $\mu^3\text{He}^+$ are the same as the ratio of $\delta_{D1}(\text{Li}^{2+})/\delta_{D1}(\mu^3\text{He}^+)$. Results for muonic lithium are reported in Table 5.1. We truncate the corrections at the level of 1 meV, considering the remaining digits as insignificant.

For comparison, we also quote the results of δ_{pol} from Ref. [119] which were obtained using experimental data: $\delta_{\text{pol}}(\mu^6\text{Li}^{2+}) = -15 \pm 4$ meV and $\delta_{\text{pol}}(\mu^7\text{Li}^{2+}) = -21 \pm 4$ meV. It is worth noting that in order to compare on the same footing, we must remove the non-dipole sum rules and the electron vacuum polarization from our calculations, given that the non-dipole and the eVP corrections are not included in Ref. [119]. As a result, we obtain $\delta_{\text{pol}}(\mu^6\text{Li}^{2+}) = -12$ meV and $\delta_{\text{pol}}(\mu^7\text{Li}^{2+}) = -23$ meV, which are in agreement with Ref. [119]. Comparing to the previous works, we have given the complete nuclear structure correction to the Lamb-shift of muonic lithium, calculated within the framework of the η-expansion, and up to order $(Z\alpha)^5$ with the further inclusion of the eVP-correction of order $\alpha(Z\alpha)^5$ and the Coulomb distortion effects.

Important remarks. This preliminary analysis is useful to illuminate some important and general features. Firstly, as qualitatively argued at the beginning of Section 2.2, the energy-shift is negative, which means that the nuclear structure

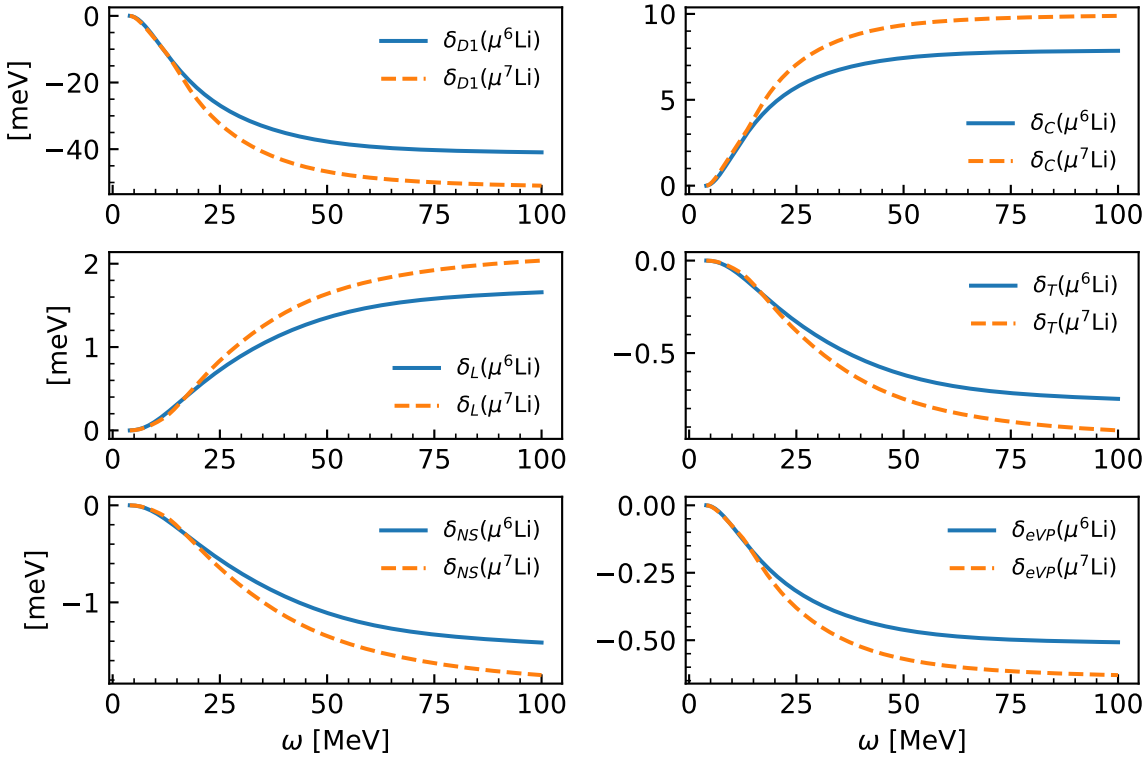

Figure 5.1.: Running sum rules as a function of the energy for the polarizability corrections related to the electric-dipole response function as a function of the integration endpoint.

effects at order $(Z\alpha)^5$ lower the energy of atomic $2S$-state and enhance the magnitude of the Lamb-shift $E_{LS} = E(2P_{1/2}) - E(2S_{1/2})$. Secondly, as clearly shown in Table 5.1, the most important corrections are δ_{R3}, δ_{Z3}, δ_{Z1}, δ_{R1} and δ_{D1}. However, as discussed in the theory chapter, the analytical cancellations between the elastic and the inelastic $(Z\alpha)^5$ corrections make δ_{Z3} and δ_{Z1} irrelevant to the total energy shift considering that these two terms appear in both elastic and inelastic corrections with opposite signs. The relevant corrections are then δ_{R3}, δ_{R1}, and δ_{D1}. Finally, the high but not exactly known correlations among the terms in Table 5.1 make it difficult to quantify the uncertainties of our results. The problem can be addressed by performing an order-by-order analysis of the corrections using interactions derived from the chiral effective field theory. This task is left to the future.

5.2. Uncertainties due to the η-expansion

In this section we use the Bayesian methods developed in Chapter 4 to quantify the uncertainties in our calculation of the nuclear structure corrections to the Lamb-shift due to the truncation of the η-expansion. This work is published in *Journal of Physics G* [3].

The η-expansion originates from the Taylor expansion of the structure functions $I_{\rm NR}(z)$, $I_{\rm N}(z)$, $J(z)$, $\bar{J}(z)$, $K(z)$ and $\bar{K}(z)$ which are defined in Section 2.2. The nuclear polarizability corrections to the energies of muonic atoms are related to all five structure functions, see Eq. (2.28). However, instead of studying the expansion of the complete energy shift, we decided to study the truncation uncertainties of the non-relativistic correction shown in Eq. (2.24) which is related to only one structure function, $I_{\rm NR}(z)$. This is justified by the fact that, in muonic atoms, the relativistic terms are significantly smaller than the non-relativistic ones. We expect that the relativistic terms do not significantly modify the conclusions of our analysis.

From Eq. (2.27) the nuclear polarizability correction to the atomic $2S$-state can be expressed as

$$\begin{aligned}\delta_{\rm pol} &= \frac{2\pi}{3}\,\alpha^2\,\phi_{2S}^2\,(2m)^{-\frac{1}{2}}\sum_{N\neq 0}(\omega_N)^{-\frac{3}{2}}\int d^3x\,d^3y\;\langle 0|\,\rho_{\rm ch}^{\dagger}(\mathbf{y})\,|N\rangle\,\langle N|\,\rho_{\rm ch}(\mathbf{x})\,|0\rangle \\ &\times \left[\eta^2-\frac{1}{4}\eta^3+\frac{1}{20}\eta^4+\mathcal{O}(\eta^5)\right]. \end{aligned} \tag{5.2}$$

Comparing to Eq. (2.27) we re-define the correction as $\Delta E_{20}^{\rm NR}\equiv\delta_{\rm pol}$ and we write $\eta=\sqrt{2m\omega_N}|\mathbf{x}-\mathbf{y}|$, where m is the mass of the muon. Following Ref. [39], one can argue by using the uncertainty principle that $|\mathbf{x}-\mathbf{y}|$ scales inversely with the momentum boost, q, of the traveling proton. It is thus roughly related to the nuclear excitation energy by $\omega_N\sim q^2/2m_p\sim(2m_p)^{-1}|\mathbf{x}-\mathbf{y}|^{-2}$, where m_p is the mass of the proton. Therefore η is a small parameter in light-nuclear systems, since it is of the order $\eta\sim\sqrt{m/m_p}\ll 1$. This justifies performing and truncating the Taylor expansion of the structure function $I_{\rm NR}(z)$ as in Eq. (2.26).

Our goal is to quantify the uncertainties associated with the truncation in Eq. (5.2). The way we tackle the problem was explained in Section 4.2. We write the nuclear polarizability as a sum of the partial calculation terms $\{D_2, D_3, D_4, ...\}$

$$\begin{aligned}\delta_{\rm pol} &= D_2+D_3+D_4+... \\ &= X_{\rm ref}\left[\,c_2\,\eta^2+c_3\,\eta^3+c_4\,\eta^4+...\,\right], \end{aligned} \tag{5.3}$$

where $X_{\rm ref}$ sets the natural scale of the observable, η is the expansion parame-

ter of Eq. (5.3), and $\{c_2, c_3, c_4, ...\}$[1] are the dimensionless coefficients that are expected to be of $\mathcal{O}(1)$ and set the converging pattern of the nuclear polarizability. Following Section 4.2 we assume that the expansion coefficients are uncorrelated with each other and the expression is set by the dimensionless scale parameter $\bar{c}$ through the probability distribution $\mathrm{pr}(c_n|\bar{c})$. The values for the partial calculations $\{D_2, D_3, D_4, ...\}$ used in this work are listed in Table 5.2[2].

	Corrections	^{2}H	^{3}H	^{3}He	^{4}He
D_2	$\delta^{(0)}_{D1}$	-1.912	-0.7848	-6.633	-4.701
D_3	$\delta^{(1)}_{R3} + \delta^{(1)}_{Z3}$	0.359	0.1844	-0.384	0.809
D_4	$\delta^{(2)}_{Q} + \delta^{(2)}_{D1D3} + \delta^{(2)}_{R^2}$	-0.037	-0.0247	0.83	0.101
$\sum_{k=2}^{4} D_k$	-	-1.590	-0.6251	-6.187	-3.791
X_{ref}	-	-1.664	-0.6986	-14.564	-8.220

Table 5.2.: Nuclear polarizability correction to the Lamb shift (in meV) for several light muonic atoms at various orders in the η-expansion. The reference X_{ref} are the δ_{TPE} values evaluated using the AV18+UIX interaction. Data from Ref. [39].

To proceed with the statistical analysis, we need to specify the prior probability distributions $\mathrm{pr}(\bar{c})$, $\mathrm{pr}(c_n|\bar{c})$ and $\mathrm{pr}(\eta)$. Whenever feasible, we will adhere to the principle of maximum entropy [113] in order to determine the least informative priors. Below we list a few considerations on the choice of the priors:

- The parameter $\bar{c}$ sets the overall scale of the dimensionless coefficients c_n. Our unbiased expectations of $\bar{c}$ can be encoded by adopting the Jeffreys' prior, $\mathrm{pr}(\bar{c}) \propto 1/\bar{c}$ [112], with only one constraint: $\bar{c}$ is a positive definite quantity. In order to work with a normalizable distribution, we introduce a slight modification and restrict the range of $\bar{c}$ from a minimum value of $c_< = 10^{-4}$ to a maximum value of $c_> = 10^4$ by multiplying with step functions $\theta(x)$.

- For $\mathrm{pr}(c_n|\bar{c})$, we present two different reasonable choices. The sensitivity of the obtained posterior distributions to these choices will indicate whether the data set provides enough information to dominate the analysis or not. Our first choice, labelled as prior A, assumes that the magnitude of the dimensionless coefficients can not be larger than $\bar{c}$. The maximum-entropy principle then leads to a uniform distribution in the range $-\bar{c} < c_i < \bar{c}$ with

[1] Again, these should not be confused with the sub-leading pion-nucleus LECs introduced in Section 3.2.

[2] The corrections of Table 5.2 are reported with the notation of Ref. [39], the superscript indicates at what order the correction appears in the η-expansion.

$i = m, ..., k$. Our second choice, labelled as prior B, is a Gaussian distribution with zero mean and standard deviation $\bar{c}$. This was initially introduced in nuclear effective field theories [120] and is motivated by the maximum-entropy principle. It assumes that there is testable information available regarding the means and standard deviations of the dimensionless coefficients.

- For $\text{pr}(\eta)$, we first note that this parameter is constrained to be positive. In the following discussion, we assume that the simple estimate of $\eta \sim 0.33$ can be considered as an informative measure for the mean of $\text{pr}(\eta)$. As shown in Section 4.3, the exponential distribution is the least-informative prior for a parameter which is positive definite and whose mean is known. We label this choice as α_η. In order to assess the stability of the statistical analysis conclusions under reasonable modifications of η-prior, we compare this choice with a β-distribution, denoted as $\beta(a, b)$, that constrains $\eta \in [0, 1]$. This alternative prior choice is referred to as β_η. The choice of the parameters of β_η should keep its mean equal to 0.33. There is an infinite set of β-distributions that satisfy this constraint. We select $a = 3.0$ and $b = 6.0$, because it holds a reasonable standard deviation for both the prior and the data to be informative.

We list in Table 5.3 the prior-choices for $\text{pr}(\bar{c})$ and $\text{pr}(c_n|\bar{c})$, while the prior choices for $\text{pr}(\eta)$ are listed in Table 5.4.

Priors	$\text{pr}(c_i\|\bar{c})$	$\text{pr}(\bar{c})$
A	$\frac{1}{2\bar{c}}\theta(\bar{c} - \lvert c_i\rvert)$	$\frac{1}{\ln(\bar{c}_>/\bar{c}_<)\bar{c}}\theta(\bar{c} - \bar{c}_<)\theta(\bar{c}_> - \bar{c})$
B	$\frac{1}{\sqrt{2\pi}\bar{c}}\exp\left(-\frac{c_i^2}{2\bar{c}^2}\right)$	$\frac{1}{\ln(\bar{c}_>/\bar{c}_<)\bar{c}}\theta(\bar{c} - \bar{c}_<)\theta(\bar{c}_> - \bar{c})$

Table 5.3.: Priors for the scale parameter $\bar{c}$ and for the dimensionless coefficients c_n.

Priors	$\text{pr}(\eta)$
α_η	$\frac{1}{\lambda}\exp(-\frac{\eta}{\lambda})$
β_η	$\beta(a, b)$

Table 5.4.: Priors for the expansion parameter η. The mean of the exponential distribution is $\lambda = 0.33$, while for the β-distribution we take $a = 3.0$ and $b = 6.0$.

Having specified the priors and described all the important aspects of the analysis, we now move on to the exposition of the results. Our first goal is to obtain a posterior probability distribution for the values of the expansion parameter η using Eq. (4.13). The results are shown in Figure 5.2 for different choices of the priors

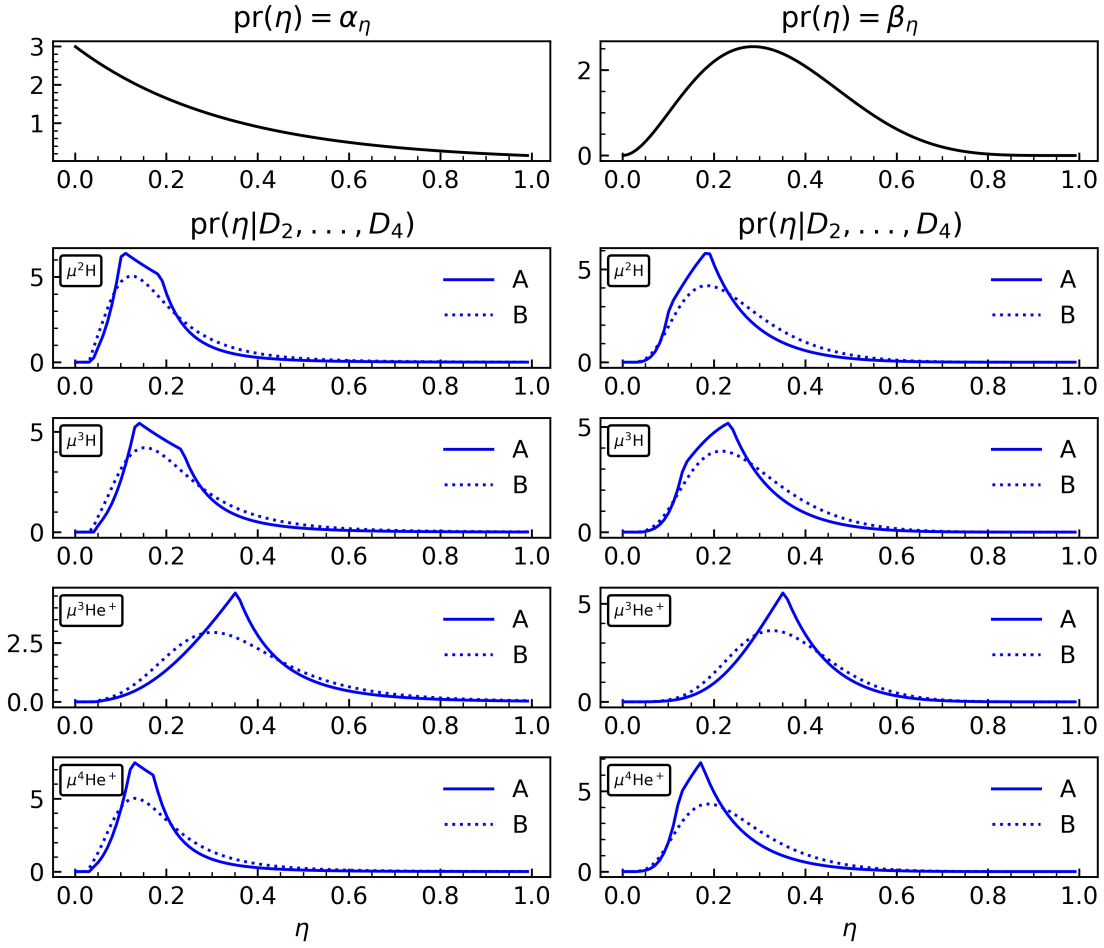

Figure 5.2.: (Upper panel) Prior probability distributions $\mathrm{pr}(\eta)$: α_η choice (left) and β_η choice (right). (Lower panels) Posterior probability distributions $\mathrm{pr}(\eta|\ D_2, D_3, D_4)$ for the choice of $\mathrm{pr}(\eta) = \alpha_\eta$ (left) and $\mathrm{pr}(\eta) = \beta_\eta$ (right) and two choices (A and B) of priors for $\mathrm{pr}(\bar{c})$ and $\mathrm{pr}(c_i|\bar{c})$.

$\mathrm{pr}(\eta)$, $\mathrm{pr}(c_n|\bar{c})$ and $\mathrm{pr}(\bar{c})$. Overall, the posterior distributions are quite stable under modifications of the priors, suggesting that there is enough information in the data sets to dominate the analysis. For $\mathrm{pr}(\eta)$ in particular, we note that the exponential distribution only assumes $\eta > 0$, whereas the β-distribution constrains $\eta \in [0, 1]$. We find only weak deviations in the results with the two priors, which increase the credibility of the assumption $\eta \in [0, 1]$, and that the expansion in Eq. (5.2) converges. Our Bayesian analysis indicates that the most likely η-value is smaller than the estimate obtained from the uncertainty principle for the μ^2H, μ^3H and μ^4He$^+$ systems, because the maximum-likelihood value of η is approximately 0.15.

As a next step, we address the evaluation of the truncation errors in the expansion of Eq. (5.3). By utilizing the posterior distributions $\mathrm{pr}(\eta|D_2, ..., D_4)$ of Figure 5.2, we calculate distributions for the truncation uncertainty $\mathrm{pr}(\Delta_4^{(1)}|D_2, ..., D_4)$

through a process of marginalization, as shown in Eq. (4.17). The results are shown in Figure 5.3. We also illustrate the confidence interval (CI) at the 68% and 95% level in Table 5.5. Again, the distributions show good stability when we modify the prior choices. We find a fairly good agreement between the 68% CI uncertainties of this work and the estimates in Refs. [39], with the exception of the truncation uncertainties in the $\mu^3\mathrm{He}^+$ system, which are roughly four times larger compared to Refs. [39]. We note that the 95% CIs in Table 5.5 are much larger than twice the size of the corresponding 68% CIs for all systems and all prior choices, indicates that the posterior probability distributions are not Gaussian. The η-prior α_η efficiently summarizes, through the maximum-entropy principle, the information available on the parameter η before the calculation of the data sets. On the other hand, the analysis with prior β_η makes additional assumptions about the value of η, e.g. it constrains η to a value smaller than 1. While this assumption is well supported by both prior and posterior information that is available, it does not allow us to diagnose divergences of the expansion in Eq. (5.2). Furthermore, the analysis with prior B for $\mathrm{pr}(c_i|\bar{c})$ is more sensitive to details of the distributions of the coefficients c_n comparing with the analysis with prior A. Based on our analysis, we conclude that the uncertainty estimates obtained with the combinations of priors α_η and B exhibit better calibration compared to other choices. Therefore, we recommend using the results obtained with these specific priors for future studies.

Atom	Prior	68% CI (α_η)	68% CI (β_η)	95% CI (α_η)	95% CI (β_η)	Ref. [39]
$\mu^2\mathrm{H}$	A	0.60	1.03	2.81	3.72	0.4
	B	0.79	1.38	3.46	4.07	
$\mu^3\mathrm{H}$	A	1.18	1.73	5.44	6.67	1.3
	B	1.52	2.29	6.88	7.73	
$\mu^3\mathrm{He}^+$	A	4.95	4.90	14.47	13.05	1.1
	B	4.81	4.74	14.99	13.87	
$\mu^4\mathrm{He}^+$	A	0.63	1.02	3.32	4.86	0.8
	B	0.89	1.55	4.70	5.80	

Table 5.5.: Truncation uncertainties of Eq. (5.2) expressed as confidence interval % for various prior choices.

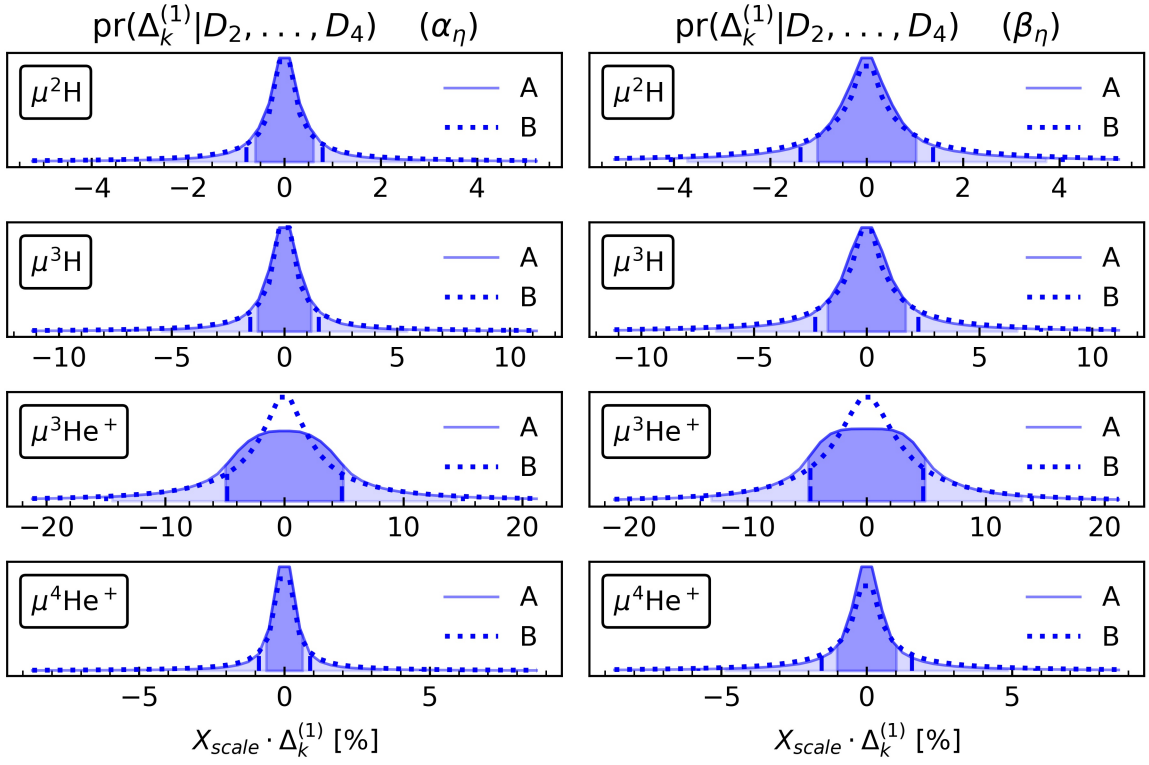

Figure 5.3.: Posterior distributions for the truncation uncertainties of Eq. (5.2). Results with $\mathrm{pr}(\eta)=\alpha_\eta$ (left) and $\mathrm{pr}(\eta)=\beta_\eta$ (right). Solid lines (dotted lines) denote posterior distributions obtained with choices A (B) for priors of Table 5.3. The 68% and 95% CI are reported as dark and light shaded areas for the prior choice A, respectively, while for the prior choice B they are reported as vertical dashed lines.

5.3. Benchmark tests of the local-chiral interaction in helium nuclei

With the goal of applying Bayesian inference to the nuclear structure corrections in muonic atoms, we have implemented a local version of the chiral interaction in our computational methods. This interaction was developed in Refs. [63, 94–96] up to N2LO. Here, we show the benchmark tests of this interaction on three- and four-body nuclei, published in *Frontiers in Physics* [2], as well as a new calculation of the photoabsorption cross-section of ^{4}He published in the same Journal [4].

In our calculations of the nuclear charge radii, $r_c^2 \equiv \langle r_c^2 \rangle$, we use

$$r_c^2 = r_{\rm pt}^2 + r_p^2 + \frac{A-Z}{Z} r_n^2 + \frac{3\hbar^2}{4m_p^2c^2}\,, \tag{5.4}$$

where $r^2_{\rm pt} \equiv \langle r^2_{\rm pt} \rangle$ is the calculated point-proton radius, $r_p = 0.8751(61)$ fm [121] is the root-mean-square (rms) charge radius of the proton, and $r^2_n = -0.1161(22)$ fm^2 [121] is the squared charge radius of the neutron. The last term is the Darwin-Foldy relativistic correction to the proton-charge radius [30]. We neglect the spin-orbit relativistic contribution, because it is negligible in s-shell nuclei [122], as well as two-body currents. Since the goal of this section is to benchmark our calculation against the available Monte-Carlo results, we have used the same numerical values for r_p and r_n as in Ref. [63], which follows the CODATA-2014 recommendations [121]. However we note that, nowadays there are more precise results coming from muonic atoms spectroscopy [25,123] and we recommend using these updated values when providing new predictions.

For a given observable, O, the numerical uncertainty, $\delta(O)$, is estimated as

$$\delta(O) = |O(K_{\rm max}) - O(K_{\rm max} - 2)| + |O(K_{\rm max} - 2) - O(K_{\rm max} - 4)| + \delta_{\rm res} \ , \quad (5.5)$$

where $O(K_{\rm max})$ is the expectation value of the observable computed by setting a given maximal value of $K_{\rm max}$, which is the maximal grand-angular momentum quantum number in the expansion of the wavefunction. $\delta_{\rm res}$ is the residual uncertainty (independent of K_{max}) obtained by varying the number of radial grid points (from 70 to 90), the maximal values of the angular momentum in the construction of the two-body effective interaction (from 60 to 120), and the maximal number of three-body angular momentum (from 5/2 to 7/2) in the partial wave expansion of the 3N force.

In the following, we first address and discuss the benchmarks of the interaction at LO and NLO in order to have a clean test on the NN interaction. Then we move to the N2LO, where the three-body forces are included.

Benchmarks at LO and NLO. We study the maximally-local chiral interactions with two different regulator cut-offs, $r_0 = 1.0$ fm and $r_0 = 1.2$ fm. The latter gives rise to a softer interaction compared to the former. For the benchmarks at LO and NLO, the ^{4}He is used as a testing ground. We compute point-proton charge radii $r^2_{\rm pt}$, and ground-state energies E_0, at increasing values of the grand-angular momentum quantum number and compare them to the GFMC calculations. The results are shown in Table 5.6, where the uncertainty is estimated as explained above with $K_{\rm max} = 22$. Taking into account the uncertainties, our final EIHH results agree well with the GFMC calculations, which is a strong validation of our implemented interaction up to this order.

Benchmarks at N2LO. We now turn to the benchmark at the next order. At N2LO we have the first appearance of 3N forces, so this serves as a check of our irreducible tensor representation. The 3N interaction involves two new LECs, c_D and c_E, coming from the one-pion-exchange and the contact term of the 3N forces,

	LO			NLO		
	Cut-off [fm]	E_0 [MeV]	$\sqrt{\langle r^2_{pt} \rangle}$ [fm]	Cut-off [fm]	E_0 [MeV]	$\sqrt{\langle r^2_{pt} \rangle}$ [fm]
EIHH	1.0	-42.830(6)	1.0370(3)	1.0	-21.55(4)	1.575(1)
	1.2	-46.6054(7)	1.01765(4)	1.2	-22.974(6)	1.5278(6)
GFMC	1.0	-42.83(1)	1.02(1)	1.0	-21.56(1)	1.57(1)
	1.2	-46.62(1)	1.00(1)	1.2	-22.94(6)	1.53(1)
Nature		-28.29566	1.46(1)		-28.29566	1.46(1)

Table 5.6.: Ground-state energies and point-proton radii for the ^{4}He nuclear system at LO and NLO computed with the EIHH method. For comparison we report the GFMC results and the experimental values (Nature) taken from Ref. [124,125].

respectively, which can not be fitted in the NN sector. In Ref. [96] these couplings have been fitted to reproduce the ^{4}He binding energy and the n-^{4}He scattering P-wave phase shift and the values reported in Table 5.7 were obtained. We employed the same values in [2] for the benchmark.

3N force	r_0 [fm]	c_E	c_D	c_1 [GeV^{-1}]	c_3 [GeV^{-1}]	c_4 [GeV^{-1}]
N2LO	1.0	-0.63	0.0	-0.81	-3.40	3.40
	1.2	0.085	3.5	-0.81	-3.40	3.40

Table 5.7.: Fit values for the couplings c_D and c_E for different choices of 3N cut-offs as reported in [63,96]. The constants $c_{1,3,4}$ are tuned in the pion-nucleon sector, see Ref. [50].

As a testing ground for our N2LO Hamiltonian expressed in terms of spherical tensors, we study the three-body ^{3}He, and ^{3}H and the four-body ^{4}He nuclear systems. We calculate ground-state energies E_0, and charge radii r^2_c, for the two different cut-off choices $r_0 = 1.0$ and 1.2 fm and carefully study the convergence with increasing K_{max} values. The K_{max} convergence is explicitly shown in a graphical manner in Fig. 5.4, Fig. 5.5, and Fig. 5.6, where we compare with the GFMC method. Our final EIHH results with numerical uncertainties quantified as explained in Eq. (5.5) with $K_{max} = 22$ are shown in Table 5.8 comparing with the GFMC, the auxiliary-field diffusion Monte-Carlo (AFDMC) method and the experimental data. The theoretical computations agree with each other at a similar level as observed in other benchmarks [126]. Note that for the harder cut-off $r_0 = 1.0$ fm, EIHH and GFMC results are in agreement within error bars while AFDMC

	Cut-off [fm]	^{3}He		^{3}H		^{4}He	
		E_0 [MeV]	$\sqrt{\langle r_c^2 \rangle}$ [fm]	E_0 [MeV]	$\sqrt{\langle r_c^2 \rangle}$ [fm]	E_0 [MeV]	$\sqrt{\langle r_c^2 \rangle}$ [fm]
EIHH	1.0	-7.630(6)	1.976(7)	-8.338(5)	1.759(6)	-28.34(5)	1.656(6)
	1.2	-7.619(4)	1.974(5)	-8.332(3)	1.758(5)	-28.31(2)	1.651(4)
GFMC	1.0	-7.65(2)	1.97(2)	-8.34(1)	1.72(3)	-28.30(1)	1.65(2)
	1.2	-7.63(4)	1.97(1)	-8.35(4)	1.72(4)	-28.30(1)	1.64(1)
AFDMC	1.0	-7.55(8)	1.96(2)	-8.33(7)	1.72(2)	-27.64(13)	1.68(2)
	1.2	-7.64(4)	1.95(5)	-8.27(5)	1.73(2)	-28.37(8)	1.65(1)
Nature		-7.718043(2)	1.973(14)	-8.481798(2)	1.759(36)	-28.29566	1.681(4)

Table 5.8.: Ground-state energies and charge radii for the nuclear ^{3}He, ^{3}H and ^{4}He systems at N2LO in the chiral expansion computed with the EIHH, GFMC and AFDMC method. The GFMC and AFDMC results are from [63, 96, 124, 127]. Experimental values (Nature) are from Ref. [125, 128–130].

ones have some discrepancy. Given that the AFDMC method is known to be less accurate, we do not consider this difference to be significant. In summary, all these results constitute a successful benchmark for our implementation of 3N forces.

A much improved agreement with experiment is obtained at N2LO. In fact, if one compares the experimental binding energies with the LO and NLO calculations in Table 5.6 one observes that these low orders either overbind (LO) or underbind (NLO) the few-body nuclei, while N2LO nicely agree with experiments. For ^{4}He it is well expected, given that 3N forces are fit to reproduce the ^{4}He binding energy. A good agreement is also found for ^{3}He and ^{3}H due to the strong correlation between the three- and four-body binding energy.

A nice converging pattern is also found for the nuclear charge radii. From a closer look at Table 5.8, one would appreciate that our EIHH calculations are more precise than the GFMC and AFDMC results in the three-nucleon sector and that our numerical uncertainty for the radii is comparable to the experimental values. This is expected, since the nuclear radii are sensitive to the tails of the wavefunction which is usually well reproduced with the hyperspherical harmonics. While this may be an advantage of our method, it is important to note that the error bars quoted in this table do not include the uncertainties coming from the ChEFT expansion and do not constitute the full uncertainty of the theory. In light nuclei, the ChEFT dominates the uncertainty budget.

We expect the uncertainty coming from the ChEFT expansion to dominate the uncertainty budget in observables of light nuclei.

To further check the quality of the interaction, we calculate the inclusive photoabsorption cross-section of ^{4}He in the unretarded-dipole approximation, see

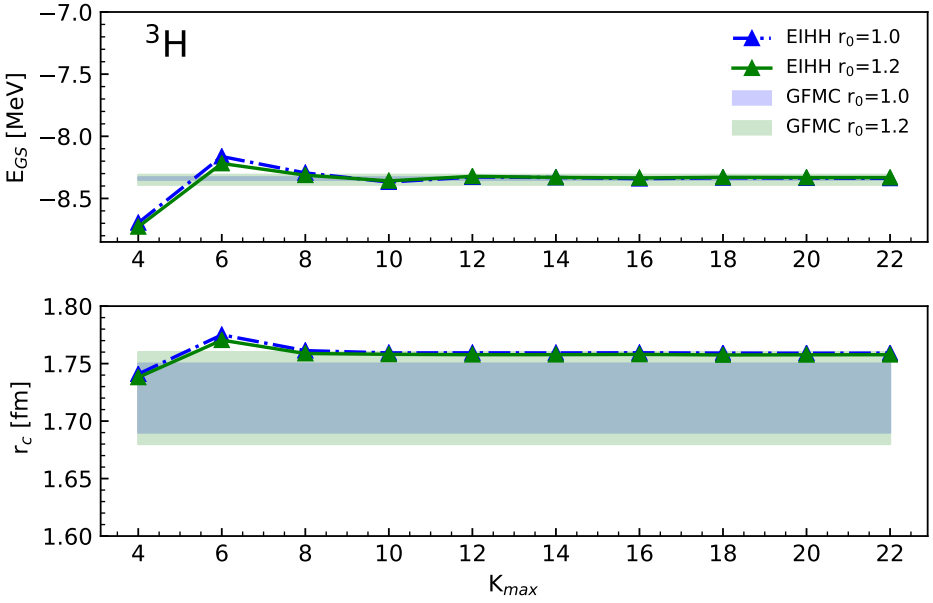

Figure 5.4.: Ground-state energy and charge radius of the nuclear ^{3}H system as a function of the grand-angular momentum quantum number $K_{\max}$. The green and blue error-bands are the GFMC results with the relative statistical uncertainty.

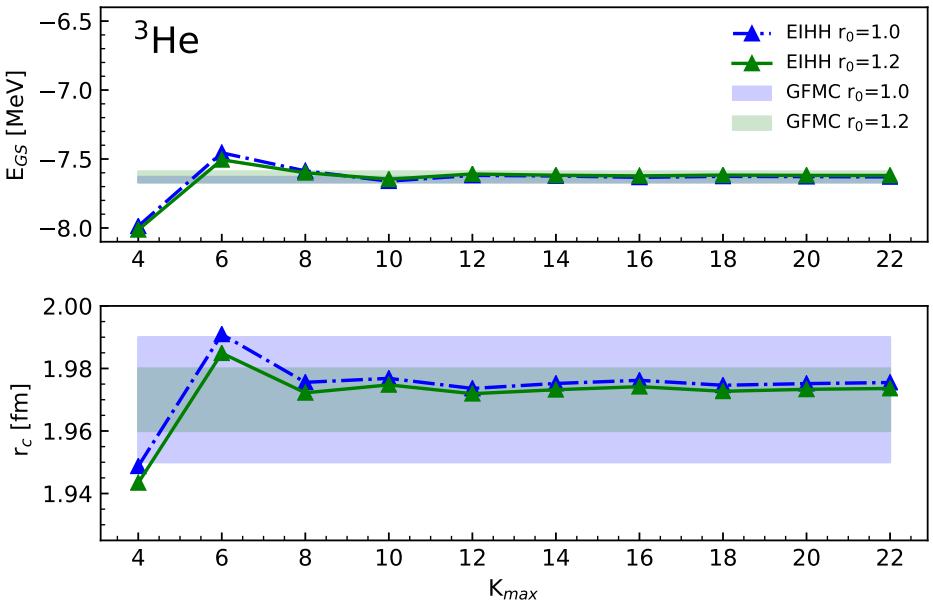

Figure 5.5.: Ground-state energy and charge radius of the nuclear ^{3}He system as a function of the grand-angular momentum quantum number $K_{\max}$. The green and blue error-bands are the GFMC results with the relative statistical uncertainty.

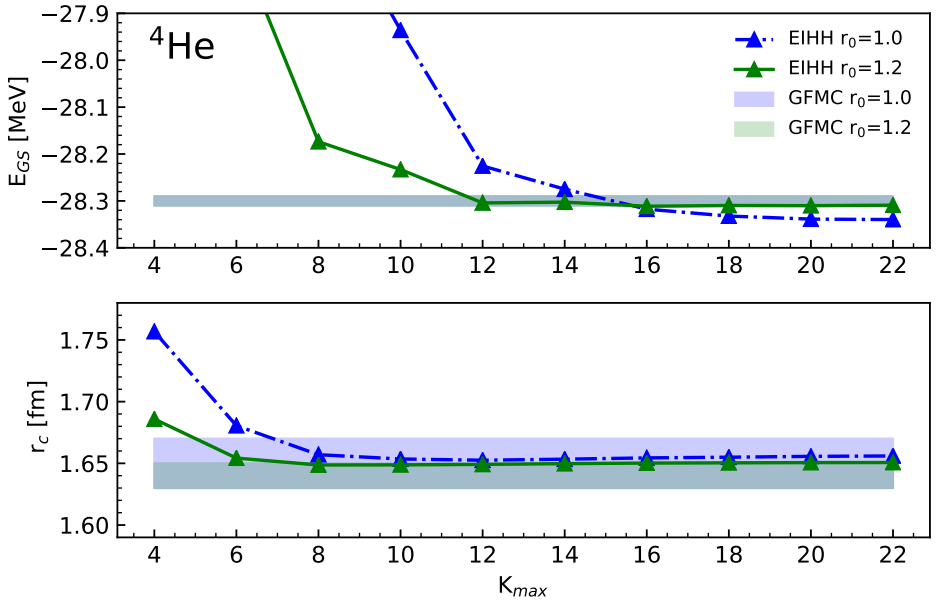

Figure 5.6.: Ground-state energy and charge radius of the nuclear ^{4}He system as a function of the grand-angular momentum quantum number $K_{\max}$. The green and blue error-bands are the GFMC results with the relative statistical uncertainty.

Eq. (5.1), and compare against experimental data [131]. We estimate the uncertainty due to the ChEFT truncation using the algorithm proposed in Ref. [132]. The results are shown in Figure 5.7. We find a good agreement with the data once the ChEFT truncation uncertainties are included, see Figure 5.7 (right panel).

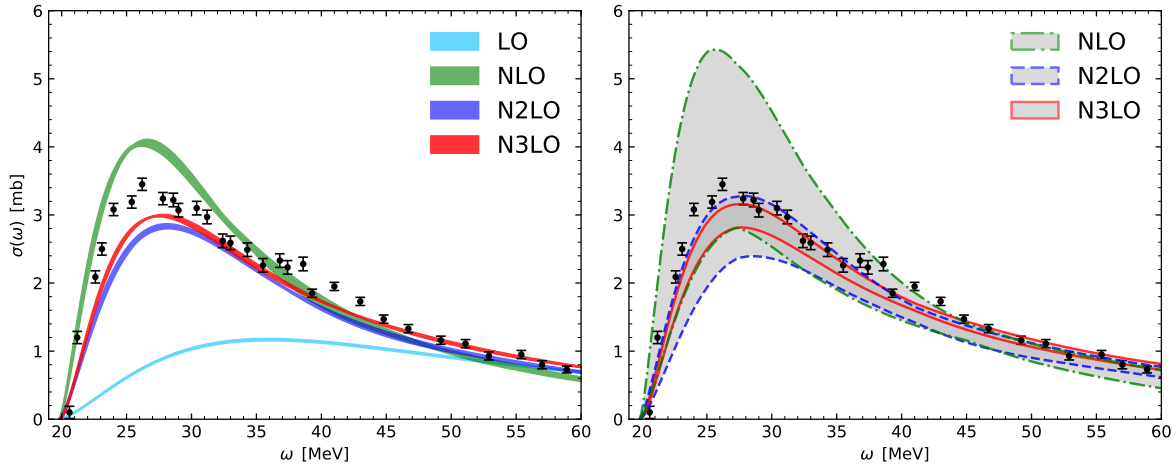

Figure 5.7.: Inclusive ^{4}He photoabsorption cross-section calculated at different orders in ChEFT. Left panel: bands display the numerical uncertainty. Right panel: bands display the ChEFT truncation uncertainty estimated with the algorithm proposed in [132]. Experimental data from Ref. [131].

5.4. Nuclear polarizabilities in muonic helium atoms

In this section we perform an order-by-order calculation of the nuclear structure effects in muonic helium ions and assess the theory uncertainty with Bayesian statistics. The paper on this work is currently in preparation [6].

First, to compare with Ref. [39], we include in the calculation of the two-photon-exchange not only the terms obtained in Chapter 2 in Eq. (2.85–2.98), but also the very small magnetic dipole term, denoted below as δ_{M1}. Since we did not derive this correction ourselves, we directly use the definition given in Ref. [39]. We perform calculations without including the electron vacuum polarization corrections of Eq. (2.97) and Eq. (2.98). It is because Eq. (2.98) requires the evaluation of the radius r_L shown in Eq. (2.84) which is not an easy observable to obtain, and in Ref. [5] it was only estimated as $r_L \sim 2\, r_c$, with r_c being the nuclear charge radius. To have a better quantification of uncertainties, we prefer to use Bayesian methods to quantify only the uncertainties of the calculated, as opposed of the estimated, terms. Accordingly, we take the value of $\delta_{\rm eVP}$ from Ref. [5].

We first calculate the terms listed in Section 2.4 at N2LO in ChEFT. The results obtained with the two short-range cut-offs are shown in Fig. 5.8 for $\mu^3{\rm He}^+$ and Fig. 5.9 for $\mu^4{\rm He}^+$. The differences between the two cut-offs emerge as regulator artifacts [63]. In order to maximally reduce our sensitivity to these unphysical effects, we take as our final results the calculations with the lower cut-off $r_0 = 1.0$ fm, as they are expected to be less affected by possible regulator artifacts. These are shown in Table 5.9.

Our next goal is to estimate the uncertainties due to the truncation of ChEFT. This is done by performing an order-by-order analysis. Namely we re-calculate the terms shown in section 2.4 but by using chiral interaction at LO and NLO. This allows us to employ the Bayesian techniques developed in the previous chapter and study the convergence pattern of the two-photon-exchange correction to the $2S$-states in muonic helium, $\delta_{\rm TPE}$, as[3]

$$\begin{aligned} \delta_{\rm TPE} &= D_0 + D_2 + D_3 + ... \\ &= X_{\rm ref} \left[\, c_0 \, + c_2 \, Q^2 + c_3 \, Q^3 + ... \, \right], \end{aligned} \tag{5.6}$$

where D_0 is the result of $\delta_{\rm TPE}$ obtained using the LO chiral interaction, D_2 is obtained using the NLO interaction, D_3 is obtained using the N2LO interaction. Q is the expansion parameter in ChEFT, $Q = \max\{m_\pi, p\}/\Lambda$ with p being the average nucleon momenta, m_π the pion mass and Λ the breakdown scale of

[3]Note that there is no operator of order Q in the ChEFT hamiltonian, thus the NLO is already of order Q^2 and in Eq. (5.6) we have $c_1 = 0$.

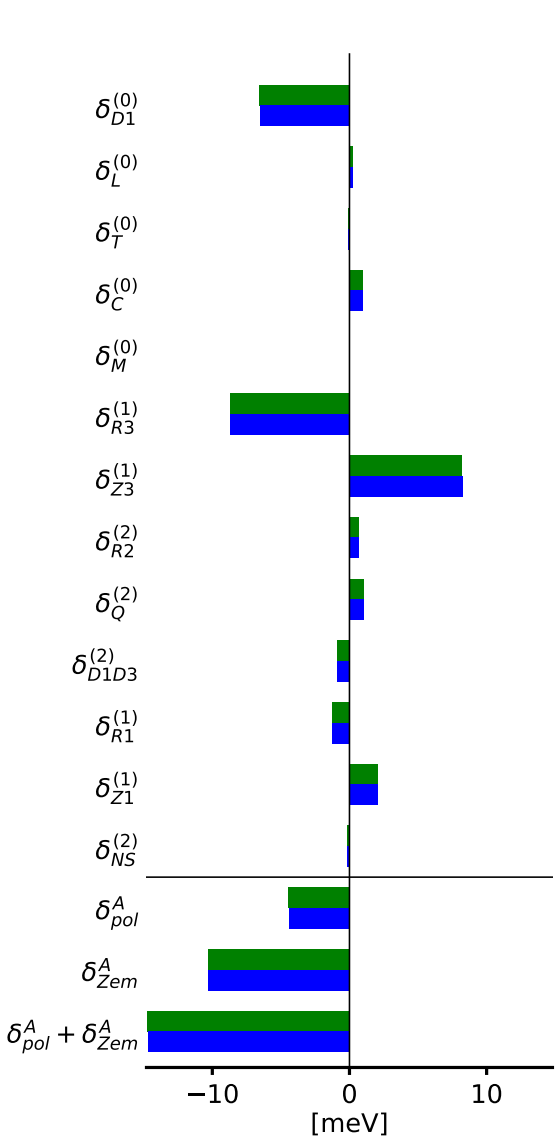

	$r_0 = 1.2$	$r_0 = 1.0$
$\delta^{(0)}_{D1}$	-6.562	-6.552
$\delta^{(0)}_{L}$	0.232	0.232
$\delta^{(0)}_{T}$	-0.104	-0.104
$\delta^{(0)}_{C}$	1.018	1.015
$\delta^{(0)}_{M}$	0.008	0.008
$\delta^{(1)}_{R3}$	-8.674	-8.691
$\delta^{(1)}_{Z3}$	8.223	8.255
$\delta^{(2)}_{R2}$	0.67	0.701
$\delta^{(2)}_{Q}$	1.043	1.062
$\delta^{(2)}_{D1D3}$	-0.877	-0.899
$\delta^{(1)}_{R1}$	-1.297	-1.302
$\delta^{(1)}_{Z1}$	2.054	2.057
$\delta^{(2)}_{NS}$	-0.191	-0.193
δ^{A}_{pol}	-4.458	-4.411
δ^{A}_{Zem}	-10.277	-10.312
$\delta^{A}_{pol} + \delta^{A}_{Zem}$	-14.735	-14.723

Figure 5.8.: Relative strengths of the nuclear structure corrections to the $2S$-states of $\mu^3\mathrm{He}^+$ at order $(Z\alpha)^5$ with the inclusion of the higher-order Coulomb distortion $\delta^{(0)}_C$ which is of order $(Z\alpha)^6 \log(Z\alpha)$.

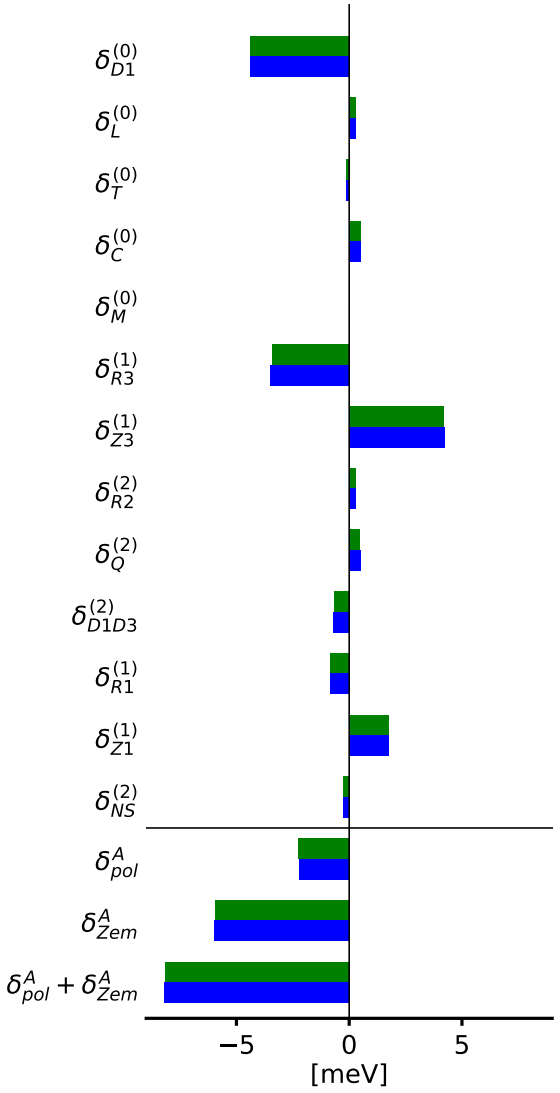

	$r_0 = 1.2$	$r_0 = 1.0$
$\delta^{(0)}_{D1}$	-4.386	-4.373
$\delta^{(0)}_{L}$	0.272	0.287
$\delta^{(0)}_{T}$	-0.124	-0.125
$\delta^{(0)}_{C}$	0.517	0.514
$\delta^{(0)}_{M}$	0.011	0.011
$\delta^{(1)}_{R3}$	-3.422	-3.477
$\delta^{(1)}_{Z3}$	4.171	4.23
$\delta^{(2)}_{R2}$	0.267	0.285
$\delta^{(2)}_{Q}$	0.484	0.505
$\delta^{(2)}_{D1D3}$	-0.668	-0.69
$\delta^{(1)}_{R1}$	-0.846	-0.856
$\delta^{(1)}_{Z1}$	1.749	1.758
$\delta^{(2)}_{NS}$	-0.272	-0.277
δ^{A}_{pol}	-2.254	-2.208
δ^{A}_{Zem}	-5.92	-5.988
$\delta^{A}_{pol} + \delta^{A}_{Zem}$	-8.174	-8.196

Figure 5.9.: Relative strengths of the nuclear structure corrections to the $2S$-states of $\mu^4\mathrm{He}^+$ at order $(Z\alpha)^5$ with the inclusion of the higher-order Coulomb distortion $\delta^{(0)}_C$ which is of order $(Z\alpha)^6 \log(Z\alpha)$.

	μ^3He [meV]	μ^4He [meV]
δ_{D1}	-6.552	-4.373
δ_C	1.015	0.514
δ_L	0.232	0.287
δ_T	-0.104	-0.125
δ_{M1}	0.008	0.011
δ_{R3}	-8.691	-3.477
δ_{Z3}	8.255	4.230
δ_{R2}	0.701	0.285
δ_Q	1.062	0.505
δ_{D1D3}	-0.899	-0.690
δ_{R1}	-1.302	-0.856
δ_{Z1}	2.057	1.758
δ_{NS}	-0.193	-0.277
δ_{pol}	-4.411	-2.208
δ_{Zem}	-10.312	-5.988
δ_{TPE}	-14.723	-8.196

Table 5.9.: Nuclear structure corrections to the $2S$-states in $\mu^3\text{He}^+$ and $\mu^4\text{He}^+$ at N2LO in the chiral expansion with the cut-off choice of $r_0 = 1.0$ fm.

ChEFT. In this work, we made the following choices for the expansion parameters: $Q(\mu^3\text{He}^{2+}) = 0.279$ and $Q(\mu^4\text{He}^{2+}) = 0.356$. These correspond to assuming a breakdown scale of $\Lambda = 500$ MeV and a low-energy scale of m_π in ^{3}He, while in ^{4}He we estimate that $p > m_\pi$ and use $p = 178.0$ MeV. The reference scale X_{ref} is, in all cases, taken as the result in Ref. [39] with the AV18+UIX interaction.

In Ref. [39] a partial N3LO calculation of δ_{TPE} is presented, which is obtained by using NN forces at N3LO and 3N forces at N2LO[4]. The uncertainty due to the nuclear Hamiltonian was then estimated in Ref. [39] by comparing the prediction of the N3LO chiral interaction against the one of the AV18+UIX. With an order-by-order analysis of the chiral expansion, where we also include the partial N3LO calculation, we can improve that uncertainty quantification.

In fact, we propagate the uncertainty estimate of Eq. (5.6) to the next order, namely we include the term $X_{\text{ref}} c_4 Q^4$ using the result of the N3LO calculation in [39]. The full Bayesian analysis is shown in Figure. 5.10. We obtain that at each order the truncation uncertainty of the chiral expansion reduces by roughly

[4]As discussed at the end of Chapter 3, it is impossible to perform a calculation with consistent 3N forces at N3LO, since these forces have not been derived yet.

a factor of 3, which is expected given an expansion parameter $Q \sim 0.3$.

However, when going from LO to NLO the uncertainty increases, which is due to the peculiar pattern of the dimensionless expansion coefficients $\{c_0, c_2\}$: the coefficient c_0 is always much smaller than c_2. This means that, when we truncate the expansion at LO, the Bayesian analysis tends to underestimate the uncertainty since it generates a probability distribution for $\mathrm{pr}(\bar{c}|c_0)$ peaked in the neighborhood of the calculated c_0. Once the NLO expansion coefficient c_2 is included, the Bayesian analysis re-elaborates the uncertainty budget and predicts a much larger uncertainty. This is consistent with the previous calculations of δ_{TPE} shown as the vertical lines in Figure. 5.10. We expect that the LO coefficient, c_0, is the only outlier, and that all the uncertainties starting from NLO reflect the true truncation errors of the ChEFT for δ_{TPE}.

The nuclear structure corrections to the Lamb-shift of muonic atoms consist of different sources of uncertainties which are summarized in Table 8 of Ref. [39]. We update three sources of uncertainties of that table: the numerical, nuclear model, and η-expansion terms. We report an updated list of the uncertainties in Table 5.10. Our numerical precision is at the sub-percentage level which is comparable to what was previously obtained in Ref. [39]. The nuclear model uncertainties are larger at N2LO but slightly smaller when we extend the Bayesian analysis to N3LO. For the η-expansion uncertainties we get a comparable result in $\mu^4\mathrm{He}^+$ but a much larger uncertainty in $\mu^3\mathrm{He}^+$. Finally note that compared to Table 8 of Ref. [39], we removed the quoted uncertainty due to the $Z\alpha$ expansion to avoid double counting with the uncertainty given in the three-photon-exchange, see Table 1.1.

Our final predictions for the two-photon-exchange correction to the energies of $2S$-states in muonic helium ions are:

$$\delta_{\mathrm{TPE}}(\mu^3\mathrm{He}^+) = \begin{cases} -14.723(955)\ \mathrm{meV} & (\mathrm{N2LO}) \\ -14.868(357)\ \mathrm{meV} & (\mathrm{N3LO}) \end{cases}, \tag{5.7}$$

$$\delta_{\mathrm{TPE}}(\mu^4\mathrm{He}^+) = \begin{cases} -8.196(900)\ \mathrm{meV} & (\mathrm{N2LO}) \\ -8.751(303)\ \mathrm{meV} & (\mathrm{N3LO}) \end{cases}, \tag{5.8}$$

which, compared to Ref. [5], include the Coulomb distortion effects but not the two-photon exchange of individual nucleons. Following Ref. [5] we then include the two-photon exchange terms of individual nucleons, the electron-vacuum polarization, the three-photon exchange, the very small muon self energy, and muon vacuum polarization corrections. We obtain

$$\delta_{\mathrm{NS}}(\mu^3\mathrm{He}^+) = \begin{cases} -15.499(981)\ \mathrm{meV} & (\mathrm{N2LO}) \\ -15.644(421)\ \mathrm{meV} & (\mathrm{N3LO}) \end{cases}, \tag{5.9}$$

$$\delta_{\mathrm{NS}}(\mu^4\mathrm{He}^+) = \begin{cases} -8.986(917)\ \mathrm{meV} & (\mathrm{N2LO}) \\ -9.541(351)\ \mathrm{meV} & (\mathrm{N3LO}) \end{cases}. \tag{5.10}$$

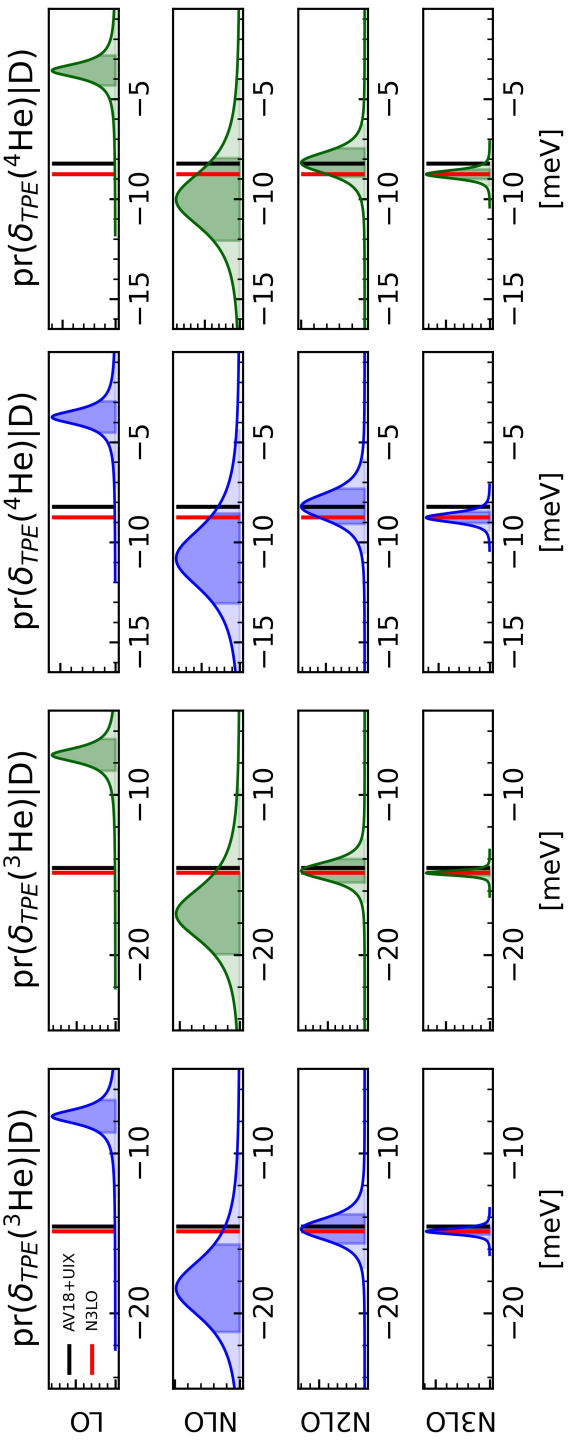

Figure 5.10.: Bayesian analysis of the ChEFT truncation errors in the two-photon-exchange correction of muonic helium ions. Results in blue are obtained using the cut-off a $r_0 = 1.0$ fm, while results in green are obtained with the choice $r_0 = 1.2$ fm. The vertical lines are the previous calculations of Ref. [39]. The last row is obtained from the calculation of Ref. [39], denoted with N3LO.

5.4.1. Nuclear charge radii and helium isotope shift

In a recent review, currently submitted to *Review of Modern Physics* [5], we summarized the theory of the Lamb-shift in light-muonic ions. This summary of the atomic, nuclear and hadronic effects in the Lamb-shift is important, because it allows to extract the nuclear charge radii from spectroscopy experiments in muonic ions.

We start from Eq. (1.1), and by using the value of E_{LS} from the recent laser spectroscopy experiments in muonic helium [26, 27], the updated QED theory, E_{QED}, of Ref. [5] and our new values of the nuclear structure corrections from Eq. (5.9) and Eq. (5.10), we can extract updated charge radii of the ^{3}He and ^{4}He nuclei, obtaining

$$r_c(^3\mathrm{He}) = \begin{cases} 1.9700(24)\ \mathrm{fm} & (\mathrm{N2LO}) \\ 1.9704(10)\ \mathrm{fm} & (\mathrm{N3LO}) \end{cases} , \tag{5.11}$$

$$r_c(^4\mathrm{He}) = \begin{cases} 1.6777(26)\ \mathrm{fm} & (\mathrm{N2LO}) \\ 1.6793(10)\ \mathrm{fm} & (\mathrm{N3LO}) \end{cases} . \tag{5.12}$$

These are compared to previous extractions in Figure. 5.11 and Figure. 5.12, for μ^3He and μ^4He, respectively.

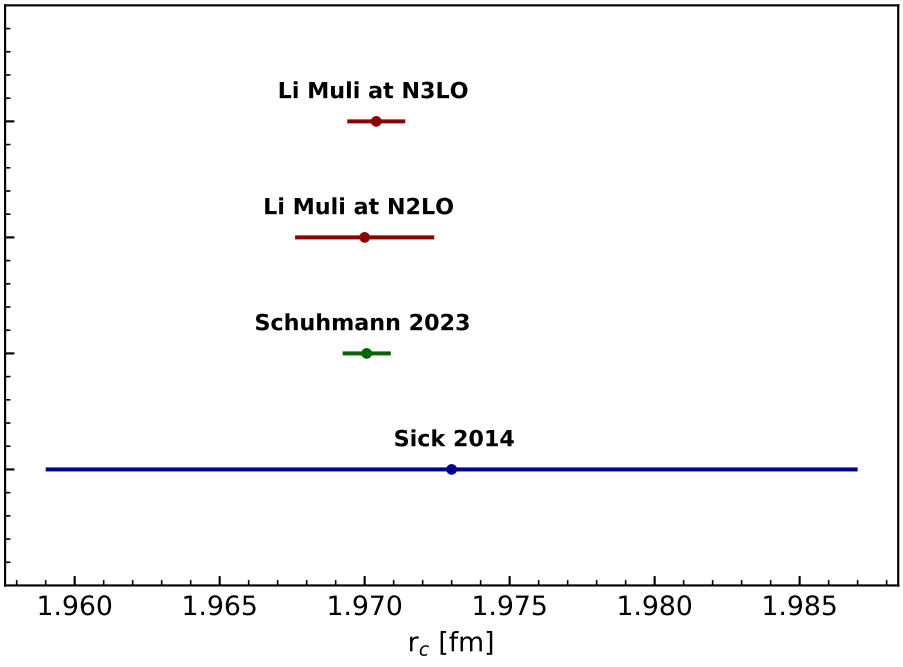

Figure 5.11.: Recent determinations of the ^{3}He charge radius. The blue line is the electron scattering experiments of [128], the green line is the spectroscopy of $\mu^3\mathrm{He}^+$ [27] using the theory in Ref. [5]. Red points are the results in [6].

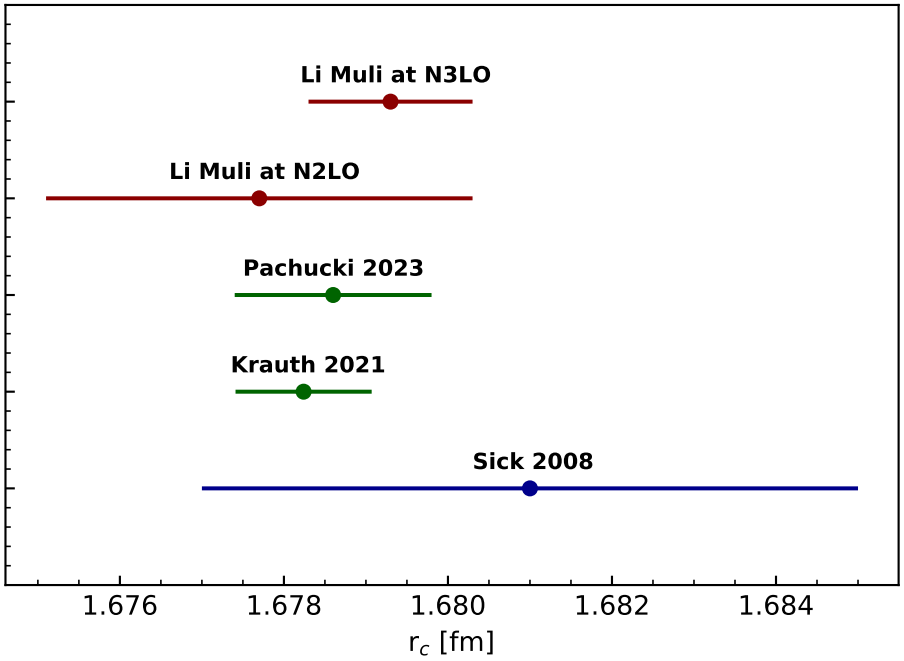

Figure 5.12.: Recent determinations of the ^{4}He charge radius. The blue line is the electron scattering experiments from [133], the green line is the spectroscopy of $\mu^4\mathrm{He}^+$ from [26] using the theory of the nuclear structure effects in [39] (Krauth 2021) and in [5] (Pachucki 2023). Red points are the results in [6].

The helium isotope shift. Due to partial cancellation of uncertainties, Eq. (1.1) can be used to obtain the difference of the squared nuclear charge radii, $\delta r^2 = r_c^2(^3\mathrm{He}) - r_c^2(^4\mathrm{He})$, with better precision than the individual charge radii. Furthermore, an independent value of δr^2 can be obtained by combining the isotope shift theory of ordinary helium atoms [5,134,135], with the results of laser spectroscopy experiments in neutral helium [136–140]. Comparing the predictions of δr^2 from muonic and ordinary atoms is important, since it allows to perform consistency checks between experiment and theory and can probe possible violations of lepton universality. Recently, two values for δr^2 from muonic and ordinary atoms have been extracted, which are in a 3.6 σ disagreement [27,140].

Here, we analyze the current discrepancy by updating the theory of the isotope shift in the $2\mathrm{P}_{1/2} - 2\mathrm{S}_{1/2}$ transition of muonic helium ions, by using our results for the nuclear structure effects in Eq. (5.9) and Eq. (5.10). We obtain

$$\delta r^2 = \begin{cases} \frac{\mathrm{E_{LS}}(\mu^3\mathrm{He}^+)}{\mathcal{C}(\mu^3\mathrm{He}^+)} - \frac{\mathrm{E_{LS}}(\mu^4\mathrm{He}^+)}{\mathcal{C}(\mu^4\mathrm{He}^+)} + 0.2612(51)\ \mathrm{fm}^2 & \text{(N2LO)} \\ \frac{\mathrm{E_{LS}}(\mu^3\mathrm{He}^+)}{\mathcal{C}(\mu^3\mathrm{He}^+)} - \frac{\mathrm{E_{LS}}(\mu^4\mathrm{He}^+)}{\mathcal{C}(\mu^4\mathrm{He}^+)} + 0.2574(31)\ \mathrm{fm}^2 & \text{(N3LO)} \end{cases} , \tag{5.13}$$

where E_{LS} are the experimentally measured values of the Lamb-shift in muonic helium ions and the values of $\mathcal{C}$ are given in Table 1.1. Using this updated theory of the isotope shift, and the recent laser spectroscopy experiments in muonic helium ions [26, 27], we obtain

$$\delta r^2 = \begin{cases} 1.0664(52)\ \text{fm}^2 & \text{(N2LO)} \\ 1.0626(32)\ \text{fm}^2 & \text{(N3LO)} \end{cases}, \tag{5.14}$$

in agreement with the previous value from muonic helium [5, 27]. When comparing with the prediction of δr^2 obtained from the isotope shift in neutral helium [134, 135, 140], at N2LO we find that the disagreement weakens, but it is then reinforced at N3LO, given our updated central value and reduced uncertainty. The results are shown in Figure 5.13 and prove the relevance of the calculations performed in this thesis in the context of precision atomic physics.

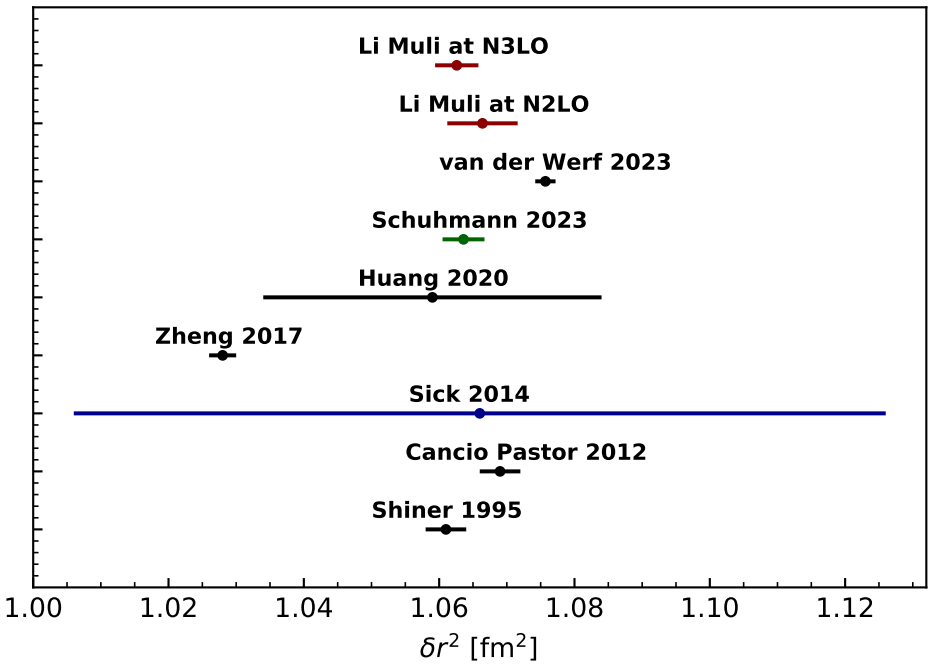

Figure 5.13.: Squared charge radius difference between the ^{3}He and ^{4}He. The blue point is from electron scattering [128]. Points in black are spectroscopy of ordinary atoms: Shiner [136], Cancio Pastor [137], Zheng [138], Huang [139] and van der Werf [140], respectively. The point in green is the spectroscopy of muonic helium ions [26, 27]. Red points are from [6].

	$\mu^3\mathrm{He}^+$			$\mu^4\mathrm{He}^+$		
	δ_{pol} [%]	δ_{Zem} [%]	δ_{TPE} [%]	δ_{pol} [%]	δ_{Zem} [%]	δ_{TPE} [%]
Numerical [39]	0.4	0.1	0.1	0.4	0.3	0.4
Numerical	0.1	0.2	0.1	0.4	0.3	0.2
Nuclear model [39]	0.7	1.8	1.5	3.9	4.6	4.4
Nuclear model (N2LO)	4.8	6.9	6.2	14.5	9.4	11
Nuclear model (N3LO)	1.6	1.6	1.4	4.1	2.8	3
η-expansion [39]	1.1	–	0.3	0.8	–	0.2
η-expansion	4.8	–	1.4	0.9	–	0.2
$Z\alpha$ [39]	1.5	0.0	0.4	1.5	0.0	0.4
$Z\alpha$	–	–	–	–	–	–
ISB [39]	1.8	0.2	0.5	2.2	0.5	0.5
Nucleon-size [39]	1.2	1.3	0.9	2.7	2.0	1.2
Relativistic [39]	0.4	–	0.1	0.1	–	0.0
Coulomb [39]	3.0	–	0.9	0.4	–	0.1
Total [39]	4.2	2.2	2.1	5.5	5.1	4.6
Total (N2LO)	7.6	6.9	6.5	10.6	9.6	10.9
Total (N3LO)	6.3	2.1	2.4	5.3	3.5	3.5

Table 5.10.: Relative uncertainties of the two-photon-exchange (plus the Coulomb distortion) correction in muonic helium atoms, compared with the previous estimates of Ref. [39]. The total uncertainties are obtained by a quadrature sum.

6. Conclusions

In this thesis, we have studied the nuclear structure corrections to the Lamb-shift of muonic helium and lithium hydrogen-like atoms.

In muonic lithium ions, we have theoretically estimated nuclear structure corrections to the Lamb-shift, which on the one hand agree fairly well with the independent estimates of Ref. [119] based on experimental data, and on the other hand extend Ref. [119] with the inclusion of several new terms. We used the theory summarized in Section 2.4 and calculated the corrections related to the electric dipole nuclear response function with the semi-realistic AV4′ interaction. We estimated the remaining non-dipole terms of Section 2.4 by assuming some scaling properties with the known corrections in muonic helium. The predicted energy corrections to the Lamb-shift are $E_{TPE}(^6Li^{2+}) = 196$ meV and $E_{TPE}(^7Li^{2+}) = 166$ meV. Due to the simplified version of the nuclear interaction used in this work, and to the assumptions made in scaling the missing terms from the results of muonic helium, these numbers are intended to provide only the order-of-magnitude of the nuclear structure effects, which might nevertheless be helpful for experimental physicists searching for the frequency of the atomic transition. This work is timely in view of the planned experimental activity in muonic lithium ions [28], and serves as a preparatory step for future work aiming at a complete ab-initio calculation.

For muonic helium ions, we have calculated the nuclear structure corrections originating from the two-photon-exchange diagram with realistic NN and 3N interactions using the effective interaction hyperspherical harmonics method. Compared to what was previously done in Refs. [39,40], we have: calculated δ_{TPE} at various orders in ChEFT, included for the first time the electron-vacuum-polarization correction to the leading nuclear polarizabilities, see Eq. (2.97) and Eq. (2.98), and quantified the uncertainties with Bayesian inference. The results of this work, together with the recent spectroscopy experiments in muonic helium ions [26, 27] and the relevant QED theory [5], allow to extract new values for the charge radii of the ^{3}He and ^{4}He nuclei. Our results at N2LO lead to $r_c(^3\text{He}) = 1.9700(24)$ fm and $r_c(^4\text{He}) = 1.6777(26)$ fm, while at N3LO we obtain $r_c(^3\text{He}) = 1.9704(10)$ fm and $r_c(^4\text{He}) = 1.6793(10)$ fm.

Due to partial cancellation of uncertainties, from Eq. (1.1) we can extract the difference of the squared nuclear charge radii with better precision than the individual charge radii. The same quantity can also be extracted from the theory

of the isotope shift of ordinary helium [134, 135] and laser spectroscopy experiments in helium atoms. In view of the recent disagreement between the values obtained from muonic helium ions [27] and helium atoms [140], we have updated the isotope shift theory of the Lamb-shift of muonic helium using the nuclear structure corrections calculated in this work. Then, the laser spectroscopy experiments in muonic helium ions [26, 27] allow us to extract new values for the difference of the squared nuclear charge radii. At N2LO we obtain $r_c^2(^3\mathrm{He}) - r_c^2(^4\mathrm{He}) = 1.0664(52)$ fm^2, while at N3LO we get $r_c^2(^3\mathrm{He}) - r_c^2(^4\mathrm{He}) = 1.0626(32)$ fm^2. The results are in perfect agreement with the previous prediction from spectroscopy of muonic atoms [27]. However, we see a slight deviation at N2LO with the result obtained from neutral helium spectroscopy [140], which is reinforced at N3LO in view of our different central value and reduced uncertainty compared to N2LO.

Finally, we present an overview of the future prospects of this research line:

1. The three-photon-exchange (3PE) correction has been calculated so far only in muonic deuterium [45]. The correction is expected to be large, and it has been roughly estimated in muonic helium with an uncertainty of 100%. In the future, it might be possible to calculate this effect with a relative precision of 20% or better, which will improve the precision of the extraction of the nuclear charge radii by $\sim 10\%$.

2. Given that the η-expansion is one of the largest source of uncertainty in $\mu^3\mathrm{He}^+$, the calculation of the next term in the expansion, see Eq. (2.66), should be addressed. This could lead to a further 10% improvement in the precision of the extracted charge radius. Another promising approach is to calculate the nuclear structure corrections in $\mu^3\mathrm{He}^+$ without making use of the η-expansion at all [38, 141]. The calculation is numerically challenging, but should be feasible in a three-body system.

3. Complete ab-initio calculations of muonic lithium should be provided. This can perhaps be achieved using the no-core-shell-model (NCSM) or a Green's-function-Monte-Carlo (GFMC) method, which work well for p-shell nuclei.

4. The most difficult uncertainty to reduce is the one related to the nuclear Hamiltonian. To improve in that respects, calculations at complete N3LO or even N4LO are required. However, the development of complete nuclear interactions at N4LO is extremely challenging, due to the large number of operators and LECs included up to this order.

5. In the framework of ChEFT, the nuclear Hamiltonian and the electromagnetic operators should be constructed consistently. It will be important in the future to extend our calculation by including two-body operators, which are required to conserve the e.m. current.

Appendices

A. The two-photon exchange amplitude

Here, we present the calculation of the scattering amplitude shown in Fig. 2.3 with the inclusion of the intermediate derivations omitted in the main part of the thesis.

We start by writing the scattering amplitude in terms of the lepton $L_{\mu\nu}(q,k)$, hadronic $H_{\mu\nu}(q,-q)$ and gauge $D_{\mu\nu}(q)$ tensors. The amplitude reads

$$i\mathcal{M} = \int \frac{d^4q}{(2\pi)^4} L_{\mu\nu}(q,k)\; D^{\nu\sigma}(q)\; D^{\mu\rho}(-q)\; H_{\sigma\rho}(q,-q)\;, \tag{A.1}$$

where q is the 4-momentum of the photon loop while k is the 4-momentum of the external muon. Since muons are fundamental Dirac particles, the evaluation of the leptonic tensor comes immediately from the QED Lagrangian

$$L^s_{\mu\nu}(q,k) = \left[-\frac{ie^2}{(k-q)^2-m^2+i\epsilon}\right]\; \bar{u}^s(k)\; \gamma_\mu \Big[(k-q)^\lambda \gamma_\lambda + m\Big]\gamma_\nu\; u^s(k)\;, \tag{A.2}$$

where $u^s(k)$ is the Dirac wavefunction of the bound muon with with spin s and 4-momentum k. The muon propagator is taken as the Dirac propagator for a free muon. This approximation generates the leading contribution to the amplitude, which is of order $(Z\alpha)^5$.

Given our definition of the Lamb-shift, which assumes no coupling between the muon and the nuclear spins, the two states associated with the possible spin orientations of the muon are degenerate. This feature can be exploited to simplify the calculation of the amplitude in Eq. (2.12) by averaging the leptonic tensor over the spin. We obtain

$$\begin{aligned}
\frac{1}{2}\sum_s L^s_{\mu\nu}(q,k) &= \frac{1}{2}\left[-\frac{ie^2}{(k-q)^2-m^2+i\epsilon}\right]\mathrm{Tr}\left[\gamma_\mu[(k-q)^\lambda\gamma_\lambda+m]\gamma_\nu\frac{k^\sigma\gamma_\sigma+m}{2m}\right] \\
&= \frac{1}{m}\left[-\frac{ie^2}{(k-q)^2-m^2+i\epsilon}\right]\Big[k_\nu(k-q)_\mu + k_\mu(k-q)_\nu + mq^0 g_{\mu\nu}\Big]\;,
\end{aligned} \tag{A.3}$$

where $g_{\mu\nu}$ is the metric tensor and we normalized the Dirac wavefunctions as in non-relativistic quantum electrodynamic, $\sum_s u^s(k)\bar{u}^s(k) = (k^\mu\gamma_\mu + m)/(2m)$. In the last step of Eq. (A.3), we assumed that the three-momentum of the bound muon can be neglected compared to its rest mass, namely that $k \sim (m, 0, 0, 0)$. This approximation is motivated by the evidence that light hydrogen-like atoms are loosely bound systems, where the momentum of the bound muon goes as $|\mathbf{k}| \sim m(Z\alpha)$. For light atoms this means that $|\mathbf{k}| \ll m$. We refer to this as the "wavefunction approximation" and since our derivations are entirely based on the applicability of this approximation, this means that our calculation works best in light systems where $(Z\alpha)$ is a small parameter. Finally, the hadronic tensor is generally written in a way that it obeys crossing symmetry $H_{\rho\sigma}(-q, q) = H_{\sigma\rho}(q, -q)$. The symmetries of the amplitude in Eq. (A.1) can then be exploited by writing the leptonic tensor in a way that it follows this symmetry as well. We label this symmetrized leptonic tensor as $L^{(S)}_{\mu\nu}(q, k)$, and write it as

$$\begin{aligned} L^{(S)}_{\mu\nu}(q,k) &= \frac{1}{2}\Big[L_{\mu\nu}(q,k) + L_{\nu\mu}(-q,k)\Big] \\ &= -\frac{i}{2m}(4\pi\alpha)\left[\frac{2m^2\delta_{\nu0}\delta_{\mu0} - q_\mu m\delta_{\nu0} - q_\nu m\delta_{\mu0} + q^0 m g_{\mu\nu}}{q^2 - 2mq^0 + i\epsilon} + (q \to -q)\right], \end{aligned} \tag{A.4}$$

where we introduced the fine-structure constant $4\pi\alpha = e^2$. Giving that every term in Eq. (A.1) obeys crossing symmetry, the substitution $1/2\sum_s L^s_{\mu\nu}(q, k) \to L^{(S)}_{\mu\nu}(q, k)$ does not modify the amplitude.

As a next step we specify a gauge for our amplitude. Our task is heavily simplified in the use of the Coulomb gauge $(\nabla \cdot \mathbf{A} = 0)$. In this Gauge, the photon propagator reads

$$D^{\mu\nu}(q) = \begin{cases} D^{00}(q) = \frac{1}{\mathbf{q}^2} \\ D^{i0}(q) = D^{0j}(q) = 0 \\ D^{ij}(q) = \frac{1}{q^2}\left(\delta^{ij} - \frac{q^i q^j}{\mathbf{q}^2}\right) \end{cases}, \tag{A.5}$$

where we follow the convention to adopt Greek letters for the components of Lorentz vectors and Roman letters to denote the space components only. The only non-trivially zero combinations in the tensor contractions, $L^{(S)}_{\mu\nu} D^{\nu\sigma} D^{\mu\rho}$, are

$$L^{(S)}_{\mu\nu}\, D^{\nu\sigma}\, D^{\mu\rho} = L^{(S)}_{00}\, D^{00}\, D^{00} + L^{(S)}_{0i}\, D^{in}\, D^{00} + L^{(S)}_{i0}\, D^{00}\, D^{in} + L^{(S)}_{ij}\, D^{jm}\, D^{in}\,. \tag{A.6}$$

However, two more of these combinations are found to be identically zero:

$$\begin{aligned} L_{0i}^{(S)}\, D^{in}\, D^{00} &= L_{i0}^{(S)}\, D^{00}\, D^{in} \\ &= -\frac{i}{2m}(4\pi\alpha)\frac{1}{\mathbf{q}^2}\frac{1}{q^2}\left[\frac{-mq_i}{q^2-2mq^0+i\epsilon}+\frac{mq_i}{q^2+2mq^0+i\epsilon}\right]T^{in}(\mathbf{q})=0\,, \end{aligned} \tag{A.7}$$

where we defined the transverse projection tensor $T^{nm}(\mathbf{q}) = \left(\delta^{nm} - (q^n q^m)/\mathbf{q}^2\right)$. The remaining two terms are

$$L_{00}^{(S)}\, D^{00}\, D^{00} = -\frac{i}{2m}(4\pi\alpha)\left[\frac{1}{\mathbf{q}^2}\right]^2\left[\frac{2m^2-mq^0}{q^2-2mq^0+i\epsilon}+\frac{2m^2+mq^0}{q^2+2mq^0+i\epsilon}\right], \tag{A.8}$$

$$L_{ij}^{(S)}\, D^{jm}\, D^{in} = \frac{i}{2}(4\pi\alpha)\left[\frac{1}{q^2}\right]^2\left[\frac{-q^0}{q^2-2mq^0+i\epsilon}+\frac{q^0}{q^2+2mq^0+i\epsilon}\right]T^{nm}(\mathbf{q})\,. \tag{A.9}$$

The sum of Eq. (A.8) and Eq. (A.9)

$$L_{\mu\nu}^{(S)}\, D^{\nu\sigma}\, D^{\mu\rho} = \frac{i}{2}(4\pi\alpha)\frac{4m}{(q^2+i\epsilon)^2-4m^2q_0^2}\left[\frac{g_{00}}{\mathbf{q}^2}+\frac{q_0^2}{(q^2+i\epsilon)^2}\,T^{nm}(\mathbf{q})\right], \tag{A.10}$$

defines the leptonic-gauge part of the scattering amplitude in Eq. (A.1).

Finally, we derive the hadronic tensor. This tensor is formally defined as the time-ordered product of two nuclear currents over the nuclear ground state

$$\begin{aligned} i\Pi_{\mu\nu}(x,x') &= \langle 0|\,\mathrm{T}\left[J_\mu(x)J_\nu(x')\right]|0\rangle \\ &= \sum_N\Big[\langle 0|\,J_\mu(x)\,|N\rangle\,\langle N|\,J_\nu(x')\,|0\rangle\,\theta(t-t') \\ &+ \langle 0|\,J_\nu(x')\,|N\rangle\,\langle N|\,J_\mu(x)\,|0\rangle\,\theta(t'-t)\Big]\,, \end{aligned} \tag{A.11}$$

where we expressed the time-ordered product in terms of the unit step function, $\theta(t)$, and inserted a complete set of states. The nuclear currents are written in the Heisenberg picture $J_\mu(x) = e^{iHt}J_\mu(\mathbf{x})e^{-iHt}$, with H being the nuclear Hamiltonian, $H\,|N\rangle = E_N\,|N\rangle$. By rewriting $\tau = t - t'$, the previous equation becomes

$$\begin{aligned} i\Pi_{\mu\nu}(x,x') &= \sum_N\Big[\langle 0|\,J_\mu(\mathbf{x})\,|N\rangle\,\langle N|\,J_\nu(\mathbf{x}')\,|0\rangle\,e^{i(E_0-E_N)\tau}\theta(\tau) \\ &+ \langle 0|\,J_\nu(\mathbf{x}')\,|N\rangle\,\langle N|\,J_\mu(\mathbf{x})\,|0\rangle\,e^{i(E_N-E_0)\tau}\theta(-\tau)\Big]. \end{aligned} \tag{A.12}$$

Taking the Fourier transform over τ, we arrive at the following expression

$$H_{\mu\nu}(q,-q) = \sum_N \left[\frac{\langle 0|\, J_\mu(\mathbf{q})\, |N\rangle \langle N|\, J_\nu(-\mathbf{q})\, |0\rangle}{E_0 - E_N + q_0 + i\epsilon} + \frac{\langle 0|\, J_\nu(-\mathbf{q})\, |N\rangle \langle N|\, J_\mu(\mathbf{q})\, |0\rangle}{E_0 - E_N - q_0 + i\epsilon} \right] . \tag{A.13}$$

This tensor preserves crossing symmetry, i.e., $H_{\rho\sigma}(-q,q) = H_{\sigma\rho}(q,-q)$. However, it does not fulfill the gauge condition written in the form $q^\mu H_{\mu\nu} = 0$, when we model nucleons as non-relativistic particles, which is the case in our calculations. Thus the hadronic tensor of Eq. (A.13) breaks the gauge invariance of the two-photon amplitude in Eq. (A.1). Gauge invariance is restored by the inclusion of the seagull (or two-photon) operator, $B_{\mu\nu}(\mathbf{q})$. As a result we write our full hadronic tensor as

$$\begin{aligned} H_{\mu\nu}(q,-q) &= \sum_N \left[\frac{\langle 0|\, J_\mu(\mathbf{q})\, |N\rangle \langle N|\, J_\nu(-\mathbf{q})\, |0\rangle}{E_0 - E_N + q_0 + i\epsilon} + \frac{\langle 0|\, J_\nu(-\mathbf{q})\, |N\rangle \langle N|\, J_\mu(\mathbf{q})\, |0\rangle}{E_0 - E_N - q_0 + i\epsilon} \right] \\ &+ B_{\mu\nu}(\mathbf{q}) \, . \end{aligned} \tag{A.14}$$

The total amplitude of Eq. (A.1) reads

$$i\mathcal{M} = i(4\pi\alpha)^2 \int \frac{d^4q}{(2\pi)^4} \, \frac{2m}{(q^2+i\epsilon)^2 - 4m^2 q_0^2} \left[\frac{1}{\mathbf{q}^2} \, H_L + \frac{q_0^2}{(q^2+i\epsilon)^2} \, H_T \right] , \tag{A.15}$$

where we took out a factor of $(4\pi\alpha)$ outside of the definition of $H_{\rho\sigma}$. This amplitude defines a complex potential that shift the energy of the bound muon, see for instance Refs. [36,37], by

$$\begin{aligned} \Delta E_{nL} &= \langle n\mathrm{L}|\, \mathrm{Re}\big[i\mathcal{M}\big]\, |n\mathrm{L}\rangle \\ &= (4\pi\alpha)^2 \, \phi_{nL}^2 \, \mathrm{Im} \int \frac{d^4q}{(2\pi)^4} \, \frac{2m}{(q^2+i\epsilon)^2 - 4m^2 q_0^2} \left[\frac{1}{\mathbf{q}^2} \, H_L + \frac{q_0^2}{(q^2+i\epsilon)^2} \, H_T \right] , \end{aligned} \tag{A.16}$$

where the shorthand ϕ_{nL}^2 stands for the modulus square of the muon's wavefunction at the origin of the coordinate system.

A.1. Solving the time-like integral

Here, we solve the integration over the time-like component in Eq. (A.16) analytically, and express the energy correction to the Lamb-shift in terms of quantity that can be evaluated from nuclear theory.

We firstly focus on the correction to the Lamb-shift coming from the longitudinal component of the hadronic tensor. We denote this energy correction as $\Delta E_{nL}^{(L)}$. Following Eq. (A.14), Eq. (A.16), and defining $\omega_N = E_N - E_0$, we write

$$H_L = \sum_{N\neq 0} \frac{\langle 0|\,\rho_{\rm ch}(-\mathbf{q})\,|N\rangle\,\langle N|\,\rho_{\rm ch}(\mathbf{q})\,|0\rangle}{q_0-\omega_N+i\epsilon} - \frac{\langle 0|\,\rho_{\rm ch}(-\mathbf{q})\,|N\rangle\,\langle N|\,\rho_{\rm ch}(\mathbf{q})\,|0\rangle}{q_0+\omega_N-i\epsilon}\,, \tag{A.17}$$

$$\Delta E_{nL}^{(\rm L)} = (4\pi\alpha)^2\,\phi_{nL}^2 \sum_{N\neq 0} {\rm Im}\int \frac{d^3q}{(2\pi)^3}\,\frac{2m}{\mathbf{q}^2}\,\langle 0|\,\rho_{\rm ch}(-\mathbf{q})\,|N\rangle\,\langle N|\,\rho_{\rm ch}(\mathbf{q})\,|0\rangle\;Q_N^{(L)}\,, \tag{A.18}$$

$$Q_N^{(L)} = \int \frac{dq_0}{2\pi}\,\frac{1}{(q^2+i\epsilon)^2-4m^2q_0^2}\left[\frac{2\omega_N}{q_0^2-(\omega_N-i\epsilon)^2}\right]. \tag{A.19}$$

Compared to Eq. (A.14), we are taking only the inelastic part of the hadronic tensor, since we are interested in polarizability effects. In order to solve the integral in Eq. (A.19), we write it in a more convenient form

$$Q_N^{(L)} = \frac{\omega_N}{\pi}\int dq_0\,\frac{1}{(q_0-m)^2-E_q^2+i\epsilon}\,\frac{1}{(q_0+m)^2-E_q^2+i\epsilon}\,\frac{1}{q_0^2-\omega_N^2+i\epsilon}\,, \tag{A.20}$$

where $E_q^2 = \mathbf{q}^2+m^2$. We now make use of the following identities, which hold as long as we take the limit $\epsilon\to 0$ at the end of the calculation

$$\begin{aligned}
\frac{1}{(q_0-m)^2-E_q^2+i\epsilon} &= \frac{1}{(q_0-m)+(E_q-i\epsilon)}\,\frac{1}{(q_0-m)-(E_q-i\epsilon)}\,,\\
\frac{1}{(q_0+m)^2-E_q^2+i\epsilon} &= \frac{1}{(q_0+m)+(E_q-i\epsilon)}\,\frac{1}{(q_0+m)-(E_q-i\epsilon)}\,,\\
\frac{1}{q_0^2-\omega_N^2+i\epsilon} &= \frac{1}{q_0+(\omega_N-i\epsilon)}\,\frac{1}{q_0-(\omega_N-i\epsilon)}\,.
\end{aligned}$$

Using the previous transformations, is easy to see that the integrand of Eq. (A.20) has six poles, three of which lie in the upper-half of the complex q_0-plane, at $q_0 = m-E_q+i\epsilon$, $q_0=-m-E_q+i\epsilon$ and $q_0=-\omega_N+i\epsilon$. The integral in Eq. (A.20) can then be solved as a contour integration by closing the contour with a large

semi-circle, Γ_R, in the upper half of the complex plane. We obtain

$$Q_N^{(L)} = -\frac{i}{4mE_q}\left[\frac{1}{(m-E_q)(m-E_q-\omega_N)} - \frac{1}{(m+E_q)(m+E_q+\omega_N)}\right] . \quad \text{(A.21)}$$

We insert Eq. (A.21) back in Eq. (A.18), obtaining the longitudinal part of the energy correction

$$\Delta E_{nL}^{(\mathrm{L})} = -(4\pi\alpha)^2\,\phi_{nL}^2 \sum_{N\neq 0}\int \frac{d^3q}{(2\pi)^3}\,\frac{g(\omega_N,q)}{\mathbf{q}^2}\,\langle 0|\,\rho_{\mathrm{ch}}(-\mathbf{q})\,|N\rangle\,\langle N|\,\rho_{\mathrm{ch}}(\mathbf{q})\,|0\rangle\ , \quad \text{(A.22)}$$

with

$$\begin{aligned} g(\omega_N,q) &= \frac{1}{2E_q}\left[\frac{1}{(E_q-m)(E_q-m+\omega_N)} - \frac{1}{(E_q+m)(m+E_q+\omega_N)}\right] \\ &= \frac{m}{E_q}\,\frac{(2E_q+\omega_N)}{\mathbf{q}^2\left[(E_q+\omega_N)^2-m^2\right]} . \end{aligned} \quad \text{(A.23)}$$

It is possible to combine the two previous equations in a more compact form

$$\Delta E_{nL}^{(\mathrm{L})} = -8\alpha^2 m\,\phi_{nL}^2 \sum_{N\neq 0}\int \frac{d^3q}{4\pi}\,|\langle N|\,\rho_{\mathrm{ch}}(\mathbf{q})\,|0\rangle|^2\,\frac{(2E_q+\omega_N)}{\mathbf{q}^4 E_q\left[(E_q+\omega_N)^2-m^2\right]} . \quad \text{(A.24)}$$

The next step is to evaluate the time-like integral of the transverse part of Eq. (A.16). We separate this transverse part in a term proportional to the nuclear currents, and a term proportional to the two-photon operator. We discuss the term proportional to the nuclear currents first. Similarly to the longitudinal part of the equation, we write

$$H_T = \sum_{N\neq 0} |\langle 0|\,\mathbf{J}_\perp\,|N\rangle|^2\left[\frac{1}{q_0-\omega_N+i\epsilon} - \frac{1}{q_0+\omega_N-i\epsilon}\right] , \quad \text{(A.25)}$$

$$\Delta E_{nL}^{(T)} = (4\pi\alpha)^2\,\phi_{nL}^2 \sum_{N\neq 0} \mathrm{Im}\int \frac{d^3q}{(2\pi)^3}\,|\langle 0|\,\mathbf{J}_\perp\,|N\rangle|^2\ 2m\,Q_N^{(T)} , \quad \text{(A.26)}$$

and

$$Q_N^{(T)} = \frac{\omega_N}{\pi}\int dq_0 \left[\frac{1}{(q_0-m)^2-E_q^2+i\epsilon}\,\frac{1}{(q_0+m)^2-E_q^2+i\epsilon}\,\frac{1}{q_0^2-\omega_N^2+i\epsilon}\right] \times \frac{q_0^2}{(q_0^2-\mathbf{q}^2+i\epsilon)^2}\,. \tag{A.27}$$

Here, we defined the transverse part of the vector current $\mathbf{J}_\perp(\mathbf{q}) = \hat{q}\times\mathbf{J}(\mathbf{q})$. In performing the contour integral in Eq. (A.27), we see that the terms in the square brackets have the same simple poles that we found in our evaluation of $Q_N^{(L)}$. Their contribution to the integral is

$$\begin{aligned} Q_{N,1}^{(T)} &= \frac{\omega}{\pi}2\pi i\left[-\frac{1}{2E_q}\,\frac{1}{4m^2-4mE_q}\,\frac{1}{(m-E_q)^2-\omega_N^2}\,\frac{1}{4m^2}\right. \\ &- \frac{1}{2E_q}\,\frac{1}{4m^2+4mE_q}\,\frac{1}{(m+E_q)^2-\omega_N^2}\,\frac{1}{4m^2} \\ &\left.- \frac{1}{2\omega_N}\,\frac{1}{(m+\omega_N)^2-E_q^2}\,\frac{1}{(m-\omega_N)^2-E_q^2}\,\frac{\omega_N^2}{(\omega_N^2-\mathbf{q}^2)^2}\right] \\ &= -\frac{i}{2m}\left[\frac{1}{4m^2}\,g(\omega_N,\mathbf{q}) - \frac{1}{2m}\,\frac{1}{(\omega_N^2-\mathbf{q}^2)^2}\right]. \end{aligned} \tag{A.28}$$

The last term of Eq. (A.27) has a 2nd order singularity at $q_0 = -|\mathbf{q}|+i\epsilon$, we obtain

$$Q_{N,2}^{(T)} = -\frac{i}{2m}\,\frac{\omega_N}{2m}\frac{3|\mathbf{q}|^2-\omega_N^2}{2|\mathbf{q}|^3}\,\frac{1}{(\omega_N^2-\mathbf{q}^2)^2}\,. \tag{A.29}$$

In summary, we can rewrite Eq. (A.27) as $Q_N^{(T)} = Q_{N,1}^{(T)} + Q_{N,2}^{(T)}$, obtaining:

$$Q_N^{(T)} = -\frac{i}{2m}\left[\frac{\mathbf{q}^2}{4m^2}\frac{g(\omega_N,\mathbf{q})}{\mathbf{q}^2} - \frac{1}{4m|\mathbf{q}|^3}\,\frac{\omega_N+2|\mathbf{q}|}{(\omega_N+|\mathbf{q}|)^2}\right]. \tag{A.30}$$

Inserting Eq. (A.30) back in Eq. (A.26) we get

$$\begin{aligned} \Delta E_{nL}^{(T)} &= -8\alpha^2 m\,\phi_{nL}^2\sum_{N\neq 0}\int\frac{d^3q}{4\pi}\,|\langle 0|\,\mathbf{J}_\perp\,|N\rangle|^2 \\ &\times \left[\frac{\mathbf{q}^2}{4m^2}\,\frac{(2E_q+\omega_N)}{\mathbf{q}^4E_q\left[(E_q+\omega_N)^2-m^2\right]} - \frac{1}{4m^2|\mathbf{q}|^3}\,\frac{\omega_N+2|\mathbf{q}|}{(\omega_N+|\mathbf{q}|)^2}\right]. \end{aligned} \tag{A.31}$$

Lastly, we evaluate the time-like integral of the term proportional to the two-photon operator $B_{\mu\nu}(\mathbf{q})$. According to Eq. (A.16), and similarly to what was done before, we write

$$\Delta E_{nL}^{(S)} = (4\pi\alpha)^2\,\phi_{nL}^2\;\mathrm{Im}\int\frac{d^3q}{(2\pi)^3}\,2m\,B_\perp(\mathbf{q})\,Q_N^{(S)}\,, \tag{A.32}$$

$$Q_N^{(S)} = \int\frac{dq_0}{2\pi}\,\frac{1}{(q^2+i\epsilon)^2-4m^2q_0^2}\left[\frac{q_0^2}{(q^2+i\epsilon)^2}\right] = \frac{i}{16m^2\mathbf{q}^2}\left(\frac{1}{E_q}-\frac{1}{|\mathbf{q}|}\right), \tag{A.33}$$

where $B_\perp(\mathbf{q}) = T^{nm}(\mathbf{q})B_{nm}(\mathbf{q})$. We insert the solution of Eq (A.33) back in Eq (A.32) and rearranging terms we find

$$\Delta E_{nL}^{(S)} = -8\alpha^2 m\,\phi_{nL}^2\int\frac{d^3q}{4\pi}\,B_\perp(\mathbf{q})\,\frac{1}{8m^2\mathbf{q}^2}\left(\frac{1}{|\mathbf{q}|}-\frac{1}{E_q}\right). \tag{A.34}$$

The total energy. The total energy correction comes as the sum of Eq. (A.24), Eq. (A.31) and Eq. (A.34)

$$\begin{aligned}\Delta E_{nL} &= -8\alpha^2 m\,\phi_{nL}^2\int\frac{d^3q}{4\pi}\left\{\sum_{N\neq0}|\langle N|\,\rho_{\rm ch}(\mathbf{q})\,|0\rangle|^2\,\frac{(2E_q+\omega_N)}{\mathrm{q}^4E_q\left[(E_q+\omega_N)^2-m^2\right]}\right.\\ &+ \sum_{N\neq0}|\langle0|\,\mathbf{J}_\perp(\mathbf{q})\,|N\rangle|^2\left[\frac{\mathrm{q}^2}{4m^2}\,\frac{(2E_q+\omega_N)}{\mathrm{q}^4E_q\left[(E_q+\omega_N)^2-m^2\right]}-\frac{1}{4m^2\mathrm{q}^3}\,\frac{\omega_N+2\mathrm{q}}{(\omega_N+\mathrm{q})^2}\right]\\ &+ \left.B_\perp(\mathbf{q})\,\frac{1}{8m^2\mathrm{q}^2}\left(\frac{1}{\mathrm{q}}-\frac{1}{E_q}\right)\right\},\end{aligned} \tag{A.35}$$

where we have redefined $\mathrm{q} = |\mathbf{q}|$.

B. Relativistic structure functions

Here, we derive the electromagnetic sum rules contributing to the nuclear polarizability corrections to the Lamb-shift with relativistic lepton kinematic. The correction can be separated into a longitudinal $\Delta E_{nL}^{(\mathrm{L})}$, transverse $\Delta E_{nL}^{(\mathrm{T})}$ and seagull-transverse $\Delta E_{nL}^{(\mathrm{S})}$ components. It is best to treat these component separately, and combine the contributions only at the very end. This appendix follow closely the discussion in Ref. [32].

B.1. The longitudinal correction

The longitudinal polarizability correction to the Lamb-shift is written in Eq. (A.24), and is for convenience reported below

$$\Delta E_{nL}^{(\mathrm{L})} = -8\alpha^2 m\, \phi_{nL}^2 \sum_{N\neq 0} \int \frac{d^3q}{4\pi}\, |\langle N|\, \rho_{\mathrm{ch}}(\mathbf{q})\, |0\rangle|^2\, \frac{(2E_q+\omega_N)}{\mathbf{q}^4 E_q\left[(E_q+\omega_N)^2-m^2\right]}\,. \tag{B.1}$$

The momentum space matrix elements of the nuclear charge distribution operator are defined as Fourier transform of the coordinate space matrix elements

$$|\langle N|\, \rho_{\mathrm{ch}}(\mathbf{q})\, |0\rangle|^2 = \int d^3x\, d^3y\ \langle 0|\, \rho_{\mathrm{ch}}^{\dagger}(\mathbf{y})\, |N\rangle\, \langle N|\, \rho_{\mathrm{ch}}(\mathbf{x})\, |0\rangle\ e^{i\mathbf{q}\cdot\mathbf{z}}\,, \tag{B.2}$$

where $\mathbf{z} = \mathbf{x} - \mathbf{y}$. We insert Eq. (B.2) in Eq. (B.1) and solve the angular integral over the momentum transfer, obtaining

$$\Delta E_{nL}^{(\mathrm{L})} = -8\alpha^2 m\, \phi_{nL}^2 \sum_{N\neq 0} \int d^3x\, d^3y\ \langle 0|\, \rho_{\mathrm{ch}}^{\dagger}(\mathbf{y})\, |N\rangle\, \langle N|\, \rho_{\mathrm{ch}}(\mathbf{x})\, |0\rangle\ \mathrm{I_N}(z)\,, \tag{B.3}$$

where the coupling between nucleus and lepton is now found within the relativistic structure function $\mathrm{I_N}(z)$ which depends only on the radial part of $\mathbf{z}$

$$\mathrm{I_N}(z) = \frac{1}{\omega_N z} \int d\mathrm{q}\, \frac{\sin(\mathrm{q}z)}{\mathrm{q}^3}\, \frac{(2E_q\omega_N+\omega_N^2)}{E_q\left[(E_q+\omega_N)^2-m^2\right]}\,. \tag{B.4}$$

The problem reduces into the evaluation of the integrals in Eq. (B.3) and Eq. (B.4). To find a solution to Eq. (B.4), it is best to define two parameters depending only on the two relevant scales of the problem $\xi = \omega_N + m$, $\xi' = \omega_N - m$. For normal

electronic atoms both ξ, $\xi' > 0$, while for muonic atoms we usually have that the low-lying nuclear transitions are smaller than the mass of the muon, this means that for the first few terms of the sum in Eq. (B.3) we have $\xi' < 0$. We define

$$\bar{I}(\xi, z) = \xi I_0(z) + \int_0^\infty d\mathrm{q}\, \frac{\sin(\mathrm{q}z)}{\mathrm{q}E_q}\, \frac{1}{E_q + \xi}\,, \tag{B.5}$$

which allow us to rewrite the relativistic longitudinal structure function as

$$I_N(z) = \frac{1}{2m\omega_N z}\left[\bar{I}(\xi, z) - \bar{I}(\xi', z)\right]. \tag{B.6}$$

The function $\bar{I}(\xi, z)$ is well defined for any value of ξ and ξ', but smoothly changes form in different regions of the allowed domain. We make use of the field-theory trick

$$\frac{1}{E_1 E_2 (E_1 + E_2)} = \frac{2}{\pi}\int_0^\infty d\lambda\, \frac{1}{(\lambda^2 + E_1^2)(\lambda^2 + E_2^2)}\,, \tag{B.7}$$

and the solution of the integral [142]

$$\int_0^\infty \frac{\sin(ax)}{x(\beta^2 + x^2)}\, dx = \frac{\pi}{2\beta^2}\left[1 - e^{-a\beta}\right], \tag{B.8}$$

to write Eq. (B.5) as

$$\bar{I}(\xi, z) = \xi I_0(z) + \xi\int_0^\infty d\lambda\, \frac{1}{(\lambda^2 + \xi^2)(\lambda^2 + m^2)} - \xi\int_0^\infty d\lambda\, \frac{e^{-z\sqrt{\lambda^2+m^2}}}{(\lambda^2 + \xi^2)(\lambda^2 + m^2)}\,. \tag{B.9}$$

The first integral in Eq. (B.9) has a standard solution [142]

$$\xi\int_0^\infty d\lambda\, \frac{1}{(\lambda^2 + \xi^2)(\lambda^2 + m^2)} = \frac{\pi}{2m}\, \frac{1}{\xi + m}\,. \tag{B.10}$$

The second integral in Eq. (B.9) requires further manipulations. Firstly, we define $\mu^2 = \xi^2/m^2 - 1$ and then we use partial fraction to split the integral in two parts

$$\begin{aligned}\int_0^\infty d\lambda\, \frac{e^{-z\sqrt{\lambda^2+m^2}}}{(\lambda^2 + \xi^2)(\lambda^2 + m^2)} &= \frac{1}{\mu^2 m^2}\int_0^\infty d\lambda \left[\frac{e^{-z\sqrt{\lambda^2+m^2}}}{(\lambda^2 + m^2)} - \frac{e^{-z\sqrt{\lambda^2+m^2}}}{(\lambda^2 + m^2) + \mu^2 m^2}\right] \\ &= \frac{1}{\mu^2 m^3}\int_0^\infty dx \left[\frac{e^{-\beta x}}{x\sqrt{x^2-1}} - \frac{x e^{-\beta x}}{(x^2 + \mu^2)\sqrt{x^2-1}}\right],\end{aligned} \tag{B.11}$$

where in the last step we made a change of variable $z^2\lambda^2 = \beta^2(x^2 - 1)$ and re-defined $\beta = mz$. The first integral in Eq. (B.11) can be solved by using standard

methods [143], the result is

$$\frac{1}{\mu^2 m^3}\int_0^\infty \frac{e^{-\beta x}}{x\sqrt{x^2-1}}dx = \frac{1}{\mu^2 m^3}\left[\frac{\pi}{2} - \int_0^\beta K_0(\beta')\,d\beta'\right], \tag{B.12}$$

where $K_0(\beta)$ is the modified Bessel function of 0^{th} order. The last integral of Eq. (B.11), which we label $\bar{I}(\beta,\mu)$, is more difficult to solve. As shown in Ref. [42], the solution can be found by recognizing that $\bar{I}(\beta,\mu)$ is the solution of the differential equation $\partial^2_\beta \bar{I}(\beta,\mu) + \mu^2 \bar{I}(\beta,\mu) = K_0'(\beta)$ with the boundary condition that $\bar{I}(+\infty,\mu) \to 0$ exponentially. Instead of solving the integral we then solve the differential equation, which can be done with conventional techniques. The solution is

$$\bar{I}(\beta,\mu) \;=\; \frac{m}{\xi}\left[\sin(\mu\beta)\sinh^{-1}(\mu) + \frac{\pi}{2}\cos(\mu\beta)\right] + \int_0^\beta d\beta'\; K_0(\beta')\cos\big(\mu(\beta-\beta')\big)\,. \tag{B.13}$$

In summary, from Eq. (B.13), Eq. (B.12) and Eq. (B.10) we obtain

$$\begin{aligned}\bar{I}(\xi,\beta) \;&=\; \frac{\pi}{2m^2\mu^2}\Big(\cos(\mu\beta)-1\Big) + \frac{1}{\mu^2 m^2}\sin(\mu\beta)\sinh^{-1}(\mu) - \\ &-\; \frac{\xi}{\mu^2 m^3}\int_0^\beta K_0(\beta')d\beta'\left[\cos\Big(\mu(\beta-\beta')\Big) - 1 + \frac{\mu^2}{2}(\beta-\beta')^2\right]. \end{aligned}\tag{B.14}$$

The evaluation of $\bar{I}(\xi',\beta)$ is done similarly. The main difference is that $\mu'^2 = \xi'^2/m - 1$ now takes negative values for the low-lying nuclear transitions, where $\omega_N < 2m$. In these region, we define the (positive) parameter $\nu'^2 = -\mu'^2$ which allows us to find a solution for $\bar{I}(\xi',\beta)$ with the same techniques used for $\bar{I}(\xi,\beta)$. The solution is

$$\begin{aligned}\bar{I}(\xi',\beta) \;&=\; -\frac{\pi}{2m^2\nu'^2}\Big(\cosh(\nu'\beta)-1\Big) + \frac{\mathcal{B}(\omega_N/m)}{m^2} + \\ &+\; \frac{\xi'}{\nu'^2 m^3}\int_0^\beta K_0(\beta')d\beta'\left[\cosh\Big(\nu'(\beta-\beta')\Big) - 1 + \frac{\mu^2}{2}(\beta-\beta')^2\right], \end{aligned}\tag{B.15}$$

were we defined the function

$$\mathcal{B}(\omega_N/m) \;=\; \begin{cases} \sin(\mu'\beta)\sinh^{-1}(\mu')/\mu'^2 & \omega_N > 2 \\ \sinh(\nu'\beta)\sin^{-1}(\nu')/\nu'^2 & 1 \le \omega_N \le 2 \\ \sinh(\nu'\beta)\big[\pi - \sin^{-1}(\nu')\big]/\nu'^2 & \omega_N < 1 \end{cases}. \tag{B.16}$$

Most of the changes between Eq. (B.14) and Eq. (B.15) are trivial because they came from the substitution $\mu \to i\nu'$. We insert Eq. (B.14) and Eq. (B.15) back into

Eq. (B.6) and obtain

$$I_N(z) = \frac{\pi}{4m^3\omega_N z}\mathcal{Z}(\mu,\nu'\beta) + \frac{1}{2m^4\omega_N z}\mathcal{Q}(\mu,\nu',\beta) + \frac{1}{2m^3\omega_N z}\mathcal{D}(\mu,\nu',\beta)\ , \quad \text{(B.17)}$$

where, to simplify the notation, we defined three new functions

$$\mathcal{Z}(\mu,\nu'\beta) = \frac{1}{\nu'^2}\cosh(\nu'\beta) + \frac{1}{\mu^2}\cos(\mu\beta) - \frac{1}{\mu^2} - \frac{1}{\nu'^2}\ , \quad \text{(B.18)}$$

$$\begin{aligned}\mathcal{Q}(\mu,\nu',\beta) &= \int_0^\beta K_0(\beta')\left[\frac{\xi'}{\nu'^2} + \frac{\xi}{\mu^2} + \frac{(\beta-\beta')^2}{2}(\xi'-\xi)\right.\\ &- \left.\cosh\Big(\nu'(\beta-\beta')\Big)\frac{\xi'}{\nu'^2} - \cos\Big(\mu(\beta-\beta')\Big)\frac{\xi}{\mu^2}\right], \quad \text{(B.19)}\end{aligned}$$

$$\begin{aligned}\mathcal{D}(\mu,\nu',\beta) &= \frac{1}{\mu^2}\sin(\mu\beta)\sinh^{-1}(\mu) - \mathcal{B}(\omega_N/m)\\ &= \begin{cases} \frac{1}{\mu^2}\sin(\mu\beta)\sinh^{-1}(\mu) - \frac{1}{\mu'^2}\sin(\mu'\beta)\sinh^{-1}(\mu') & \omega_N > 2\\ \frac{1}{\mu^2}\sin(\mu\beta)\sinh^{-1}(\mu) - \frac{1}{\nu'^2}\sinh(\nu'\beta)\sin^{-1}(\nu') & 1 \le \omega_N \le 2\\ \frac{1}{\mu^2}\sin(\mu\beta)\sinh^{-1}(\mu) - \frac{1}{\nu'^2}\sinh(\nu'\beta)\left[\pi - \sin^{-1}(\nu')\right] & \omega_N < 1 \end{cases}.\end{aligned} \quad \text{(B.20)}$$

To obtain expressions for the nuclear polarizabilities that can be more easily calculated numerically, we expand the previous functions in terms of the small parameters $\mu\beta$ and $\nu'\beta$. We obtain

$$\mathcal{Z}(\mu,\nu'\beta) = \frac{1}{6}\omega_N m^3 z^4 + \mathcal{O}(z^6)\ , \quad \text{(B.21)}$$

$$\mathcal{Q}(\mu,\nu',\beta) = \frac{\omega_N^2 m^4 z^5}{20}\left(\gamma + \ln(\beta/2) - \frac{137}{60}\right) + \mathcal{O}(z^6)\ , \quad \text{(B.22)}$$

$$\begin{aligned}\mathcal{D}(\mu,\nu',\beta) &= -\frac{m^3z^3}{6}\mathcal{D}^{(1)}(\mu,\nu',\beta) + \frac{m^5z^5}{120}\mathcal{D}^{(3)}(\mu,\nu',\beta)\\ &= -\frac{m^3z^3}{6}\begin{cases} \mu\sinh^{-1}(\mu) - \mu'\sinh^{-1}(\mu') & \omega_N > 2m\\ \mu\sinh^{-1}(\mu) + \nu'\sin^{-1}(\nu') & m \le \omega_N \le 2m\\ \mu\sinh^{-1}(\mu) + \nu'\left[\pi - \sin^{-1}(\nu')\right] & \omega_N < m \end{cases}\\ &+ \frac{m^5z^5}{120}\begin{cases} \mu^3\sinh^{-1}(\mu) - \mu'^3\sinh^{-1}(\mu') & \omega_N > 2m\\ \mu^3\sinh^{-1}(\mu) - \nu'^3\sin^{-1}(\nu') & m \le \omega_N \le 2m\\ \mu^3\sinh^{-1}(\mu) - \nu'^3\left[\pi - \sin^{-1}(\nu')\right] & \omega_N < m \end{cases}\\ &+ \mathcal{O}(z^7)\ . \end{aligned} \quad \text{(B.23)}$$

We neglected terms in the expansions that can not generate nuclear transitions and we defined the first two relevant orders of $\mathcal{D}(\mu,\nu',\beta)$ as $\mathcal{D}^{(1)}(\mu,\nu',\beta)$ and $\mathcal{D}^{(3)}(\mu,\nu',\beta)$. To connect the notations in Ref. [32] and in Ref. [39], we define $(m/2\omega_N)\mathcal{D}^{(1)}(\mu,\nu',\beta) = \mathcal{F}(\omega_N/m)$, where $\mathcal{F}(\omega_N/m)$ is the function that generates the unretarded electric dipole sum rule in [39]. With the previous substitution and by moving Eq. (B.21), Eq. (B.22) and Eq. (B.23) back in Eq. (B.17) we obtain

$$\begin{aligned} I_N(z) &= \frac{\mathcal{F}(\omega_N/m)}{6m}z^2 + \frac{\pi}{24}z^3 \\ &+ \left[\frac{m^2}{240\omega_N}\mathcal{D}^{(3)}(\mu,\nu',\beta) + \frac{\omega_N}{40}\left(\gamma + \ln(mz/2) - \frac{137}{60}\right)\right]z^4 \\ &+ \mathcal{O}(z^5)\,. \end{aligned} \tag{B.24}$$

B.2. The transverse correction

The transverse polarizability correction to the Lamb-shift was obtained in Eq. (A.31), and it is for convenience reported here :

$$\begin{aligned} \Delta E_{nL}^{(T)} &= -8\alpha^2 m\,\phi_{nL}^2 \sum_{N\neq 0}\int d^3x\, d^3y\ \langle 0|\, J_i^\dagger(\mathbf{y})\,|N\rangle\,\langle N|\, J_j(\mathbf{x})\,|0\rangle \\ &\times \int\frac{d^3q}{4\pi}\left[\frac{\mathrm{q}^2}{4m^2}\,\frac{(2E_q+\omega_N)}{\mathrm{q}^4E_q\left[(E_q+\omega_N)^2-m^2\right]} - \frac{1}{4m^2\mathrm{q}^3}\,\frac{\omega_N+2\mathrm{q}}{(\omega_N+\mathrm{q})^2}\right]\left(\delta_{ij}+\frac{\nabla_i^z\nabla_j^z}{\mathrm{q}^2}\right)e^{i\mathbf{q}\cdot\mathbf{z}} \\ &\equiv -8\alpha^2 m\,\phi_{nL}^2 \sum_{N\neq 0}\int d^3x\, d^3y\,\langle 0|\, J_i^\dagger(\mathbf{y})\,|N\rangle\,\langle N|\, J_j(\mathbf{x})\,|0\rangle\left(\delta_{ij}J_N(z) + z^i z^j \bar{J}_N(z)\right). \end{aligned} \tag{B.25}$$

The two structure functions, $J_N(z)$ and $\bar{J}_N(z)$, are defined through matching terms with $\delta_{ij}J_0(z) + \nabla^{z_i}\nabla^{z_j}J_{CG}(z)$, where $J_0(z)$ and $J_{CG}(z)$ are functions defined as

$$J_0(z) = \int\frac{d^3q}{4\pi}\left[\frac{\mathrm{q}^2}{4m^2}\,\frac{(2E_q+\omega_N)}{\mathrm{q}^4E_q\left[(E_q+\omega_N)^2-m^2\right]} - \frac{1}{4m^2\mathrm{q}^3}\,\frac{\omega_N+2\mathrm{q}}{(\omega_N+\mathrm{q})^2}\right]e^{i\mathbf{q}\cdot\mathbf{z}}\,, \tag{B.26}$$

$$J_{CG}(z) = \int\frac{d^3q}{4\pi}\frac{1}{4m^2}\left[\frac{(2E_q+\omega_N)}{\mathrm{q}^4E_q\left[(E_q+\omega_N)^2-m^2\right]} - \frac{\omega_N+2\mathrm{q}}{\mathrm{q}^5(\omega_N+\mathrm{q})^2}\right]e^{i\mathbf{q}\cdot\mathbf{z}}\,. \tag{B.27}$$

The solutions for the integrals in Eq. (B.26) and Eq. (B.27) can be easily found by using the derived expression for $I_N(z)$. Starting from Eq. (B.4) one can show that

$$J_0(z) = -\frac{1}{4m^2}\frac{1}{z}\frac{d^2}{dz^2}z\Big[I_N(z) - \lim_{m\to 0} I_N(z)\Big] , \tag{B.28}$$

$$J_{CG}(z) = \frac{1}{4m^2}\Big[I_N(z) - \lim_{m\to 0} I_N(z)\Big] . \tag{B.29}$$

The longitudinal structure function is logarithmic divergent in the limit of zero lepton mass, we find

$$\lim_{m\to 0}\frac{1}{6m}\mathcal{F}(\omega_N/m) = -\frac{1}{6m}\Big[1+\ln\big(\omega_N/\lambda\big)\Big] , \tag{B.30}$$

$$\lim_{m\to 0} m^2\mathcal{D}^{(3)}(\mu,\nu',\beta) = 6\omega_N^2\Big[\frac{1}{3}+\ln\big(\omega_N/\lambda\big)\Big] , \tag{B.31}$$

where we wrote $2\lambda = m$ in divergent logarithms. With the results of Eq. (B.30) and Eq. (B.31) the limit of the longitudinal structure function can be written as

$$\begin{aligned}\lim_{m\to 0} I_N(z) &= -\frac{1}{6\omega_N}\Big[1+\ln\big(\omega_N/\lambda\big)\Big]z^2 + \frac{\pi}{24}z^3 + \frac{\omega_N}{40}\Big[\gamma - \frac{39}{20} + \ln\big(\omega_N z\big)\Big]z^4 \\ &+ \mathcal{O}\big(z^5\big) .\end{aligned} \tag{B.32}$$

By using Eq. (B.24), Eq. (B.32) and the definitions of J_0 and J_{CG} in Eq. (B.28) and Eq. (B.29) we obtain

$$\begin{aligned}J_0(z) &= -\frac{1}{4m^3}\Big[\mathcal{F}(\omega_N/m) + \frac{m}{\omega_N}\Big(1+\ln\big(\omega_N/\lambda\big)\Big)\Big] - \frac{\mathcal{D}^{(3)}(\omega_N/m)}{48\omega_N}z^2 \\ &- \frac{\omega_N}{8m^2}\Big[\ln\Big(\frac{m}{2\omega_N}\Big) - \frac{1}{3}\Big]z^2 + \mathcal{O}\big(z^3\big) ,\end{aligned} \tag{B.33}$$

$$\begin{aligned}J_{CG}(z) &= \frac{z^2}{24m^3}\Big[\mathcal{F}(\omega_N/m) + \frac{m}{\omega_N}\Big(1+\ln\big(\omega_N/\lambda\big)\Big)\Big] + \frac{z^4}{960\omega_N}\mathcal{D}^{(3)}(\omega_N/m) \\ &+ \frac{\omega_N}{160m^2}z^4\Big[\ln\Big(\frac{m}{2\omega_N}\Big) - \frac{1}{3}\Big] + \mathcal{O}\big(z^5\big) .\end{aligned} \tag{B.34}$$

Performing the contraction $\delta_{ij}J_0(z) + \nabla_i^z \nabla_j^z J_{CG}(z)$ and doing the matching with Eq. (B.25) we obtain

$$\bar{J}_N(z) = \frac{\mathcal{D}^{(3)}(\omega_N/m)}{120\omega_N} + \frac{\omega_N}{20m^2}\left[\ln\left(\frac{m}{2\omega_N}\right) - \frac{1}{3}\right], \tag{B.35}$$

$$J_N(z) = -\frac{1}{6m^3}\mathcal{F}(\omega_N/m) - \frac{1}{6\omega_N m^2}\Big[1 + \ln(\omega_N/\lambda)\Big] - 2\bar{J}_N(z)z^2\,. \tag{B.36}$$

B.3. The Seagull correction

We write the transverse seagull correction, Eq. (A.34), as

$$\begin{aligned}\Delta E_{nL}^{(S)} &= -8\alpha^2 m\,\phi_{nL}^2 \int d^3x\, d^3y\, B^{ij}(\mathbf{x},\mathbf{y}) \\ &\times \int \frac{d^3q}{4\pi}\frac{1}{8m^2\mathrm{q}^2}\left(\frac{1}{\mathrm{q}} - \frac{1}{E_q}\right)\left(\delta_{ij} + \frac{\nabla^{z_i}\nabla^{z_j}}{\mathrm{q}^2}\right)e^{i\mathbf{q}\cdot\mathbf{z}} \\ &\equiv -8\alpha^2 m\,\phi_{nL}^2 \int d^3x\, d^3y\, B^{ij}(\mathbf{x},\mathbf{y})\,\frac{1}{2}\Big[\delta_{ij}K(z) + z_i z_j \bar{K}(z)\Big]\,. \end{aligned} \tag{B.37}$$

The structure functions, $K(z)$ and $\bar{K}(z)$, are obtained by matching from $\delta_{ij}K_0(z) + \nabla^{z_i}\nabla^{z_j}K_{CG}(z)$, where $K_0(z)$ and $K_{CG}(z)$ are defined as

$$K_0(z) = \int \frac{d^3q}{4\pi}\frac{1}{8m^2q^2}\left(\frac{1}{q} - \frac{1}{E_q}\right)e^{i\mathbf{q}\cdot\mathbf{z}}\,, \tag{B.38}$$

$$K_{CG}(z) = \int \frac{d^3q}{4\pi}\frac{1}{8m^2q^4}\left(\frac{1}{q} - \frac{1}{E_q}\right)e^{i\mathbf{q}\cdot\mathbf{z}}\,. \tag{B.39}$$

These integrals can be written as variants of

$$I_0(z) = -\frac{1}{2m^3}\int_0^\beta K_0(\beta')(\beta - \beta')^2\,, \tag{B.40}$$

and here we merely quote the result in Ref. [42]

$$\bar{K}(z) = -\frac{1}{120}\left[\gamma + \ln(\beta/2) - \frac{31}{30}\right] + \mathcal{O}(z^2)\,, \tag{B.41}$$

$$K(z) = -\frac{\ln(2\lambda/m)}{6m^2} - 2z^2\left(\bar{K}(z) + \frac{1}{480}\right). \tag{B.42}$$

C. Leading order chiral NN interaction in coordinate space

The ChEFT diagrams contributing to generating the nuclear potential and at leading order in Weinberg power counting are shown in Figure C.1. These are the static one-pion-exchange (1PE) and two contact interactions given by the low-energy constants (LECs) C_S and C_T.

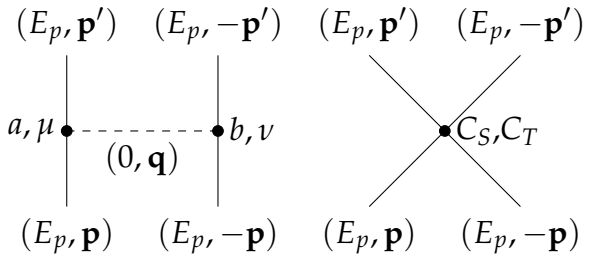

Figure C.1.: Feynman diagrams for the amplitudes contributing to the leading order chiral interaction in Weinberg power counting.

The contact diagrams generate a potential with the following spin-isospin structure

$$V_{12}^{ct}(r_{12}) = \Big[C_S + C_T(\boldsymbol{\sigma}_1 \cdot \boldsymbol{\sigma}_2)\Big]\delta(r_{12}) \,, \tag{C.1}$$

where $\delta(r_{12})$ is the Dirac delta function. The OPE diagram leads to the following potential

$$V_{12}^{\pi}(r_{12}) = -\left(\frac{g_A}{2f_\pi}\right)^2 (\boldsymbol{\tau}_1 \cdot \boldsymbol{\tau}_2) \int \frac{d^3q}{(2\pi)^3} \frac{(\boldsymbol{\sigma}_1 \cdot \mathbf{q})(\boldsymbol{\sigma}_2 \cdot \mathbf{q})}{\mathbf{q}^2 + m_\pi^2} \, e^{i\mathbf{q}\cdot\mathbf{r}_{12}} \,. \tag{C.2}$$

In the previous two equations we defined $\mathbf{r}_{12}$ as the distance between nucleon 1 and nucleon 2, while $r_{12} = |\mathbf{r}_{12}|$. The Fourier transform in Eq. (C.2) is easily found. In fact, it is well known that the Fourier transform of the Yukawa potential is

$$Y(r_{12}) = \int \frac{d^3q}{(2\pi)^3} \, \frac{1}{\mathbf{q}^2 + m_\pi^2} \, e^{i\mathbf{q}\cdot\mathbf{r}_{12}} = \frac{1}{4\pi} \frac{e^{-m_\pi r_{12}}}{r_{12}} \,. \tag{C.3}$$

Eq. (C.2) can then be expressed as

$$V_{12}^{\pi}(r_{12}) = \left(\frac{g_A}{2f_\pi}\right)^2 (\boldsymbol{\tau}_1 \cdot \boldsymbol{\tau}_2)\ \sigma_1^i \sigma_2^j\ \nabla_{r_{12}^i} \nabla_{r_{12}^j} Y(r_{12})\ . \tag{C.4}$$

After performing the derivatives of the Yukawa potential and rearranging terms, it is possible to express the OPE potential as

$$\begin{aligned} V_{12}^{\pi}(r_{12}) \;&=\; \left(\frac{g_A}{2f_\pi}\right)^2 \frac{m_\pi^3}{12\pi}\ \frac{e^{-m_\pi r_{12}}}{m_\pi r_{12}} \\ &\times\; \left[\left(1 + \frac{3}{m_\pi r_{12}} + \frac{3}{(m_\pi r_{12})^2}\right)(\boldsymbol{\tau}_1 \cdot \boldsymbol{\tau}_2) S_{12} + (\boldsymbol{\tau}_1 \cdot \boldsymbol{\tau}_2)(\boldsymbol{\sigma}_1 \cdot \boldsymbol{\sigma}_2)\right], \end{aligned} \tag{C.5}$$

where $S_{12} = 3(\boldsymbol{\sigma}_1 \cdot \hat{r}_{12})(\boldsymbol{\sigma}_2 \cdot \hat{r}_{12}) - (\boldsymbol{\sigma}_1 \cdot \boldsymbol{\sigma}_2)$ is the standard tensor operator.

D. Three-nucleon forces as spherical tensors

The 3N chiral forces derived in Chapter 3 are written here as irreducible spherical tensors in configuration-spin space and isospin space.

Notation. We denote the general spin space Σ^{λ}_{ij}, $\Sigma^{\lambda,\Lambda}_{ij,k}$ and configuration space X^{λ}_{ij}, $X^{(\lambda,\lambda')\Lambda}_{ij,ij}$ irreducible tensor operators as

$$\begin{aligned}
\Sigma^{\lambda}_{ij} &= [\boldsymbol{\sigma}_i \times \boldsymbol{\sigma}_j]^{\lambda}, \\
\Sigma^{\lambda,\Lambda}_{ij,k} &= \left[[\boldsymbol{\sigma}_k \times [\boldsymbol{\sigma}_i \times \boldsymbol{\sigma}_j]^{\lambda}\right]^{\Lambda}, \\
X^{\lambda}_{ij} &= [\hat{\boldsymbol{r}}_{1i} \times \hat{\boldsymbol{r}}_{1j}]^{\lambda}, \\
X^{(\lambda,\lambda')\Lambda}_{ij,ij} &= \left[[\hat{\boldsymbol{r}}_{1i} \times \hat{\boldsymbol{r}}_{1j}]^{\lambda} \times [\hat{\boldsymbol{r}}_{1i} \times \hat{\boldsymbol{r}}_{1j}]^{\lambda'}\right]^{\Lambda},
\end{aligned}$$

where, contrary to the main part of the thesis, here we follow Ref. [2] and denote the generic particle indexes with i, j, k. With $\hat{\boldsymbol{r}}_{1i}$ we mean the rank 1 normalized spherical tensor associated to the relative distance between particle 1 and particle i. With the notation $[\hat{\boldsymbol{r}}_{1i} \times \hat{\boldsymbol{r}}_{1j}]^{\lambda}$ we intend the two rank-one coordinate space tensors coupled into a rank-λ tensor, and analogously for $[\boldsymbol{\sigma}_i \times \boldsymbol{\sigma}_j]^{\lambda}$ and $[\boldsymbol{\tau}_i \times \boldsymbol{\tau}_j]^{\lambda}$ in spin and isospin space, respectively. Furthermore, we define

$$X^{\lambda}(\hat{\boldsymbol{r}}_{ij}, \hat{\boldsymbol{r}}_{ij}) = [\hat{\boldsymbol{r}}_{ij} \times \hat{\boldsymbol{r}}_{ij}]^{\lambda} ,$$

where $\hat{\boldsymbol{r}}_{ij}$ is the rank-1 normalized spherical tensor associated to the relative distance between particles i and j.

In writing the 3N forces we follow Ref. [63]. The 3N interaction reads

$$W_{123} = \sum_{\text{cyc}} W_{1,23} = \sum_{\text{cyc}} \left[W^{2\pi,c_1}_{1,23} + W^{2\pi,c_3}_{1,23} + W^{2\pi,c_4}_{1,23} + W^{1\pi,c_D}_{1,23} + W^{ct,c_E}_{1,23} \right] ,$$

where the sum runs over the cyclic permutations of the particle triplet and the notation highlights the symmetry of the interaction over the exchange of particles 2 and 3. Each term is denoted with a label that includes the associated LEC. The

2π exchange $3N$ terms are given by

$$W_{1,23}^{2\pi,c_1} = A\, U_{12} Y_{12} U_{13} Y_{13}\, (\boldsymbol{\tau}_2 \cdot \boldsymbol{\tau}_3)\, (\boldsymbol{\sigma}_2 \cdot \hat{\boldsymbol{r}}_{12})\, (\boldsymbol{\sigma}_3 \cdot \hat{\boldsymbol{r}}_{13})\,, \tag{D.1}$$

$$W_{1,23}^{2\pi,c_3} = B\, \{\boldsymbol{\tau}_1 \cdot \boldsymbol{\tau}_2, \boldsymbol{\tau}_1 \cdot \boldsymbol{\tau}_3\}\, \{\chi_{12}, \chi_{13}\}\,, \tag{D.2}$$

$$W_{1,23}^{2\pi,c_4} = -C\, [\boldsymbol{\tau}_1 \cdot \boldsymbol{\tau}_2, \boldsymbol{\tau}_1 \cdot \boldsymbol{\tau}_3]\, [\chi_{12}, \chi_{13}]\,, \tag{D.3}$$

where we have defined the coupling constants A, B and C as

$$A = c_1 \frac{g_A^2 m_\pi^4 (\hbar c)^2}{16\pi^2 F_\pi^4}\,, \tag{D.4}$$

$$B = c_3 \frac{g_A^2 m_\pi^4 (\hbar c)^2}{1152\pi^2 F_\pi^4}\,, \tag{D.5}$$

$$C = c_4 \frac{g_A^2 m_\pi^4 (\hbar c)^2}{2304\pi^2 F_\pi^4}\,, \tag{D.6}$$

while the other functions and operators are

$$U_{12} \equiv U(r_{12}) = 1 + \frac{1}{m_\pi r_{12}}\,, \tag{D.7}$$

$$\begin{aligned} \chi_{12} &\equiv \chi(r_{12}) = X_{12} - \frac{4\pi}{m_\pi^2}\, \delta(r_{12})\, \left(\boldsymbol{\sigma}_1 \cdot \boldsymbol{\sigma}_2\right) \\ &= T(r_{12}) S_{12} + \tilde{Y}_{12}\, \left(\boldsymbol{\sigma}_1 \cdot \boldsymbol{\sigma}_2\right)\,, \end{aligned} \tag{D.8}$$

$$X_{12} \equiv X(r_{12}) = T(r_{12}) S_{12} + Y(r_{12}) \left(\boldsymbol{\sigma}_1 \cdot \boldsymbol{\sigma}_2\right)\,, \tag{D.9}$$

$$\tilde{Y}_{12} \equiv \tilde{Y}(r_{12}) = Y(r_{12}) - \frac{4\pi}{m_\pi^2}\, \delta(r_{12})\,, \tag{D.10}$$

$$Y(r_{12}) = \frac{e^{-m_\pi r_{12}}}{r_{12}}\,, \tag{D.11}$$

$$T(r_{12}) = \left(1 + \frac{3}{m_\pi r_{12}} + \frac{3}{(m_\pi r_{12})^2}\right) Y(r_{12})\,. \tag{D.12}$$

The 1π-interaction and contact terms used in this work read

$$W_{1,23}^{1\pi,c_D 2} = D\left(\boldsymbol{\tau}_2 \cdot \boldsymbol{\tau}_3\right)\, \chi_{23}\, \left[\delta(r_{12}) + \delta(r_{13})\right]\,, \tag{D.13}$$

$$W_{1,23}^{ct,c_E \tau} = E\left(\boldsymbol{\tau}_2 \cdot \boldsymbol{\tau}_3\right)\, \delta(r_{12})\, \delta(r_{13}) \tag{D.14}$$

with

$$D = c_D \frac{g_A m_\pi^2 (\hbar c)^4}{96\pi \Lambda_\chi F_\pi^4} , \tag{D.15}$$

$$E = c_E \frac{(\hbar c)^6}{\Lambda_\chi F_\pi^4} . \tag{D.16}$$

We now write the 3N interactions in terms of irreducible tensors in isospin space and in the coupled spin-configuration space. They are:

the $2\pi - c_1$ term

$$\begin{aligned} W_{1,23}^{2\pi,c_1} &= A U_{12} Y_{12} U_{13} Y_{13} (\boldsymbol{\tau}_2 \cdot \boldsymbol{\tau}_3)(\boldsymbol{\sigma}_2 \cdot \hat{\boldsymbol{r}}_{12})(\boldsymbol{\sigma}_3 \cdot \hat{\boldsymbol{r}}_{13}) \\ &= -\sqrt{3} A [\boldsymbol{\tau}_2 \times \boldsymbol{\tau}_3]^0 F_{UU} \left(\Sigma_{23}^0 \cdot X_{23}^0 - \Sigma_{23}^1 \cdot X_{23}^1 + \Sigma_{23}^2 \cdot X_{23}^2 \right) , \end{aligned} \tag{D.17}$$

the $2\pi - c_3$ term

$$\begin{aligned} W_{1,23}^{2\pi,c_3} &= B \{ \boldsymbol{\tau}_1 \cdot \boldsymbol{\tau}_2, \boldsymbol{\tau}_1 \cdot \boldsymbol{\tau}_3 \} \{ \chi_{12}, \chi_{13} \} \\ &= -2\sqrt{3} B [\boldsymbol{\tau}_2 \times \boldsymbol{\tau}_3]^0 \Big(\\ &\qquad \Sigma_{23}^0 \cdot (+F_{TT} X_{23}^0 - \frac{1}{\sqrt{3}} (3F_{YY} + F_{TY} + F_{YT})) \\ &\quad + \Sigma_{23}^1 \cdot (-F_{TT} X_{23}^1) \\ &\quad + \Sigma_{23}^2 \cdot (+F_{TT} X_{23}^2 + F_{TY} X_{22}^2 + F_{YT} X_{33}^2) \Big) , \end{aligned} \tag{D.18}$$

the $2\pi - c_4$ term

$$\begin{aligned} W_{1,23}^{2\pi,c_4} &= -C [\boldsymbol{\tau}_1 \cdot \boldsymbol{\tau}_2, \boldsymbol{\tau}_1 \cdot \boldsymbol{\tau}_3] [\chi_{12}, \chi_{13}] \\ &= 4\sqrt{3} C [\boldsymbol{\tau}_1 \times [\boldsymbol{\tau}_2 \times \boldsymbol{\tau}_3]^1]^0 \Big[\\ &\qquad \Sigma_{23,1}^{1,0} \cdot \Big(- F_{TT} X_{23,23}^{(1,1)0} - \frac{1}{\sqrt{3}} (3F_{YY} + F_{TY} + F_{YT}) \Big) \\ &\quad + \Sigma_{23,1}^{0,1} \cdot \Big(+ F_{TT} X_{23,23}^{(1,0)1} \Big) \\ &\quad + \Sigma_{23,1}^{2,1} \cdot \Big(+ F_{TT} X_{23,23}^{(1,2)1} \Big) \\ &\quad + \Sigma_{23,1}^{1,2} \cdot \Big(- F_{TT} X_{23,23}^{(1,1)2} - \frac{1}{2} (F_{TY} X_{22}^2 + F_{YT} X_{33}^2) \Big) \\ &\quad + \Sigma_{23,1}^{2,2} \cdot \Big(- F_{TT} X_{23,23}^{(1,2)2} - \frac{\sqrt{3}}{2} (F_{TY} X_{22}^2 - F_{YT} X_{33}^2) \Big) \\ &\quad + \Sigma_{23,1}^{2,3} \cdot \Big(+ F_{TT} X_{23,23}^{(1,2)3} \Big) \Big] . \end{aligned} \tag{D.19}$$

Where we have introduced the following definitions

$$\begin{aligned} F_{UU} &= U_{12}Y_{12}U_{13}Y_{13}, \\ F_{TT} &= 18T_{12}T_{13}, \\ F_{YY} &= 2(\tilde{Y}_{12}-T_{12})(\tilde{Y}_{13}-T_{13}), \\ F_{TY} &= 6T_{12}(\tilde{Y}_{13}-T_{13}), \\ F_{YT} &= 6(\tilde{Y}_{12}-T_{12})T_{13}\,. \end{aligned} \tag{D.20}$$

Finally we have:

the D term

$$\begin{aligned} W_{1,23}^{1\pi,c_D 2} &= D(\boldsymbol{\tau}_2\cdot\boldsymbol{\tau}_3)\chi_{23}(\delta_{12}+\delta_{13}) \\ &= -\sqrt{3}D[\boldsymbol{\tau}_2\times\boldsymbol{\tau}_3]^0\Big[\\ &\qquad \Sigma_{23}^0\cdot\Big(-\sqrt{3}(\delta_{12}+\delta_{13})\tilde{Y}_{23}\Big) \\ &\qquad +\Sigma_{23}^2\cdot\Big(3(\delta_{12}+\delta_{13})T_{23}X^2(\hat{\boldsymbol{r}}_{23},\hat{\boldsymbol{r}}_{23})\Big)\Big]\,, \end{aligned} \tag{D.21}$$

the E term

$$W_{1,23}^{ct,c_E\tau} = E(\boldsymbol{\tau}_2\cdot\boldsymbol{\tau}_3)\delta_{12}\delta_{13} = -\sqrt{3}E[\boldsymbol{\tau}_2\times\boldsymbol{\tau}_3]^0\delta_{12}\delta_{13}\,. \tag{D.22}$$

Bibliography

[1] S. Li Muli, A. Poggialini, and S. Bacca, "Muonic Lithium atoms: nuclear structure corrections to the Lamb shift," SciPost Phys. Proc., vol. 3, p. 028, 2020.

[2] S. S. Li Muli, S. Bacca, and N. Barnea, "Implementation of local chiral interactions in the hyperspherical harmonics formalism," Frontiers in Physics, vol. 9, 2021.

[3] S. S. Li Muli, B. Acharya, O. J. Hernandez, and S. Bacca, "Bayesian analysis of nuclear polarizability corrections to the Lamb shift of muonic H-atoms and He-ions," J. Phys. G, vol. 49, no. 10, p. 105101, 2022.

[4] B. Acharya et al., "Uncertainty quantification in electromagnetic observables on nuclei," Frontiers in Physics, vol. 10, 2023.

[5] K. Pachucki, V. Lensky, F. Hagelstein, S. S. Li Muli, S. Bacca, and R. Pohl, "Comprehensive theory of the lamb shift in in light muonic atoms," 2023.

[6] S. S. Li Muli and S. Bacca, "In preparation for 2023,"

[7] J. J. Sakurai and J. Napolitano, Modern Quantum Mechanics. Cambridge University Press, 2 ed., 2017.

[8] D. J. Griffiths and D. F. Schroeter, Introduction to Quantum Mechanics. Cambridge University Press, 3 ed., 2018.

[9] P. A. M. Dirac, "The quantum theory of the electron," Proc. Roy. Soc. Lond. A, vol. 117, pp. 610–624, 1928.

[10] W. E. Lamb and R. C. Retherford, "Fine structure of the hydrogen atom by a microwave method," Phys. Rev., vol. 72, pp. 241–243, 1947.

[11] S.-I. Tomonaga and J. R. Oppenheimer, "On infinite field reactions in quantum field theory," Phys. Rev., vol. 74, pp. 224–225, 1948.

[12] J. Schwinger, "On quantum-electrodynamics and the magnetic moment of the electron," Phys. Rev., vol. 73, pp. 416–417, 1948.

[13] R. P. Feynman, "Space-time approach to quantum electrodynamics," Phys. Rev., vol. 76, pp. 769–789, 1949.

[14] A. Beyer et al., "The Rydberg constant and proton size from atomic hydrogen," Science, vol. 358, no. 6359, pp. 79–85, 2017.

[15] H. Fleurbaey et al., "New measurement of the $1s - 3s$ transition frequency of hydrogen: Contribution to the proton charge radius puzzle," Phys. Rev. Lett., vol. 120, p. 183001, 2018.

[16] N. Bezginov, T. Valdez, M. Horbatsch, A. Marsman, A. C. Vutha, and E. A. Hessels, "A measurement of the atomic hydrogen lamb shift and the proton charge radius," Science, vol. 365, no. 6457, pp. 1007–1012, 2019.

[17] V. A. Yerokhin, K. Pachucki, and V. Patkos, "Theory of the Lamb Shift in Hydrogen and Light Hydrogen-Like Ions," Annalen Phys., vol. 531, no. 5, p. 1800324, 2019.

[18] E. Tiesinga, P. J. Mohr, D. B. Newell, and B. N. Taylor, "Codata recommended values of the fundamental physical constants: 2018," Rev. Mod. Phys., vol. 93, p. 025010, 2021.

[19] R. Aaij et al., "Test of lepton universality in beauty-quark decays," Nature Phys., vol. 18, no. 3, pp. 277–282, 2022.

[20] M. S. Safronova, D. Budker, D. DeMille, D. F. J. Kimball, A. Derevianko, and C. W. Clark, "Search for new physics with atoms and molecules," Rev. Mod. Phys., vol. 90, p. 025008, 2018.

[21] L. Gurung, T. J. Babij, S. D. Hogan, and D. B. Cassidy, "Precision microwave spectroscopy of the positronium $n = 2$ fine structure," Phys. Rev. Lett., vol. 125, p. 073002, 2020.

[22] B. Ohayon, G. Janka, I. Cortinovis, Z. Burkley, L. d. S. Borges, E. Depero, A. Golovizin, X. Ni, Z. Salman, A. Suter, C. Vigo, T. Prokscha, and P. Crivelli, "Precision measurement of the lamb shift in muonium," Phys. Rev. Lett., vol. 128, p. 011802, 2022.

[23] G. Janka et al., "Measurement of the transition frequency from $2S_{1/2}, F = 0$ to $2P_{1/2}, F = 1$ states in Muonium," Nature Commun., vol. 13, no. 1, p. 7273, 2022.

[24] R. Pohl et al., "The size of the proton," Nature, vol. 466, pp. 213–216, 2010.

[25] A. Antognini et al., "Proton structure from the measurement of 2s-2p transition frequencies of muonic hydrogen," Science, vol. 339, no. 6118, pp. 417–420, 2013.

[26] J. Krauth et al., "Measuring the -particle charge radius with muonic helium-4 ions," Nature, vol. 589, pp. 527–531, 2021.

[27] K. Schuhmann et al., "The helion charge radius from laser spectroscopy of muonic helium-3 ions," 2023.

[28] A. Antognini et al., "Muonic-Atom Spectroscopy and Impact on Nuclear Structure and Precision QED Theory," 2022.

[29] J. Friar, "Nuclear finite-size effects in light muonic atoms," Annals of Physics, vol. 122, no. 1, pp. 151–196, 1979.

[30] J. L. Friar, J. Martorell, and D. W. L. Sprung, "Nuclear sizes and the isotope shift," Phys. Rev. A, vol. 56, pp. 4579–4586, 1997.

[31] M. I. Eides, H. Grotch, and V. A. Shelyuto, Theory of Light Hydrogenic Bound States, vol. 222. Berlin: Springer-Verlag, 2007.

[32] J. L. Friar, "Nuclear polarization corrections to μ-d atoms in zero-range approximation," Phys. Rev. C, vol. 88, p. 034003, 2013.

[33] H. Gao and M. Vanderhaeghen, "The proton charge radius," Rev. Mod. Phys., vol. 94, p. 015002, 2022.

[34] O. Tomalak and M. Vanderhaeghen, "Two-photon exchange correction to muon–proton elastic scattering at low momentum transfer," Eur. Phys. J. C, vol. 76, no. 3, p. 125, 2016.

[35] H. Arenhovel, "Meson exchange and isobar current effects in nuclear photon scattering," Z. Phys. A, vol. 297, pp. 129–139, 1980.

[36] S. Weinberg, The Quantum Theory of Fields, Volume 1: Foundations. Cambridge University Press, 2005.

[37] W. Leidemann and R. Rosenfelder, "Deuteron nuclear polarization shifts with realistic potentials," Phys. Rev. C, vol. 51, pp. 427–430, 1995.

[38] O. J. Hernandez, C. Ji, S. Bacca, and N. Barnea, "Probing uncertainties of nuclear structure corrections in light muonic atoms," Phys. Rev. C, vol. 100, p. 064315, 2019.

[39] C. Ji, S. Bacca, N. Barnea, O. J. Hernandez, and N. N. Dinur, "Ab initio calculation of nuclear-structure corrections in muonic atoms," Journal of Physics G: Nuclear and Particle Physics, vol. 45, no. 9, p. 093002, 2018.

[40] C. Ji, N. Nevo Dinur, S. Bacca, and N. Barnea, "Nuclear polarization corrections to the $\mu^4\mathrm{He}^+$ Lamb shift," Phys. Rev. Lett., vol. 111, p. 143402, 2013.

[41] N. Nevo Dinur, C. Ji, S. Bacca, and N. Barnea, "Nuclear structure corrections to the lamb shift in μhe+3 and μh3," Physics Letters B, vol. 755, pp. 380–386, 2016.

[42] J. L. Friar and G. L. Payne, "Higher-order nuclear-polarizability corrections in atomic hydrogen," Phys. Rev. C, vol. 56, pp. 619–630, 1997.

[43] K. Pachucki and A. Wienczek, "Nuclear structure effects in light muonic atoms," Phys. Rev. A, vol. 91, p. 040503, 2015.

[44] C. Patrignani, "Review of particle physics," Chinese Physics C, vol. 40, no. 10, p. 100001, 2016.

[45] K. Pachucki, V. c. v. Patkóš, and V. A. Yerokhin, "Three-photon-exchange nuclear structure correction in hydrogenic systems," Phys. Rev. A, vol. 97, p. 062511, 2018.

[46] O. Hernandez, C. Ji, S. Bacca, N. Nevo Dinur, and N. Barnea, "Improved estimates of the nuclear structure corrections in μd," Physics Letters B, vol. 736, pp. 344–349, 2014.

[47] M. Kalinowski, "Deuteron charge radius from the lamb-shift measurement in muonic deuterium," Phys. Rev. A, vol. 99, p. 030501, 2019.

[48] S. G. Karshenboim, E. Y. Korzinin, V. A. Shelyuto, and V. G. Ivanov, "$\alpha(Z\alpha)^5 m$ finite-nuclear-size contribution to the energy levels in light muonic atoms," Phys. Rev. A, vol. 98, p. 062512, 2018.

[49] K. Pachucki, "Nuclear structure corrections in muonic deuterium," Phys. Rev. Lett., vol. 106, p. 193007, 2011.

[50] R. Machleidt and D. Entem, "Chiral effective field theory and nuclear forces," Physics Reports, vol. 503, no. 1, pp. 1 – 75, 2011.

[51] E. Epelbaum, H. Krebs, and P. Reinert, "High-precision nuclear forces from chiral eft: State-of-the-art, challenges, and outlook," Front. Phys., vol. 8, p. 98, 2020.

[52] E. A. Hylleraas, "Reminiscences from early quantum mechanics of two-electron atoms," Rev. Mod. Phys., vol. 35, pp. 421–430, 1963.

[53] V. I. Korobov, J.-P. Karr, M. Haidar, and Z.-X. Zhong, "Hyperfine structure in the h_2^+ and hd^+ molecular ions at order $m\alpha^6$," Phys. Rev. A, vol. 102, p. 022804, 2020.

[54] M. Haidar, V. I. Korobov, L. Hilico, and J.-P. Karr, "Higher-order corrections to spin-orbit and spin-spin tensor interactions in hydrogen molecular ions: Theory and application to h_2^+," Phys. Rev. A, vol. 106, p. 022816, 2022.

[55] V. I. Korobov, "Coulomb three-body bound-state problem: Variational calculations of nonrelativistic energies," Phys. Rev. A, vol. 61, p. 064503, 2000.

[56] N. Barnea, E. Friedman, and A. Gal, "On the difth of the k-d atom ground state," Nuclear Physics A, vol. 1006, p. 122112, 2021.

[57] J. Mitroy, S. Bubin, W. Horiuchi, Y. Suzuki, L. Adamowicz, W. Cencek, K. Szalewicz, J. Komasa, D. Blume, and K. Varga, "Theory and application of explicitly correlated gaussians," Rev. Mod. Phys., vol. 85, pp. 693–749, 2013.

[58] M. Viviani, L. E. Marcucci, S. Rosati, and et al., "Variational Calculation on A = 3 and 4 Nuclei with Non-Local Potentials.," Few-Body Systems, vol. 39, pp. 159–176, 2006.

[59] L. E. Marcucci, J. Dohet-Eraly, L. Girlanda, A. Gnech, A. Kievsky, and M. Viviani, "The hyperspherical harmonics method: a tool for testing and improving nuclear interaction models," Front. Phys., vol. 8, no. 69, 2020.

[60] B. R. Barrett, P. Navrátil, and J. P. Vary, "Ab initio no core shell model," Progress in Particle and Nuclear Physics, vol. 69, pp. 131–181, 2013.

[61] W. Glöckle, H. Witała, D. Hüber, H. Kamada, and J. Golak, "The three-nucleon continuum: achievements, challenges and applications," Physics Reports, vol. 274, no. 3, pp. 107–285, 1996.

[62] R. Lazauskas and J. Carbonell, "Description of four- and five-nucleon systems by solving Faddeev-Yakubovsky equations in configuration space," Frontiers in Physics, vol. 7, 2020.

[63] J. E. Lynn, I. Tews, J. Carlson, S. Gandolfi, A. Gezerlis, K. E. Schmidt, and A. Schwenk, "Quantum monte carlo calculations of light nuclei with local chiral two- and three-nucleon interactions," Phys. Rev. C, vol. 96, p. 054007, 2017.

[64] H. Kamada et al., "Benchmark test calculation of a four-nucleon bound state," Phys. Rev. C, vol. 64, p. 044001, 2001.

[65] N. Barnea, Exact solution of the Schrödinger and Faddeev equations for few-body systems. PhD thesis, Hebrew university, 1997.

[66] S. Bacca, Study of electromagnetic reactions on light nuclei with the Lorentz integral transform method. PhD thesis, University of Trento and Johannes Gutenberg Universität Mainz, 2005.

[67] F. Zernike and H. Brinkman Proc. K. Ned. Akad. Wett., vol. 38, p. 161, 1935.

[68] L. M. Delves, "Tertiary and general-order collisions," Nucl. Phys., vol. 9, pp. 391–399, 1959.

[69] Y. A. Simonov Sov. J. Nucl. Phys, vol. 3, p. 461, 1966.

[70] W. Zickendraht, "Construction of a complete orthogonal system for the quantum-mechanical three-body problem," Ann. Phys., vol. 35, p. 18, 1965.

[71] F. T. Smith, "Generalized angular momentum in many-body collisions," Phys. Rev., vol. 120, p. 1058, 1960.

[72] A. Kievsky, S. Rosati, M. Viviani, L. E. Marcucci, and L. Girlanda, "A high-precision variational approach to three- and four-nucleon bound and zero-energy scattering states," J. Phys. G. Nucl. Part. Phys., vol. 35, p. 063101, 2008.

[73] J. O. Hirschfelder and J. S. Dahler, "The kinetic energy of relative motion," Proceedings of the National Academy of Sciences, vol. 42, no. 6, pp. 363–365, 1956.

[74] N. Barnea, Ab-initio few-body methods and nuclear structure. Lecture notes, TALENT school Mainz (2022).

[75] V. D. Efros Sov. J. Nucl. Phys, vol. 15, p. 128, 1972.

[76] M. Fabre de la Ripelle, "The potential harmonic expansion method," Ann. Phys. (N. Y.), vol. 147, pp. 281–320, 1983.

[77] N. Barnea, W. Leidemann, and G. Orlandini, "Ground state wave functions in the hyperspherical formalism for nuclei with A greater than 4," Nucl. Phys. A, vol. 650, pp. 427–442, 1999.

[78] S. Bacca, "Structure models: from shell model to ab initio methods," Eur. Phys. J. Plus, vol. 131, no. 4, p. 107, 2016.

[79] N. Barnea, W. Leidemann, and G. Orlandini, "State dependent effective interaction for the hyperspherical formalism," Phys. Rev. C, vol. 61, p. 054001, 2000.

[80] H. Yukawa, "On the Interaction of Elementary Particles. I," Progress of Theoretical Physics Supplement, vol. 1, pp. 1–10, 1955.

[81] R. B. Wiringa, V. G. J. Stoks, and R. Schiavilla, "Accurate nucleon-nucleon potential with charge-independence breaking," Phys. Rev. C, vol. 51, pp. 38–51, 1995.

[82] V. G. J. Stoks, R. A. M. Klomp, C. P. F. Terheggen, and J. J. de Swart, "Construction of high-quality nn potential models," Phys. Rev. C, vol. 49, pp. 2950–2962, 1994.

[83] R. Machleidt, "High-precision, charge-dependent bonn nucleon-nucleon potential," Phys. Rev. C, vol. 63, p. 024001, 2001.

[84] B. S. Pudliner, V. R. Pandharipande, J. Carlson, and R. B. Wiringa, "Quantum monte carlo calculations of $A \leq 6$ nuclei," Phys. Rev. Lett., vol. 74, pp. 4396–4399, 1995.

[85] S. C. Pieper, V. R. Pandharipande, R. B. Wiringa, and J. Carlson, "Realistic models of pion-exchange three-nucleon interactions," Phys. Rev. C, vol. 64, p. 014001, 2001.

[86] W. Leidemann and G. Orlandini, "Modern ab initio approaches and applications in few-nucleon physics with $a \geq 4$," Prog. Part. Nucl. Phys., vol. 68, pp. 158–214, 2013.

[87] S. Bacca and S. Pastore, "Electromagnetic reactions on light nuclei," Journal of Physics G: Nuclear and Particle Physics, vol. 41, no. 12, p. 123002, 2014.

[88] N. Rocco, "Ab initio calculations of lepton-nucleus scattering," Frontiers in Physics, vol. 8, p. 116, 2020.

[89] S. Weinberg, "Phenomenological Lagrangians," Physica, vol. 96A, pp. 327–340, 1979.

[90] S. Weinberg, "Nuclear forces from chiral Lagrangians," Phys. Lett. B, vol. 251, pp. 288–292, 1990.

[91] S. Weinberg, "Effective chiral Lagrangians for nucleon-pion interactions and nuclear forces," Nucl. Phys. B, vol. 363, pp. 3–18, 1991.

[92] S. Weinberg, "Three-body interactions among nucleons and pions," Phys. Lett. B, vol. 295, pp. 114–121, 1992.

[93] E. Epelbaum, H.-W. Hammer, and U.-G. Meißner, "Modern theory of nuclear forces," Rev. Mod. Phys., vol. 81, pp. 1773–1825, 2009.

[94] A. Gezerlis and et al, "Local chiral effective field theory interactions and quantum monte carlo applications," Phys. Rev. C, vol. 90, p. 054323, 2014.

[95] I. Tews, S. Gandolfi, A. Gezerlis, and A. Schwenk, "Quantum monte carlo calculations of neutron matter with chiral three-body forces," Phys. Rev. C, vol. 93, p. 024305, 2016.

[96] J. Lynn and et al, "Chiral three-nucleon interactions in light nuclei, neutron-α scattering and neutron matter," Phys. Rev. Lett, vol. 116, p. 062501, 2016.

[97] S. L. Adler, "Axial-vector vertex in spinor electrodynamics," Phys. Rev., vol. 177, pp. 2426–2438, 1969.

[98] J. S. Bell and R. Jackiw, "A PCAC puzzle: $\pi^0 \to \gamma\gamma$ in the σ model," Nuovo Cim. A, vol. 60, pp. 47–61, 1969.

[99] S. Weinberg, "Nonlinear realizations of chiral symmetry," Phys. Rev., vol. 166, pp. 1568–1577, 1968.

[100] S. Coleman, J. Wess, and B. Zumino, "Structure of phenomenological lagrangians. i," Phys. Rev., vol. 177, pp. 2239–2247, 1969.

[101] C. G. Callan, S. Coleman, J. Wess, and B. Zumino, "Structure of phenomenological lagrangians. ii," Phys. Rev., vol. 177, pp. 2247–2250, 1969.

[102] S. Scherer and M. R. Schindler, A Primer for Chiral Perturbation Theory, vol. 830. 2012.

[103] J. Gasser and H. Leutwyler, "Chiral perturbation theory to one loop," Annals of Physics, vol. 158, no. 1, pp. 142–210, 1984.

[104] J. Gasser, M. Sainio, and A. Švarc, "Nucleons with chiral loops," Nuclear Physics B, vol. 307, no. 4, pp. 779–853, 1988.

[105] E. Jenkins and A. V. Manohar, "Baryon chiral perturbation theory using a heavy fermion lagrangian," Physics Letters B, vol. 255, no. 4, pp. 558–562, 1991.

[106] H. Georgi, "An effective field theory for heavy quarks at low energies," Physics Letters B, vol. 240, no. 3, pp. 447–450, 1990.

[107] E. Epelbaum, W. Gloeckle, and U.-G. Meissner, "Improving the convergence of the chiral expansion for nuclear forces. 1. Peripheral phases," Eur. Phys. J. A, vol. 19, pp. 125–137, 2004.

[108] N. Fettes, U.-G. Meißner, and S. Steininger, "Pion-nucleon scattering in chiral perturbation theory (i): Isospin-symmetric case," Nuclear Physics A, vol. 640, no. 2, pp. 199–234, 1998.

[109] E. Epelbaum, H. Krebs, and P. Reinert, Semi-local Nuclear Forces From Chiral EFT: State-of-the-Art and Challenges, pp. 1–25. 2022.

[110] P. Maris et al., "Nuclear properties with semilocal momentum-space regularized chiral interactions beyond N2LO," Phys. Rev. C, vol. 106, no. 6, p. 064002, 2022.

[111] R. T. Cox, "Probability, Frequency and Reasonable Expectation," American Journal of Physics, vol. 14, no. 1, pp. 1–13, 1946.

[112] S. H. Jeffreys, The Theory of Probability. Clarendon Press, 1939.

[113] E. T. Jaynes, "Information theory and statistical mechanics," Phys. Rev., vol. 106, pp. 620–630, 1957.

[114] S. Bacca, M. A. Marchisio, N. Barnea, W. Leidemann, and G. Orlandini, "Microscopic calculation of six-body inelastic reactions with complete final state interaction: Photoabsorption of ^{6}He and ^{6}Li," Phys. Rev. Lett., vol. 89, p. 052502, 2002.

[115] S. Bacca, N. Barnea, W. Leidemann, and G. Orlandini, "Effect of p-wave interaction in ^{6}He and ^{6}Li photoabsorption," Phys. Rev. C, vol. 69, p. 057001, 2004.

[116] S. Bacca, H. Arenhoevel, N. Barnea, W. Leidemann, and G. Orlandini, "Ab initio calculation of Li-7 photodisintegration," Phys. Lett. B, vol. 603, pp. 159–164, 2004.

[117] R. B. Wiringa and S. C. Pieper, "Evolution of nuclear spectra with nuclear forces," Phys. Rev. Lett., vol. 89, p. 182501, 2002.

[118] R. B. Wiringa, R. Schiavilla, S. C. Pieper, and J. Carlson, "Nucleon and nucleon-pair momentum distributions in $a \leq 12$ nuclei," Phys. Rev. C, vol. 89, p. 024305, 2014.

[119] G. W. F. Drake and L. L. Byer, "Lamb shifts and fine-structure splittings for the muonic ions μ^--li, μ^--be, and μ^--b: A proposed experiment," Phys. Rev. A, vol. 32, pp. 713–719, 1985.

[120] M. Schindler and D. Phillips, "Bayesian methods for parameter estimation in effective field theories," Annals of Physics, vol. 324, no. 3, pp. 682–708, 2009.

[121] P. J. Mohr, D. B. Newell, and B. N. Taylor, "Codata recommended values of the fundamental physical constants: 2014," Rev. Mod. Phys., vol. 88, p. 035009, 2016.

[122] A. Ong, J. C. Berengut, and V. V. Flambaum, "Effect of spin-orbit nuclear charge density corrections due to the anomalous magnetic moment on halonuclei," Phys. Rev. C, vol. 82, p. 014320, 2010.

[123] A. A. Filin, V. Baru, E. Epelbaum, H. Krebs, D. Möller, and P. Reinert, "Extraction of the neutron charge radius from a precision calculation of the deuteron structure radius," Phys. Rev. Lett., vol. 124, p. 082501, 2020.

[124] J. E. Lynn, J. Carlson, E. Epelbaum, S. Gandolfi, A. Gezerlis, and A. Schwenk, "Quantum monte carlo calculations of light nuclei using chiral potentials," Phys. Rev. Lett., vol. 113, p. 192501, 2014.

[125] "Nudat." https://www.nndc.bnl.gov/nudat2. Accessed: 2021-01-22.

[126] N. Nevo Dinur, O. J. Hernandez, S. Bacca, N. Barnea, C. Ji, S. Pastore, M. Piarulli, and R. B. Wiringa, "Zemach moments and radii of ^{2,3}H and ^{3,4}He," Phys. Rev. C, vol. 99, p. 034004, 2019.

[127] D. Lonardoni et al., "Auxiliary field diffusion monte carlo calculations of light and medium-mass nuclei with local chiral interactions," Phys. Rev. C, vol. 97, p. 044318, 2018.

[128] I. Sick, "Zemach moments of ^{3}He and ^{4}He," Phys. Rev. C, vol. 90, p. 064002, 2014.

[129] J. Purcell, J. Kelley, E. Kwan, C. Sheu, and H. Weller, "Energy levels of light nuclei a=3," Nuclear Physics A, vol. 848, no. 1, pp. 1 – 74, 2010.

[130] I. Angeli and K. Marinova, "Table of experimental nuclear ground state charge radii: An update," Atomic Data and Nuclear Data Tables, vol. 99, no. 1, pp. 69 – 95, 2013.

[131] Y. M. Arkatov, P. I. Vatset, V. I. Voloshchuk, V. A. Zolenko, I. M. Prokhorets, and V. I. Chmil, "Energy moments of the γ-ray total-absorption cross section of ^{4}He," Yad.Fiz., vol. 19, p. 1172, 1974.

[132] E. Epelbaum, H. Krebs, and U.-G. Meißner, "Precision nucleon-nucleon potential at fifth order in the chiral expansion," Phys. Rev. Lett., vol. 115, p. 122301, 2015.

[133] I. Sick, "Precise root-mean-square radius of ^{4}He," Phys. Rev. C, vol. 77, p. 041302, 2008.

[134] K. Pachucki, V. c. v. Patkóš, and V. A. Yerokhin, "Testing fundamental interactions on the helium atom," Phys. Rev. A, vol. 95, p. 062510, 2017.

[135] V. c. v. Patkóš, V. A. Yerokhin, and K. Pachucki, "Higher-order recoil corrections for singlet states of the helium atom," Phys. Rev. A, vol. 95, p. 012508, 2017.

[136] D. Shiner, R. Dixson, and V. Vedantham, "Three-nucleon charge radius: A precise laser determination using ^{3}He," Phys. Rev. Lett., vol. 74, pp. 3553–3556, 1995.

[137] P. Cancio Pastor, L. Consolino, G. Giusfredi, P. De Natale, M. Inguscio, V. A. Yerokhin, and K. Pachucki, "Frequency metrology of helium around 1083 nm and determination of the nuclear charge radius," Phys. Rev. Lett., vol. 108, p. 143001, 2012.

[138] X. Zheng, Y. R. Sun, J.-J. Chen, W. Jiang, K. Pachucki, and S.-M. Hu, "Measurement of the frequency of the $2\,^3s - 2\,^3p$ transition of ^{4}He," Phys. Rev. Lett., vol. 119, p. 263002, 2017.

[139] Y.-J. Huang, Y.-C. Guan, J.-L. Peng, J.-T. Shy, and L.-B. Wang, "Precision laser spectroscopy of the $2^1s_0 - -3^1d_2$ two-photon transition in ^{3}He," Phys. Rev. A, vol. 101, p. 062507, 2020.

[140] Y. van der Werf, K. Steinebach, R. Jannin, H. L. Bethlem, and K. S. E. Eikema, "The alpha and helion particle charge radius difference from spectroscopy of quantum-degenerate helium," 2023.

[141] B. Acharya, V. Lensky, S. Bacca, M. Gorchtein, and M. Vanderhaeghen, "Dispersive evaluation of the Lamb shift in muonic deuterium from chiral effective field theory," Phys. Rev. C, vol. 103, no. 2, p. 024001, 2021.

[142] "3–4 - definite integrals of elementary functions," in Table of Integrals, Series, and Products (Seventh Edition) (A. Jeffrey, D. Zwillinger, I. Gradshteyn, and I. Ryzhik, eds.), pp. 247–617, Boston: Academic Press, seventh edition ed., 2007.

[143] A. M and S. I. A., Handbook of Mathematical Functions: With Formulas, Graphs, and Mathematical Tables. 1965.